Quantifying variability within the medial zone of modern distributive fluvial systems: Implications for reservoir characterisation

Rachel Elizabeth Williams

Submitted in fulfilment of the requirements for the degree of

Masters by Research in Earth Sciences

School of Geographical Earth Sciences

College of Science and Engineering

February 2023

University of Glasgow

College of Science and Engineering

Statement of Originality to Accompany Thesis Submission

Name: Rachel Elizabeth Williams

Registration Number: XXXXXXXXX

I certify that the thesis presented here for examination for a MRes degree of the University of Glasgow is solely my own work other than where I have clearly indicated that it is the work of others (in which case the extent of any work carried out jointly by me and any other person is clearly identified in it) and that the thesis has not been edited by a third party beyond what is permitted by the University's PGR Code of Practice.

I declare that the thesis does not include work forming part of a thesis presented successfully for another degree.

I declare that this thesis has been produced in accordance with the University of Glasgow's Code of Good Practice in Research.

I acknowledge that if any issues are raised regarding good research practice based on review of the thesis, the examination may be postponed pending the outcome of any investigation of the issues.

I am submitting this thesis with approval of my supervisor. I fully understand my responsibilities in this context as a researcher under the University's policies, including the Code of Good Practice in research.

Signature: …….

Date: 02/03/2023

Acknowledgements

I would like to express my sincerest thanks to my supervisors, Dr Amanda Owen, Dr Laura Quick, Professor Richard Williams, and Professor Adrian Hartley for their support and guidance throughout the duration and completion of this Masters by Research thesis, and the opportunity to undertake this project in the first place. I would also like to acknowledge the University of Glasgow for the resources provided to aid in this research. Additionally, a special thanks to the members of the Rivers Research Cluster Group for their contributions of support and feedback, and to my friends Alex and Pan for their extensive software and "tech" support. Finally, a special and heartfelt thanks to my family and friends, whom without their constant support and motivation, wherever in the world they are, this project would not have been possible.

Abstract

Distributive fluvial systems (DFS) are important reservoirs for hydrocarbons, groundwater, geothermal energy, carbon capture and hydrogen storage through the preservation of channel belt deposits. The study of these systems is important for understanding fluid flow and connectivity. However, previous studies have observed variability in channel characteristics within the rock record (e.g. storey and channel body thicknesses, channel: floodplain), predominantly within the medial zone of these systems. The first part of this study aimed to constrain the downstream position of the three DFS zones (proximal, medial, and distal) using a defined set of criteria, including channel belt width, active channel width, and channel planform. The percentage downstream for the proximal – medial transition, and the medial – distal transition have been identified to fall at approximately 25 – 35% and 65 – 75% downstream, with variation from this trend attributed to high sediment loads. Following this, the second part of the study used quantitative methods, including active channel and channel belt widths, active channel: channel belt: overbank, to characterise variability in the medial zone of modern DFS, in order to understand how the contemporary processes translate to ancient DFS deposits, and drive the observed variability. Analysis of downstream trends within the medial zone identified a downstream decrease in active channel and channel belt widths, related to the downstream decrease in sediment supply and discharge seen on system-wide DFS studies, however no trend is associated with the ratio of active channel width to channel belt width. In some systems there is a downstream decrease in the percentages of active channel and channel belt as overbank proportion increases, however this is directly influenced by the sweep angle of the DFS. Thus, DFS were further categorised as a *wide*, *moderate*, or *narrow* sweep angle DFS. Systems with a wide to moderate sweep angle are characterised by an increase in overbank deposits downstream, which therefore drives a downstream decrease in the percentage of channel belt deposits. However, in systems with a narrow sweep angle, confined by neighbouring systems or topography, the proportions of overbank, channel belt and active channel remain generally constant. Variability in the medial zone is seen through downstream trends between and within systems, and in the measured characteristics between systems, e.g. active channel and channel belt widths etc. The dataset of systems was grouped by climate type, catchment area (a proxy for sediment supply and discharge) and channel planform (a proxy for sediment concentrations and grain size), to identify any clear factors that cause variability between systems. Thus, it can be proposed that variability in the medial zone arises due to a combination of factors but is ultimately driven by variation in sediment concentrations and discharge. Further work may involve quantifying some of these factors of variability, or by using numerical models to infer how medial characteristics of modern DFS appear in the rock record.

Contents

List of Figures

Chapter 1

Chapter 2

Chapter 3

Chapter 4

Chapter 5

List of Tables

Chapter 2

Chapter 3

Chapter 4

List of Abbreviations

1. ACW: Active Channel Width
2. aW*: Normalised Active Channel Width
3. ACW/CBW: Ratio of Active channel width to channel belt width
4. CBW: Channel Belt Width
5. CV: Coefficient of Variation
6. cW*: Normalised Channel Belt Width
7. DFS: Distributive Fluvial System
8. MNDWI: Modified Normalised Difference Water Index
9. NDVI: Normalised Difference Vegetation Index
10. SA: Sweep angle

Chapter 1: Introduction

1.1 Study Rationale

Most literature explores both modern and ancient deposits, equally with their own merits. Studying ancient deposits provides understanding of fluvial architecture, particularly important with regards to reservoir distribution. However, modern systems provide important context for the system interactions that construct ancient deposits. Modern studies provide an understanding of processes involved, primarily the nodal avulsion causing the activation of new lobes (Cain and Mountney, 2009) and distribution and planform of channel networks. As these processes are integral to DFS development, studying them is vitally important in understanding how modern day physical processes and deposits subsequently become subsurface 3D deposits.

Modern DFS have been studied in the context of understanding the general trends and processes in these systems (e.g. Hartley *et al.*, 2010, 2013; Weissmann *et al.*, 2010, 2013, 2015; Davidson *et al.*, 2013). However, characteristic trends in these zones to determine where each DFS zone lies, and investigating channel characteristics in detail within each zone, particularly the medial zone, have been under studied; very few studies have evaluated the downstream positions of DFS zones (Davidson *et al.*, 2013). Furthermore, as variability in the medial zone has been observed in ancient and experimental studies (e.g. Führ Dal' Bó *et al.*, 2019; Terwisscha van Scheltinga *et al.*, 2020; Martin *et al.*, 2021; Snieder *et al.*, 2021), studying this in modern systems aids in the understanding of how variability arises, contributing to the wider understanding and research of DFS, as well as its applications for reservoir connectivity.

Therefore, the two aims and associated objectives for this study are as follows:

1. To outline criteria and create a dataset of a sample of rivers across different climate zones in order to constrain the medial zone within modern distributive fluvial systems (DFS), allowing for detailed analysis within the medial zone.
    - Produce a set of criteria that can be used to identify and constrain the medial position: including downstream trends and geomorphic characteristics.
    - Use the generated dataset to determine the distance downstream (and percentage downstream) for the proximal, medial, and distal zones of the sampled DFS.
2. To assess variability within the medial zone of modern distributive fluvial systems (DFS) by generating a dataset of measured characteristics, aiding the understanding of reservoir and resource distribution.
    - Measure determined parameters across the medial zone: active channel width, channel belt width, ratio of active channel width to channel belt, proportion of active channel and channel belt, and DFS sweep angle.
    - Evaluate downstream trends within the medial zone and compare between each DFS, using statistical tests
    - Discuss drivers of variability within the medial zone and between various systems, considering the effect this may have on ancient (rock record) DFS deposits.

This study primarily focuses on nine chosen DFS, within three climatic zones: tropical, dryland, and polar climates, in order to compare how variability in the medial zone may present in different settings. Despite this, tectonic setting remains consistent between systems to limit factors that may influence DFS characterstics. Detailed methods of site selection and further information on the chosen sites is outlined in Chapter 2.

Furthermore, a series of statistical tests will be used in order to compare downstream trends between systems, (e.g. the Spearman's rank correlation coefficient, linear regression), determine the degree of variability within a system and compared to others (e.g. coefficient of variation), and finally, statistical tests of difference (e.g. Kruskal-Wallis and Wilcoxon tests) to compare differences of magnitude between systems regarding the medians and means.

Following these aims, this thesis is organised into two key themes, and therefore two individual, but connected, results and discussion chapters. The first part (Chapter 3) aims to present the results and discussion establishing the position downstream of the proximal to medial, and medial to distal zones. Continuing from these results, Chapter 4 uses the established zones to outline the medial zone for studying variability in the medial zone of various characteristics, and then discusses the causes of variability. The wider implications are discussed in Chapter 5.

1.2 Literature Review

1.2.1 Definition of a DFS

Distributive fluvial systems occur where sediment laden water exits topographic confinements (e.g. hinterland) into an topographically unconfined zone, such as a sedimentary basin, producing a large scale fan geometry radiating from an apex (Hartley et al., 2010; Weissmann et al., 2010). The umbrella term "Distributive fluvial system" (henceforward referred to as DFS) encompasses all systems that undergo the sediment transportation transition. This includes alluvial fans, fluvial fans, humid fans, terminal fans, and mega fans, despite their own internal differences (Kelly and Olsen, 1993; Cain and Mountney, 2009). This umbrella term is used as it is often difficult to differentiate between each of the listed systems, as the processes involved in forming the fans are very similar, with the exception of alluvial fans that are dominated by debris and sheetflow processes. Therefore, for consistency the term DFS is used to encompass the previously mentioned systems, but exclude alluvial fans due to their inherent differences.

DFS exist in a range of climatic and tectonic settings and have been found to have broadly predictable downstream trends, such as a downstream decrease in channel width, floodplain to channel ratio, and sediment grain size (Weissmann *et al*., 2010) (**Figure 1.1**). For example the Bermejo DFS, Argentina, becomes progressively narrower downstream, with an average width in the upstream portion of 2500m and 440m downstream (Weissmann *et al.*, 2015). The Taquari Megafan, that radiates from its apex driven by series of avulsions (Buehler *et al.*, 2011), has an increasing downstream floodplain deposition and presence (Aliyuda and Howell, 2021).

However, DFS can also exhibit different characteristics and trends based on local tectonic and environmental conditions (Hartley et al., 2010; Weissmann et al., 2010). For example, the point at which the fan terminates (the fan toe) can vary across settings, whether the DFS extends into a lake, coast, or playa, or joins an axially draining river within the same basin (Hartley *et al*., 2010). The height at which the fan originates from can also be variable between systems, which can therefore control the stream gradient and thus channel morphology (Hartley *et al*., 2010).

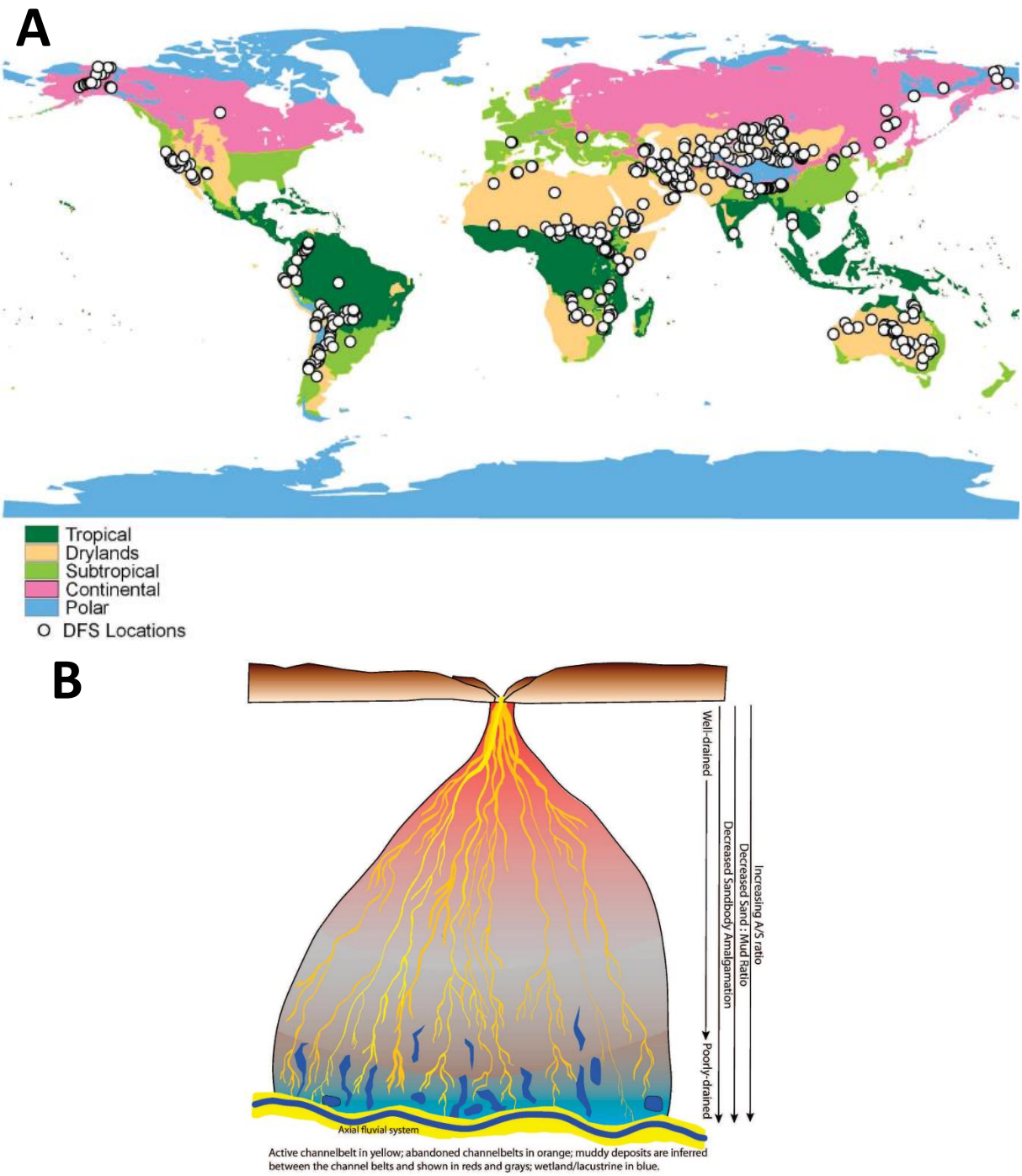

Figure 1.1: A) From Hartley et al. 2010, a map showing the global distribution of DFS and their respective climatic zones. B) Adapted from Weissmann et al 2013, conceptual diagram showing the general downstream trends associated with distributive fluvial systems.

1.2.2 Modern DFS

Controls

Studies by Hartley *et al*. (2010) and Weissmann *et al*. (2010) tested the relationships between the different DFS characteristics to determine the controls on fan development. In general, the main influences on fan development are **climate, tectonics,** and **source lithology**, all at varying levels of

interconnectivity. **Climate** is a primary influence on sediment supply, through its control on discharge and flow regimes (Hartley *et al.*, 2010) and its effect on weathering to generate the sediment supply (Arzani, 2012). The effect of climate can be variable depending on setting. For example, dryland fans, such as those in central Iran (Arzani, 2012; Arzani and Jones, 2018), experience low frequency/high magnitude hydrological events which have the ability to carry large sediment loads and are not inhibited by vegetation which may be present in more tropical climates (Arzani, 2012). Both climate and tectonic activity have a major influence over sedimentation of DFS and other fan systems. However, whilst climatic events provide significant sedimentological signatures in the rock record, they are often overlooked in favour of tectonism as the dominant control (Waters *et al.*, 2010).

The **tectonic** regime present in sedimentary basins impacts the morphology and development of the DFS, primarily through generating accommodation space, allowing the progradation or aggradation of the system (Paola *et al*., 1992; Hartley *et al.*, 2010; Weissmann *et al.*, 2013; Dingle *et al.*, 2016). Tectonics are the primary driver in generating topography, as well as driving incision or aggradation through tectonically driven base level rise or fall (Waters *et al.*, 2010). This is driven through the uplift of the mountain front and the coeval subsidence of the sedimentary basin. This may have an impact on measured DFS characteristics and channel morphology, for example, DFS in tectonically active basins (i.e. high rates of uplift and subsidence) are generally characterised by steep surface gradients and braided planforms. Furthermore, tectonic setting (e.g. foreland basin, cratonic, or extensional *etc.*) influences fluvial characteristics such as length, whereby extensional or piggyback basins are too short and narrow to allow for an extensive channel (Hartley *et al.*, 2010). In addition, tectonics can influence DFS development through the generation of sediment, such as land sliding, or through the uplift and denudation rates relationships.

Finally, **source lithology** is a major control in catchment and fan development (Hartley *et al.*, 2010), where the various physical and chemical properties of the rock influence the sediment flux and sediment grain size (Attal and Lavé, 2006; Arzani, 2012; Quick *et al.*, 2020).

The complexity and interaction of the controls that drive fan development have been studied in detail within numerical and physical modelling, isolating autogenic and allogenic processes, and identifying those that may otherwise be overwritten in the rock record (Clarke, 2015; Mouchené *et al.*, 2017). Numerical studies such as those by Duller *et al.* (2010) and, Heller and Paola (1992) show how factors such as sediment discharge and tectonics have can influence the spatial distribution and fining of sediment in a succession. These models show how autogenic factors, such as sediment flux, may influence a system, with set conditions being used to determine avulsion and channel dynamics (Reitz and Jerolmack, 2012).

Downstream Processes

Recent studies of DFS have shown how these systems display systematic downstream tends from the upstream, near the apex, to the basin-ward downstream regions. Hartley *et al.* (2010) and Weissmann *et al*. (2010) analysed the distribution and characteristics of numerous modern distributive systems and identified a series of trends spanning across all tectonic and climatic settings. It was found that DFS channels decrease in width as they progress downstream, resulting from channel bifurcation and water loss through evapotranspiration and infiltration. This has been commonly observed in DFS located within dryland environments (Kelly and Olsen, 1993; Soares *et al.*, 2018; Priddy and Clarke, 2021) as well as in subtropical environments such the Bermejo River, Argentina (Weissmann *et al*., 2015).

Furthermore, as channels progress downstream, channel morphology can change. For example, a decrease in braiding intensity may occur, or a transition in pattern from braided to meandering. As the proximal zone sediment is generally the coarsest and bedload dominated with the highest discharge rates, multithread, braided and anastomosing channels are more apparent (Nichols and Fisher, 2007; Davidson *et al.*, 2013). Downstream as the system loses energy and larger sediment, channels may become more meandering. This decline in energy may also drive an abrupt shift in grain size – the gravel-sand transition (Dingle *et al.*, 2021), which also impacts downstream channel morphology. Such effects include changes in channel gradient (steep to shallow) and meandering channels downstream of the transition in the more distal reaches (Sinha *et al.*, 2005; Dingle *et al.*, 2020; Dingle *et al*., 2021).

As sediment grain size decreases downstream, geomorphic features such as ponds or abandoned channels may be observed where sediment is finer and less permeable (Davidson *et al*., 2013). Poor drainage in the distal zone leads to the development of wet soils such as Gleysols (Hartley *et al*., 2013), however local climate conditions can also impact soil development. Well-draining coarse sediment in the proximal zone develops soils such as Entisols: permeable but undeveloped due to constant reworking of the channels (Hartley *et al*., 2013).

The effect of the previously described controls on DFS development can change as the system progresses downstream. For example, active faulting on a mountain front can drive incision within the proximal zone, consequentially altering the stream profile and sediment flux downstream (Arzani, 2012). While thought to be primarily base level controlled, downstream distal incision is likely affected by the sediment supply across the fan surface (Arzani, 2012).

Fluvial processes have been observed to change from upstream to downstream along a DFS, including avulsion. Avulsion is the processes under which a channel's flow changes, taking a new course on the fan surface (Slingerland and Smith, 2004), under this new course they may be 'full', maintaining a new course, or 'partial', later re-joining the original parent channel (**Figure 1.2**). The area over which a DFS

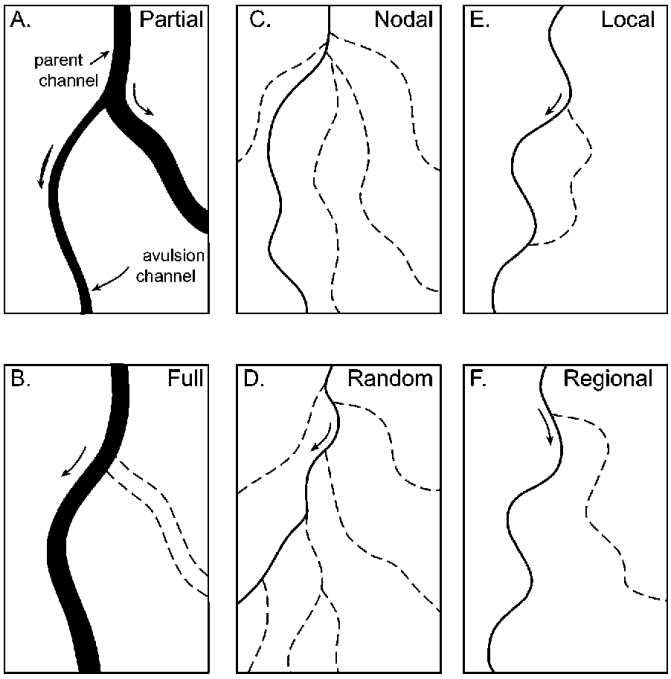

Figure 1.2: Adapted from Slingerland and Smith, 2004, illustrating the various types of avulsion: partial or full (A, B), nodal or random (C, D), and local or regional (E, F).

channel avulsion occurs increases downstream towards the distal zone, as the system becomes

considerably less confined. As a result, the floodplain to channel ratio increases downstream, producing the characteristic conical DFS shape. Therefore successive avulsion events are key in DFS development and the distribution of material across a DFS surface (Warren *et al.*, 2021), as well as the preservation of channel bodies in the rock record. Makaske *et al.* (2012) found that modern avulsion processes varied from the mid fan region to the lower fan. Avulsion within the middle portion is predominantly driven by upstream controls, including sediment supply and discharge: a function of climate and tectonics as previously discussed. High sediment supply and coarse grain sizes in the upstream portion can lead to the superelevation of the channel, triggering avulsion events. Lower stage avulsion was found to be related to sub-lobe progradation of the fan, generating a higher gradient advantage, as well as downstream base level changes. Therefore, lower fan avulsion, at least in the instance of the Taquari Mega Fan, is related to the complex relationship between upstream processes (progradation linked to sediment supply and size) and downstream processes (base level of the floodplain) (Makaske *et al*., 2012). Downstream avulsion may also arise due to low flows, leading to the backfilling and plugging of sediment in the channel, then during periods of high flow, the channels capacity is exceeded causing an avulsion (Hirst, 1991). The nature of avulsion is also thought to change downstream on a DFS. In the proximal zone channel avulsion rate may be highest; high sediment flux due to proximity to the apex driving channel instability for avulsion (Jones and Schumm, 1999; Chakraborty *et al.*, 2010). Here channel patterns may be styled by nodal avulsion, where channels switch from a fixed position, as opposed to random avulsions which can occur at any point along the system (Slingerland and Smith, 2004). An example of this is the Kosi Mega Fan, India (Chakraborty *et al.*, 2010). Channel avulsion changes the system geomorphology where old channels are overlain by floodplain, and floodplains are incised by channels, creating patterns which are preserved in the rock record.

1..3 Ancient DFS

Based on their prevalence in modern aggradational sedimentary basins, DFS are hypothesised to comprise a dominant portion of the rock record within continental sedimentary deposits (Weissmann et al., 2010; 2011). However, there is some controversy over the origin of fluvial sediments in the rock record, including the degree of prominence of DFS. Continental fluvial systems can be divided into distributive (DFS as discussed) and tributary/contributary. Deciding which occupy a larger portion of the sedimentary rock record has proved challenging. Tributary systems are described as rivers within confined settings that show a downstream increase in discharge and channel size (Weissmann *et al*., 2010), made up from a network of tributaries (Weissmann *et al*., 2011). However it has also been argued that tributary rivers in semi-arid environments also decrease in width downstream, and downstream grainsize decrease is common in most rivers whether distributive or contributive (Sambrook Smith *et al.*, 2010). Due to the confined nature of these rivers, the constant reworking over a limited area limits the preservation of potential sand bodies (Weissmann *et al*., 2015). Alternatively, this reworking may account for the large scale amalgamated channel bodies found in the rock record (Fielding *et al*., 2012), suggesting that tributary systems dominate the fluvial rock record. If DFS were to dominate the rock record, smaller channels should be more commonly observed and in higher abundance, as tributary channels have a higher areal extent in modern systems (Fielding *et al.*, 2012). However, DFS size can be difficult to determine in the rock record, thus creating an inconsistency when comparing the size between modern and ancient rivers. Nonetheless, the degradational nature, of which tributary systems are often found within, would suggest that distributary systems likely dominate the fluvial rock record, as the deposits are simply better preserved in aggradational settings (Weissmann *et al.*, 2011), where the preservation space exists for accumulation (Weissmann *et al.*, 2015).

Spatial trends of Ancient DFS

Through field studies (for example, Rittersbacher *et al*., 2014; Owen *et al*., 2015a; Owen *et al.*, 2015b; Wang and Plink-Björklund, 2019; Soares *et al.*, 2021) and virtual outcrop models (Martin *et al.*, 2021), ancient DFS have been broken into three distinct facies domains: **proximal**, **medial** and **distal**; producing varying stacking patterns depending on the systems current state of development and the autocyclic and allocyclic controls occurring at that time (Wang *et al*., 2011; Mouchené *et al.*, 2017; Owen *et al.*, 2017). These domains are described in turn below. The downstream variation in DFS characteristics identified in numerous studies has been summarised in Priddy and Clarke (2021) (**Figure 1.3**), including channel size and abundance, degree of amalgamation, and grain size. The classification of these channel geometries across a basin has been described by Owen *et al.* (2017), defining the geometry and architecture based on the internal structure, including storey presence. Channel geometry and proportion has been seen to change downstream within a DFS, as described below. Overall, as the DFS expands across a wider area downstream, the spacing and separation between channel belts increases (Weissmann *et al.*, 2013), therefore the channel percentage is expected to decrease downstream.

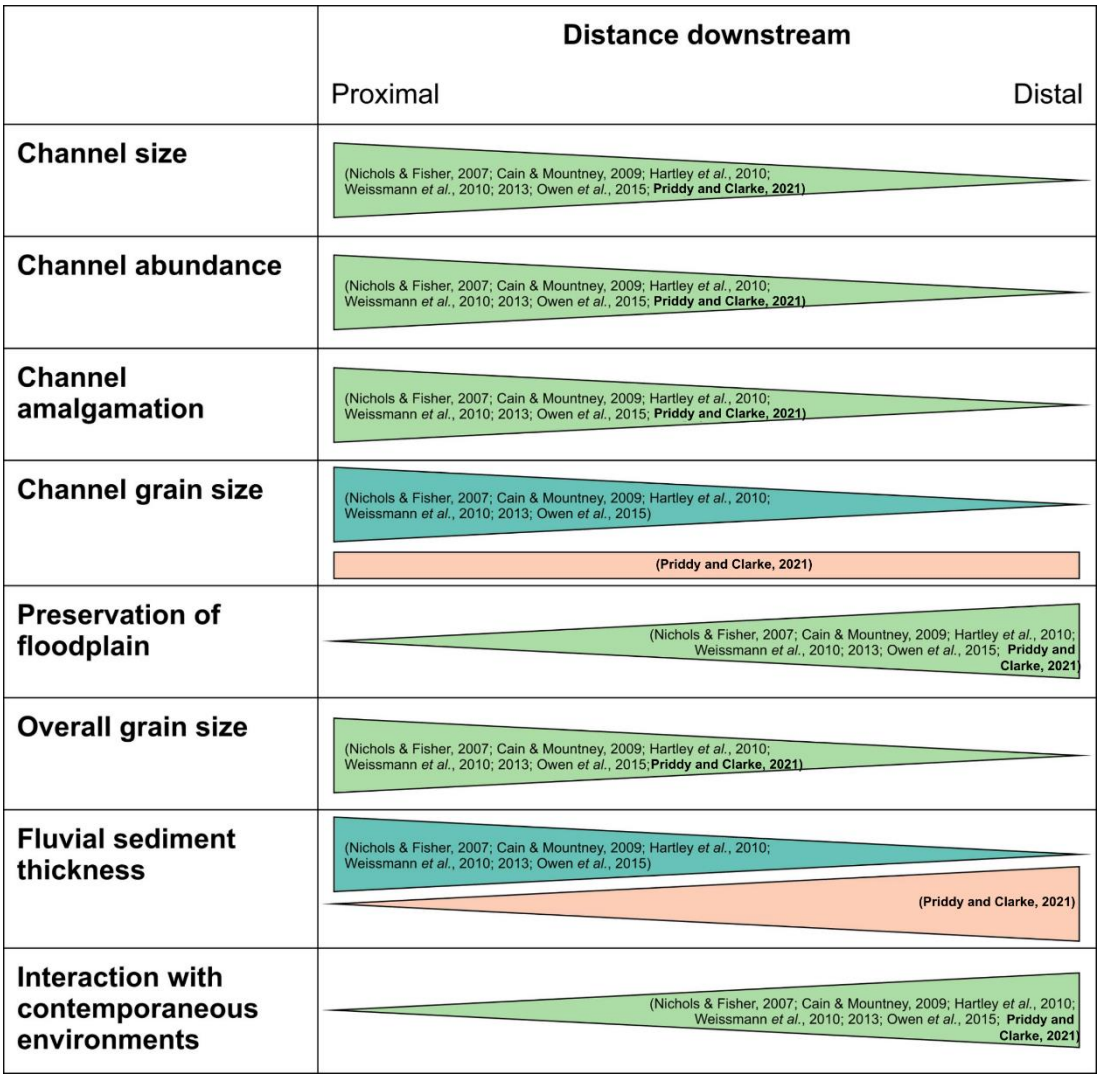

Figure 1.3: Adapted from Priddy and Clarke, 2021, showing the various downstream trends, from proximal to distal, observed in ancient DFS deposits across various studies.

Proximal

The proximal zone abuts the source and apex of the DFS, consisting of coarse grained material where energy has been highest as it exits the confined valley (Weissmann *et al.*, 2013). At this site water infiltration is highest due to the high permeability of the sediment, producing weakly developed soils (Hartley *et al.*, 2013). This zone consists of thick amalgamated sand bodies and is largely devoid of preserved floodplain deposits, due to undergoing frequent reworking and the limited accommodation space (Weissmann *et al.*, 2013, 2015), where channel return frequency is high (Wang and Plink-Björklund, 2019). For example, analysis of the Guará formation, found in the north of the Paraná Basin, Brazil, is inferred to be proximal based on its characteristic massive, amalgamated deposits, within which are numerous erosional bases lined with clasts (Reis *et al.*, 2019).

Channel belt width may be slightly narrower due to the limited area for avulsion as the system only begins to become less confined, also accounting for the constant reworking of the channel (Weissmann *et al.*, 2013). Studies of the Salt Wash DFS, Utah (Owen *et al.*, 2015a) have quantified the extent of this characteristic, indicating the proximal zone consists of the largest channel successions reaching ~170m thickness and consisting predominately of coarse sand (70%). Floodplain deposits within this zone are found to not be laterally extensive (Owen *et al.*, 2017). Similarly, the Sunnyside Delta (Wang and Plink-Björklund, 2019) shows how channel percentages in the proximal zone range from 85 – 100%.

Medial

As with modern DFS, a decrease in channel body size is apparent as the system progresses basin-ward within the rock record where water is gradually removed from the system and channel flow decreases (Weissmann *et al.*, 2013). This produces large scale deposits within which channel bodies are preserved, with distinct sheet-like geometries that are vertically separated by floodplain deposits (Chesley and Leier, 2018; Owen *et al.*, 2018). The channel bodies within the medial zone have been characterised and described as ranging from 'semi-amalgamated' to 'internally amalgamated' to 'offset stacked' with distance from the apex (Owen *et al.*, 2018).

The stacking pattern of facies in a medial succession features an increase in overbank deposits and finer channel fills than the amalgamated pebbly forms found in the proximal zone, including sheet sandstones from crevasse splays among the isolated channel fills (Nichols and Fisher, 2007). Patterns where channel fill deposits appear over these thinner sand sheets are indicative of where the channel avulsion occurs in an area previously held by these splays (Chesley and Leier, 2018). A coarsening upwards stacking pattern is seen from these progradational avulsions (Hajek and Edmonds, 2014). These features seen in the rock record can be linked to modern systems that are only studied from a planform perspective in satellite imagery. Channel fill patterns in the medial zone may be laterally extensive and amalgamated where avulsion occurs over a wider area in this zone (Martin *et al*., 2021), however the full extent of this is difficult to map within the rock record due to limitation of outcrop size and subsurface dataset (i.e. core) extent (Kukulski *et al.*, 2013). The degree of amalgamation of channel deposits is reduced within the medial zone, by 25% seen in some areas, such as the Marilia Formation, Brazil (Führ Dal' Bó *et al.*, 2019).

In studies aiming to quantify the various characteristics of DFS, the medial zone has been found to produce much lateral and vertical variability, particularly within channel storey thickness and channel proportion (Martin *et al.*, 2021). In this instance, channel percentage in the medial zone ranged from 15% to 52%, with some bodies in this zone amalgamated and others distinctly separated by floodplain deposits. Other variable patterns in channel percentage are seen in the Saltwash DFS (30 – 60%) and

the Sunnyside Delta deposits (40 – 70%) (Wang and Plink-Björklund, 2019). The dimensions of channel bodies have been noted to be more varied in the medial reaches of DFS, as identified in flume tank experiments (Terwisscha van Scheltinga *et al.*, 2020). Other studies quantifying DFS architecture note high variability in medial net to gross ratio (Führ Dal' Bó *et al.*, 2019), lateral variability of this nature is also observed at the proximal-medial transition within numerical based studies (Snieder *et al.*, 2021).

Distal

As the distal domain marks the end of the DFS, and the furthest point from the apex, this zone is often devoid of channel deposits, dominated by floodplain facies and few small isolated "ribbon" channels (Weissmann *et al.*, 2015). This is a result of high channel stability, where active channels experience less lateral migration, producing single ribbon channel bodies, as seen in Hirst's (1991) work on the Huesca DFS. Ribbon channels develop where low energy flows cause the channel to be plugged with sediment (Hirst, 1991), often producing homogenous deposits. Linked to the decreasing energy flow that drives the change in channel architecture, fine sand and mud deposits mean the palaeosols found in distal facies are often well developed, analogous with the poorly draining soils seen in modern systems (Hartley *et al.*, 2013). Additionally, many distal deposits and soils are found to interfinger with lacustrine (Hamer *et al.*, 2007) or aeolian deposits (E.g. Guara Formation in Reis *et al.*, 2019) when the DFS toe meets the far reaches of the basin. Alongside small ribbon channels, many channels are likely to be unconfined, producing thin sheet sand deposits, coined as terminal splays (Nichols and Fisher, 2007), driven by the decreasing sediment and discharge flows (Weissmann *et al.*, 2013). Distal channel deposits have been well characterised in the literature, often described as an *isolated channel body geometry* (Owen *et al.*, 2017), with channel body and storey thickness measured less than 4.4 m in some studies, and floodplain deposits dominating this portion of the rock record at >75% of the succession (Huesca DFS, Martin *et al*., 2021), and the proportion of in-channel deposits being 0 - <5% in some distal DFS sites (Hirst, 1991). Similarly, distal channel percentages range from 10 – 30 % in the Sunnyside Delta (Wang and Plink-Björklund, 2019), and 0 – 30% in the Saltwash DFS (Owen *et al*., 2015a).

Vertical trends of Ancient DFS

Rock record focused studies have also recognised vertical trends within DFS sequences, giving insights into how DFS develop through time. These trends can be seen at various scales, from grainsize to basin level. Vertical changes in the rock record are seen through a coarsening up of channel grain size as well as changes in facies tract and channel body stacking (Weissmann *et al.*, 2013; Rittersbacher et al., 2014; Owen et al., 2015b), where facies are stacked accordingly: distal to medial to proximal. Furthermore, sudden and sustained changes in grain size, from sand to gravel, may be indicative of the gravel-sand transition seen in modern Himalayan systems (Dubille and Lavé, 2015), marking an abrupt transition between the proximal and distal zones. Within a succession, there are vertical trends in the stacking patterns of channel and floodplain deposits, particularly the geometry and architecture of these (Gibling, 2006; Van Dijk *et al.*, 2016; Owen *et al.*, 2017). Driven by processes of avulsion, sedimentation rates, and accommodation space, different channel geometries described in Owen *et al*. (2017), from 'massive channel body' to 'offset stacked channel body', is related to the level of channel migration. Furthermore, this trend is also associated with trends in DFS zone, from proximal to medial to distal, which is also associated with the downstream decrease in energy levels and increase in accommodation space.

At a basin wide scale, the coarsening-up and channel stacking trends are indicative of DFS progradation where the fan migrates basin-ward, and, after successive aggradation events, the apex may also migrate basin-ward (Weissmann *et al.*, 2013). The record of progradation may be limited

where accommodation space limits preservation (Owen et al., 2015b). On a local scale, vertical changes in channel patterns arises due to avulsion and lobe progradation and the related controls (Makaske *et al.*, 2012; Owen et al., 2015b; Wang and Plink-Björklund, 2019). In most instances, the vertical and lateral trends follow the same pattern, as observed in the upper Bima Formation (Aliyuda and Howell, 2021). Lateral changes, other than the proximal to distal downstream trends, may arise due to varying degrees of avulsion (Wang and Plink-Björklund, 2019), as well as the lateral distance from the point source (Kukulski *et al.*, 2013). As a result of allocyclic and autocyclic processes concurrently occurring, vertical trends can be complex. The majority of vertical trends in DFS have noted progradational signatures. However, back stepping (retrogradation) has also been noticed in the rock record, as seen where average channel belt thickness decreases up-section (Owen *et al*., 2015b). Retrogradation is thought to be related to the shut down of the fluvial system, linked to changes in climate, or denudation rates in the hinterland impacting sediment supply (Cain and Mountney, 2009).

1.2.4 DFS Zones

In previous work, DFS have been divided into three zones, the proximal, medial and distal. Within the rock record, there are generally distinct characteristics identified within the three zones (e.g. Channel amalgamation, channel body percentage, grainsize *etc*). This has been well established in the rock record literature (e.g. Kelly and Olsen, 1993; Nichols and Fisher, 2007; Cain and Mountney, 2009; Weissmann *et al.*, 2013; Owen *et al*. 2015a). However, in literature focused on modern DFS, the zones are only broadly discussed and identified, where characteristics are less definable in planform across the zones (Davidson *et al*., 2013).

By placing ancient DFS deposits into three distinct zones based on a set of characteristics, several studies have worked to quantify this and provide empirical underpinning to each domain (e.g. Owen et al., 2017; Führ Dal' Bó et al., 2019; Wang and Plink-Björklund, 2019; Martin et al., 2021). It is noted within these studies that there is a degree of variability within the different DFS, and in some cases an overlap in characteristics. This therefore lends to the idea that there is not an abrupt change between zones within the rock record, as with modern systems, transitional phases may be recorded.

While these zones are generally apparent in the rock record they are more difficult to observe in modern systems, as with channels, the downstream trends are much more transitional in nature. In order to understand processes associated with ancient DFS deposits in each zone, it is crucial to to quantitatively study modern DFS to acertain whether the zones can be depicted on modern systems, and how they correlate to the deposits of DFS. Therefore, the first aim of this study leads to devising a method of quantifying the downstream positions of each zone within modern systems,

When exposures allow, identifying whether an outcrop is from the proximal, medial and distal zone can be done with relative ease based on the characteristics observed (e.g. channel grain size, channel: floodplain, degree of channel amalgamation/reworking; Weissmann *et al.*, 2013; Owen *et al.*, 2015). However, how these zones are defined on modern systems has been quite arbitrary within previous studies. For example, in the ancient rock record, the medial zone can be characterised and defined based on distinct facies and associations where stacked sheet like channel deposits sit within, and are separated by, preserved floodplain deposits (as seen in Owen *et al.*, 2015a, 2018; Chesley and Leier, 2018). However, in modern settings, where these systems are studied from a planform perspective, it is much more difficult to define the transition from proximal to medial zones. It is suggested that

channel size and planform changes downstream, therefore the start of the medial zone could be defined based on the processes identified in this zone. Davidson *et al*. (2013) produced a schematic to represent the different geomorphic features in each DFS zone depending on the dominant planform of the channel with the DFS (i.e., braided, or meandering rivers). In this study, Davidson *et al.* does not divide systems exclusively into three zones, often having a fourth zone as an extension of the distal zone, where deposits below the spring line may be hydromorphic in nature and surface water is prevalent. Furthermore, Hartley *et al*. (2013) identified the changes in palaeosols across a DFS relating to the changes in drainage through the system by exploiting the soil's thermal response. Therefore, it could be considered that surface soil type could be mapped and classified to determine DFS zone. However, this method may have much variability as soil type differs based on climatic setting and local hydrological conditions.

Previous studies of modern DFS defined the medial zone where channels become discrete and isolated belts or where reduced channel flow and bifurcation reduces the size of channels (Weissmann *et al.*, 2013; Chesley and Leier, 2018). This may be a defining criterion for marking the medial zone. Another may be channel form; Weissmann *et al.* (2011) discusses how the channels in the medial zone exhibit a meandering morphology, whereas the proximal zone consists of much wider multithread channels. Within the Kosi mega-fan channels, the proximal zone has been described to consist of gravel-sand braided channels, whereas the distal realm exhibits predominantly sandy meandering channels (Singh *et al*., 1993).

1.2.5 Practical Applications

Studying modern and ancient DFS has important implications for resource exploration and management, as well as environment management and remediation. Understanding the dynamic changes throughout these systems can aid in the understanding and modelling of reservoir characteristics with regards hydrocarbon and groundwater exploration (Rittersbacher *et al*., 2014; Führ Dal' Bó *et al.*, 2019), particularly within the proximal and medial zones where porosity and permeability is highest. By quantifying channel architecture within these systems, models on how the spatial distribution and heterogeneity of reservoirs may change across the system can be constructed (Anderson *et al.*, 1999; Van Dijk *et al.*, 2016; Owen *et al.*, 2018). Moreover, as sandstone architecture studies can help inform resource distribution, there are also beneficial implications for its use in carbon capture and hydrogen storage. Predictive numerical based models, such as those by Snieder *et al.* (2021), map the variability of net to gross across DFS where outcrop studies are limited, with large de-risking benefits for subsurface storage of fluids.

Resource exploitation from these systems requires a foundation understanding of the connectivity and fluid flow between the well-draining channel bodies across the proximal, medial and distal zones (Anderson *et al.*, 1999). Fluid flow in DFS is enabled by the high permeability and porosity of the sandstone channels; this was studied by Owen *et al.* (2016) in which the distribution of uranium deposits served as a proxy to map subsurface fluid flow across the system. This study also notes the benefits of DFS for mineral resource exploration. In an environmental management and sustainability context channel connectivity also has important implications. For example, by understanding the geological and geomorphic components of DFS, aquifer quality and pollution can be mapped, such as the arsenic contaminated stores on the Ganga Plain, India (Shah, 2008); as a result, reservoir quality can be predicted across a region, as well as find the source of the contaminant based on the distribution, as Owen *et al*. (2016) found.

Chapter 2: Methodology

This chapter describes the various methods used in this study, split into two parts. The first part outlines how the medial zone is defined in distributive fluvial systems, based on established criteria and parameters. Part two focuses on the methods used to characterise and quantify medial zone channels. Each part of the methods corresponds to the respective aims and objects listed in Chapter 1.

2.1 Defining the medial zone

As discussed in Chapter 1, no definitive definition as to what constitutes the boundary between proximal and medial, and medial and distal zones is present within the current literature base for modern systems. As this study concentrates on the medial zone of a DFS it is imperative that the boundary of this zone is defined.

The medial zone in modern distributive fluvial systems can be difficult to constrain as there are not necessarily clear transitional zones on the fan surface between the proximal to medial, and medial to distal, as there are in the rock record. Considering this, criteria were tested and established against a sample of DFS, covering various climatic settings (dryland, polar and tropical), to identify any trends that may indicate transitional phases between each DFS zone.

2.1.1 Criteria

The criteria used in defining the medial zone of distributive fluvial systems included:

1. **Active channel width (ACW)**

   As a defining characteristic of DFS is the downstream decrease in discharge due to infiltration and evapotranspiration (Weissmann *et al.*, 2010). Measuring active channel width can identify if these systems follow a similar downstream trend. This metric also identifies whether there are any patterns that may indicate a transition of zone. For example, the DFS transitions into the distal zone where the channels become absent.

2. **Channel belt width (CBW)**

   Modern channel belts in this study refers to the planform extent of channel morphology, including scroll and point bars from previous channel flow, bounded by floodplain/overbank deposits. This is measured in conjunction with active channel width. Channel belt width is expected to follow a similar downstream decrease, particularly where large belts are indicative of reworking and amalgamation of deposits, characteristic of the proximal zone, becoming narrower downstream in the distal. Channel belt in this context refers to the 'active' channel belt, where channel migration (of the active channel where water currently flows) has recently occurred. A major limitation of analysing modern channel belts is the true lateral extent of past channel migration being obstructed in satellite imagery by subsequently deposited overbank material and vegetation within some environments.

3. **Bifurcation**

   Bifurcation, often arising where instability, driven by changes in discharge or sediment supply (Slingerland and Smith, 2004), causes the division of sediment and water downstream (Sassi *et al.*, 2012). This could be considered one of the characteristics of distributive fluvial systems, often responsible for generating the classic radial fan morphology associated with these systems, and a cause in the downstream trend in channel width and flow (Hartley *et al.*, 2010; Weissmann *et al.*, 2010).

4. **Braided to meandering transition**

This piece of criteria for defining the medial may be more arbitrary, where some DFS systems may be entirely braided throughout, an example being Alaska's Canning River DFS (Davidson *et al.*, 2013). However, a change in channel morphology from braided to meandering, related to downstream decreases in sediment and water discharge, may be indicative of the proximal-medial transition. This pattern is coincident with the **gravel-sand transition (6)** and changes in **channel elevation (7)**, which are also considered here. The gravel-sand transition is inferred based on elevation change and channel type based on the characteristics seen in Dingle *et al.*, (2020) and Dingle *et al*. (2021).

Channels comprised of a single thread and high sinuosity are generally characterised as meandering rivers, whereas braided systems are defined by multiple channel threads separated by distinct gravel bars, typically characterised by steep slopes and straight channels. However, many braided systems may exhibit high sinuosity in the form of anastomosing channels. Furthermore, many channels may rather be classed as wandering (Buffington and Montgomery, 2022), a transitional form between meandering and braided.

Within the context of this study, the terms meandering and braided are used in reference to systems comprised of single channels exhibiting sinuosity, and multi-threaded channels characterised by a generally straight planform, thus, the terms meandering and single thread, and braided and multithreaded are used interchangeably. These two morphological characterisations are general indicators of sediment dynamics. For example, where a straight, multithreaded, braided system is characteristic of high discharge and high sediment concentrations, which have an inherent effect on DFS planform including bifurcation and channel slope gradient.

5. Channel belt and active channel ratio

Wider channel belts are a consequence of higher rates of lateral migration and migration. Where increased channel mobility is a product of high sediment flux and discharge (Wickert *et al.*, 2013). Energy levels, sediment and water supply are all highest nearer the proximal zone of DFS (based on close proximity to the source at the apex), generating wider channel belts. The ratio between the active channel and channel belt may determine how mobile channels are. Where this ratio is low (close to 0), a wide channel belt surrounding the active river where lateral migration is high is assumed. Where this value is 1, channel belts width equals the active channel width, implying less lateral migration of the river to deposit the channel belt deposits. In the distal zone, lateral migration is expected to decrease where sediment and water discharge decrease. Channel deposits are less likely to have lateral accretion sets and exhibit a ribbon morphology, corresponding with an equal channel belt and active channel width. Therefore, the proximal can be constrained by low values and the distal high.

2.1.2 Methods used for Medial Constraint

Sentinel-2 satellite imagery and Shuttle Radar Topography Mission (SRTM) digital elevation models were used within Google Earth Engine code editor for quick access to cloud-free static imagery at a 10 m resolution for multiple DFS, as well as to construct detailed elevation profiles. Intervals of 5% of the

active channel were marked for the downstream measurements. In the instance of the Alaskan DFS. The ALOS 30 m DEM was used where SRTM was unavailable.

Active Channel Width

Active channel width (ACW) measurements are collected in 5% downstream intervals, delineated by digitising across the active channel, perpendicular to the channel centreline, seen in **Figure 2.1**.

In this study, the active channel width is defined as the measure between the permanent margins of the river, often marked by the presence of permanent vegetation. While more easily observed in single thread systems, the active channel for braided systems is defined based on the active braid plain (Warburton, 1996; Kidová *et al.*, 2017), where during bank-full conditions, features such as mid-channel bars become inundated. Considering imagery of high discharge and bank-full conditions is used for better channel observation and analysis, defining the active channel this way is more suitable and reduces the complexity that individual active channels in a braided system cause. Moreover, it aids when considering that in some of the climates studied, flashy-flood, high discharge events are the primary drivers of channel planform change (Tooth, 2000).

Channel Belt Width

Similarly, to active channel width, channel belt width was measured in regular (5%) intervals downstream from apex to toe, to observe any downstream decreases that may indicate changes between DFS zones. Rivers migrating laterally leave the deposits of the previous channel position, which through time become amalgamated to form a channel belt as the river shifts and reworks deposits associated with the river channel (Dong and Goudge, 2022). These deposits are recognized in the rock record and classified as channel bodies (Gibling, 2006). The margins of these can be identified in satellite imagery where features such as point bars meet the floodplain, often with less dense and younger vegetation.

However, channel body/ belt width in the rock record can be difficult to determine due to limitations in outcrop extent. Many have attempted to link the depth of these preserved bodies to width, through the use of conversion equations (Hirst, 1991), and calculating width based on flow and cross set characteristics (Flint and Bryant, 1993; Bridge and Tye, 2000; Kukulski *et al.*, 2013; Hayden *et al.*, 2019). Channel belt widths in modern systems can help ascertain the possible widths of these deposits across difference systems (including size, climate etc.). However, outlining the channel belt in modern systems with satellite imagery also has its limitations, driven primarily by climate. For instance, in heavily vegetated systems, the full extent of the channel belt may be obstructed by vegetation coverage, and thus difficult to identify. Furthermore, as discussed above, channel belt width in this study refers to the 'active' channel belt, the area over which the channel has recently migrated.

Other quantitative methods to be considered.

The quantitative parameters to constrain the medial zone are by no means exhaustive; beyond the scope of this study, other methods may be also adopted. These may include the sinuosity index (the ratio of the length of a reach of a river to the length of a meander belt axis), used to measure downstream changes in channel mobility (Brice, 1964; Friend and Sinha, 1993), which has been utilised in other studies measuring downstream DFS trends (Weissmann *et al.*, 2015). Furthermore, other metrics such as curvature (Ahmed *et al*., 2019; Hayden *et al*., 2021), braiding index (Friend and Sinha, 1993; Egozi and Ashmore, 2008), and measuring long term channel migration rates, are but a few methods that may be useful in constraining each DFS zone.

Qualitative approaches

More qualitive approaches have been used in order to constrain the medial zone, this includes looking at where bifurcation and channel morphology occur downstream. Channel morphology in itself has been qualitatively categorised into 'braided'/'multi-thread' and 'meandering'/'single thread', and in some instances a transitional area between these two types is outlined.

2.2 Methods for Medial Variation

Once the medial zone in modern DFS has been constrained using the selected criteria, more detailed measurements within this zone can be taken with the aim of understanding variation within the zone itself. The DFS chosen for the previous stage of this study have continued to be used with the exception of the third dryland DFS – AF01_DRY. In this system the channel scale is much too small to be able to take detailed measurements within the medial zone, as opposed to the whole system measurements utilized to define the boundaries between the different zones on a DFS, despite the use of high resolution 3 m imagery from Planet Imagery.

To determine this variation, the following measurements have taken place at intervals every 5% downstream of the active channel, from the midpoint of the proximal – medial zone to the midpoint of the medial - distal. Intervals for measurements were set at every 5% of the distance downstream; this spacing provides enough detail to observe downstream geomorphic change, while remaining within the constraints of the project, which smaller or continuous intervals would exceed. In some instances, where multiple channels are active, measurements from additional channels were taken to further observe channel characteristics across the DFS surface and provide more detail to aid in the understanding of medial variability. These intervals were obtained through digitising the active

channel centreline, based on the centre point between the outer banks. The produced shapefile was then split every 5% through the *Generate points along line* tool in ArcGIS Pro.

2.2.1 Imagery

Landsat 8 and Sentinel 2 imagery were used to provide a static image to measure the stated parameters at a resolution of 15 m or 10 m respectively; both Sentinel and Landsat are readily

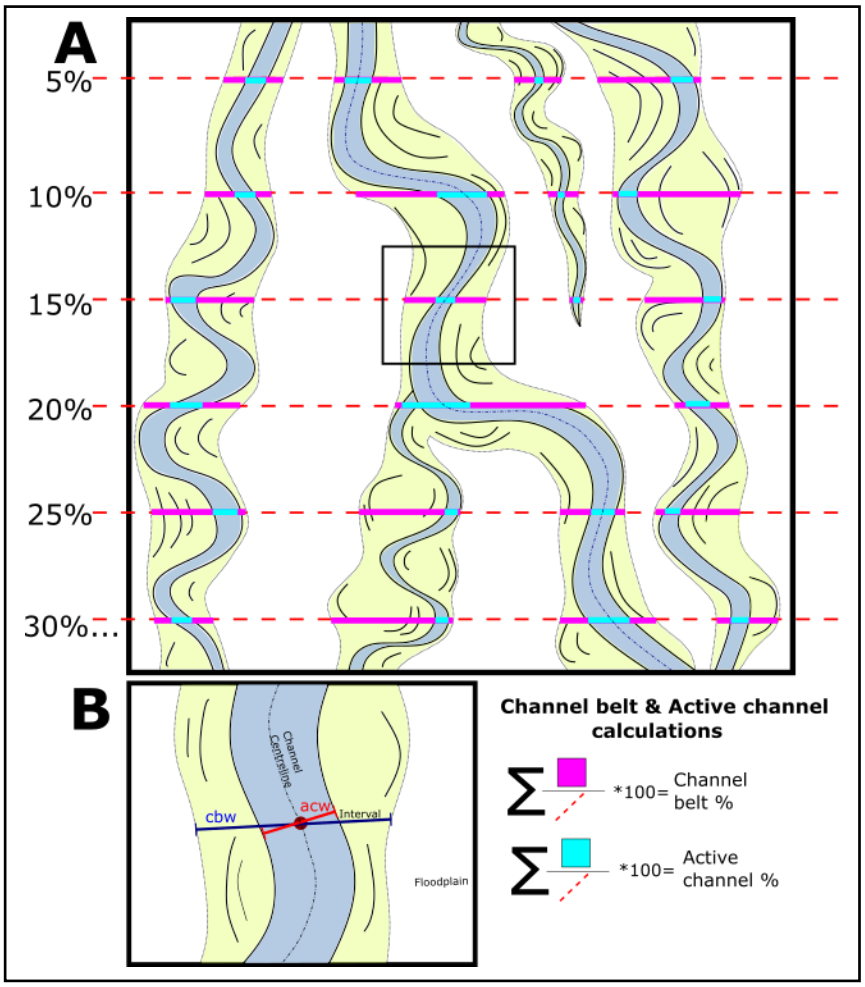

Figure 2.1: Schematic image illustrating how measurements were made. A shows the process of collecting the proportion of active channel and channel belt across a transect extending across the medial zone at intervals of every 5% downstream. B indicates how active channel width (ACW) and channel belt width (CBW) of the active channel are measured.

available at a suitable enough resolution for identifying geomorphic change, providing year-round multispectral tiles. RGB and false colour composites were constructed enabling the differentiation between channel and vegetation for some environments such as the drylands, the band combinations used for image visualisation are described below in **Table 1**. Sentinel 2 imagery was used for the majority of the systems studied due to its slightly higher resolution, with the exception of AR01_TROP and CH01_DRY where Landsat provided more suitable imagery in those instances, in terms of cloud cover and clarity in identifying active channels.

Tiles were selected and filtered based on a cloud percentage of 0% and dated during the wet season and time of high river discharge for each area. Higher discharge means channels are more visible through satellite imagery for analysis, especially important for systems where channels are ephemeral.

The processing and production of composite satellite images tool place in ArcGIS Pro.

LS 8 Band Combination	Sentinel 2 Band Combination	Composite Output
4 3 2	4 3 2	True Colour Image
5 4 3	8 4 3	Colour IR Vegetation
5 6 4	8 11 4	Land/Water

Table 2.1: Landsat 8 and Sentinel 2 band combinations used to process imagery, including true and false colour images

2.2.2 Active Channel Width (ACW) & Channel Belt Width (CBW)

As decreasing downstream active channel width, and channel belt width, are some of the characteristics that define distributive fluvial systems (Davidson *et al.*, 2013; Weissmann *et al.*, 2013), and used in constraining the medial zone, it can be beneficial to measure these in more detail within the medial zone, testing to see if these parameter vary within the medial zone across different systems, and to what extent. Therefore, using the same method described in section 2.1, the active channel and channel belt widths were measured every 5% downstream from the start to end of the medial zone (proximal – medial, medial – distal) of the dominant active channels in each system.

2.2.3 ACW/CBW

The **ratio of active channel belt to channel belt width** may help determine the degree of lateral migration downstream. Where active channel/ belt values are 1, the two parameter's widths are equal. This assumes that the active channel undergoes less lateral migration, creating narrower belts, related to a change in energy levels and bank stability, or that the channel interacts more with the belt area, in the case of braided channels (Dong and Goudge, 2022). Within the rock record, these narrow belts would exist as ribbon channel deposits, where lateral migration is minimal (Nichols *et al.*, 2012). The level of connectivity between channels as a result of this ratio can potentially be inferred; where the ratio is high, connectivity between sand bodies is likely to be low.

2.2.4 Active Channel : Channel Belt : Overbank

Channel belt Proportion

The channel belts across the medial zone were digitised within ArcGIS Pro. Similarly to the active channel, the proportion of the channel belt for each transect was measured and use to calculate a percentage. Studies quantifying ancient DFS deposits have looked at the proportion of channel deposits within a succession (e.g. Hirst, 1991; Owen *et al.*, 2018; Wang and Plink-Björklund, 2019; Martin *et al.*, 2021; Priddy and Clarke, 2021), where the system exhibits a higher percentage in the proximal region and decreasing downstream. Variability of this parameter has been noted in other studies e.g. Martin *et al.* (2021), where low percentages characteristic of the distal zone have been observed in medial deposits, particularly those closer to the proximal zone. By measuring this characteristic in a modern setting, the causes of variability can be visualised and quantified across other systems, generating a "snapshot" of what various medial rock record deposits may have once looked like.

Active Channel Proportion

Manual Approach

As active channel width is known to decrease downstream, and the proportion of overbank to increase as the system radiates out, it can be interesting to see how the proportion of active channel varies across the medial zone and different systems. This analysis provides insight into the proportion of the medial zone that is active. Therefore, by constructing cross-sectional transects across the medial at each 5% interval, the proportion of active channel and overbank on the surface can be established. Through comparison with the proportion of surface channel belt and overbank deposits, the composition of modern medial DFS surfaces and variation between different systems may be understood.

Assessing this characteristic was achieved by digitising the proportion of active channel and over bank (see **Figure 2.1)** across each transect. Per each interval, the percentage of active channel across the medial surface was calculated.

Automated Approach

The manual approach described above relies on individual interpretation of where the wetted active channels are, however, an automated approach to calculate active channel percentage was also used to find the proportion of channels to overbank across each transect. This uses the Modified Normalised Difference Water Index (MNDWI), with the work process illustrated in **Figure 2.2**. MNDWI was chosen instead of NDWI, or other indices, based on its ability to pick out open water features much more clearly (Singh *et al.*, 2015; Pereira *et al.*, 2022). When the MDWI value across the transect is plotted (Shown in **Figure 2.2**), clear peaks are present, delineating present active channels. This method has potential for quick large scale data collection, and thus holds potential as an effective tool for collecting a large data set to analyse medial variation.

In order to extract these percentages, a sample of 1000 points has been taken from the MNDWI raster, before being input into R Studio and Spyder (Python) for plotting and analysis. Using a topographic prominence approach (Llobera, 2001), peaks, indicative of wet channel, were identified. This then enabled the extraction of the peak widths, preceding a calculation of the percentage of the peaks across the transect. The resulting values were then plotted against manually collected measurements for validation. **Table 2.2 and Figure 2.4** show a comparison of the manually and automatically collected channel percentages, indicating a strongly positive correlation. Plotted based on data where automatic % = manual % (y=x), the trend line allows for visual comparison on how well the automatically extracted data reflects the manually collected, where the primary limitation is image resolution.

Comparison between the manually collected data and automated data does however show the limitations in its capacity to produce accurate results. Primarily, the automated approach is limited by climatic setting, relying on imagery from regions where vegetation is sparse, but water discharge is high (flood events or wet seasons of dryland regions). For example, CH01_DRY, CH02_DRY, and AL01_POL provide optimum conditions where channels can be clearly identified from the MNDWI rasters and plots, as well as potentially providing information for the presence of palaeochannels. However, tropical site such as AR01_TROP and AL02_TROP have too much vegetation interfering with the moisture index to be able to identify clear channels to extract from plotted peaks. Thus, this creates too much “noise” in identifying active channels across the transect.

Other limitations fall on the sensitivity of the R script, particularly the variables ‘w’ and ‘span’ that extracts the percentages from the peaks. These variables determine the ‘smoothness’ of the plots, with changes in these parameters altering the outcome of the percentages, based on if background noise is picked up. Consistent sensitivity needs to be determined across each DFS, however in some instances, sensitivity is too high where minor peaks that do not constitute as a channel are extracted, or too low through too much smoothing that prominent channels and their peaks are disregarded. After testing this methodology, it is apparent that it is not guaranteed that what may be extracted as a channel is actually a channel, therefore it is not utilized within this study.

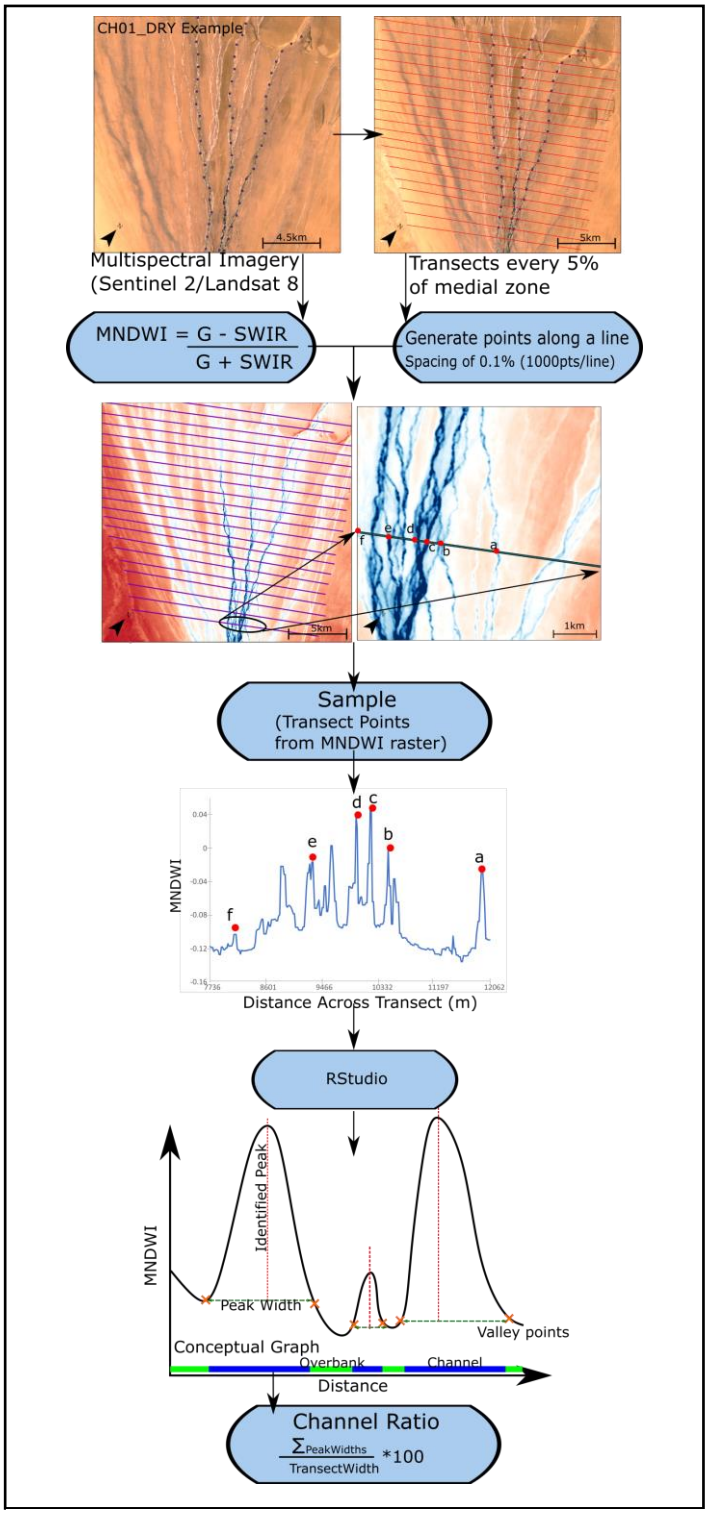

Figure 2.2: Flowchart illustrating the process to automatically extract the percentage of active channel across a measured transect using Modified Normalised Difference Water Index (MNDWI) and analysis in R Studio with a topographic prominence approach.

Downstream Interval (%)	AL01_POL		CH01_DRY		CH02_DRY	
	Manual	*Automatic*	*Manual*	*Automatic*	*Manual*	*Automatic*
0	71.3	51.65	26.8	25.4	10.1	12.69
5	67.6	68.93	28.3	29.6	6.8	9.59
10	61.5	47.35	24.3	25.4	4.8	9.99
15	64.0	46.25	23.9	26.0	4.8	9.39
20	53.3	37.06	26.1	22.0	5.0	8.59
25	47.9	43.16	25.1	24.6	6.2	9.19
30	48.7	37.96	27.1	20.8	3.7	7.29
35	49.4	43.56	29.6	27.3	3.8	7.09
40	49.8	41.46	25.0	25.9	3.8	6.59
45	45.1	37.26	30.5	22.7	3.9	6.49
50	39.9	-	22.2	22.5	4.7	5.89
55	41.0	41.96	25.8	20.8	2.6	6.29
60	34.4	44.76	21.2	21.3	2.9	4.50
65	40.2	-	22.6	22.9	3.1	6.19
70	33.8	35.66	26.3	19.8	2.6	5.39
75	31.1	-	22.3	24.2	2.9	6.99
80	33.7	37.06	19.4	21.9	2.1	5.00
85	32.4	35.66	23.8	20.2	2.1	7.39
90	27.8	36.36	24.3	23.7	2.9	4.90
95	27.5	38.36	16.5	26.8	2.6	6.29
100	27.5	44.16	15.7	21.7	3.3	6.29

Table 2.2: A comparison of the manually and automatically extracted active channel percentage for each of the three systems, where this process was viable. Missing data values for automatic AL01_POL are due to errors that arise in RStudio script.

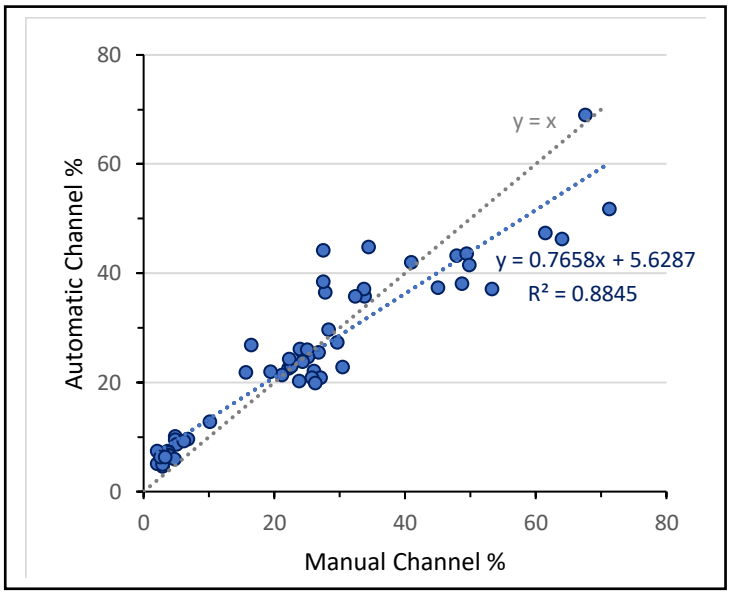

Figure 2.3: Manual channel % against Automatic channel %. Grey trendline (y=x) shows the hypothetical relationship if the automatically collected data was identical to the manually collected, allowing to visually see how well the actual data fits the model. Other line refers to the actual linear regression of the data, annotated with the line equation.

2.2.5 Sweep Angle (SA)

The shape of a DFS may vary between systems, as well as impact the observed trends within a system. Therefore, by measuring sweep angle, the angle between the outermost points of a fan (Viseras *et al.*, 2003), at different points downstream. This can be utilised to see how sweep angle varies within and between systems, and therefore the impact of DFS shape on the measured DFS characteristics. Sweep angle has been measured at four points downstream for each system: near apex, start of medial zone, end of the medial zone, and at the toe. As DFS are often characterised by radiating basin ward from the apex, it is expected that sweep angle will increase downstream. However, deviation from this trend suggests that the DFS is more confined, impacted by external factors.

2.2.6 Factors of Variability

Relative Vegetation

The Normalised Difference Vegetation Index is a robust measure of vegetation change detection using the red and near infrared bands in multispectral satellite imagery (Bajocco *et al.*, 2012; Fu and Burgher, 2015). On a scale of -1 to 1, the relative vegetation of an area can be determined per pixel, with values below 0 indicating no vegetation or a loss, and values closest to 1 indicating high vegetation coverage. Across the medial, the NDVI pixel value can be averaged and used as general quantitative proxy for assessing the extent of vegetation coverage. Vegetation coverage has an influence on channel morphology, with channels in vegetated areas expected to migrate less due to increased channel stability (Wickert *et al.*, 2013). Therefore, dryland areas, absent in vegetation, would expect wider channel belts. It should be considered that the mean NDVI value for the whole medial zone is not wholly representative of vegetation coverage across the entire medial zone (Fu and Burgher, 2015), due to differences between channel margins or by the presence of agricultural land. However, the mean NDVI value acts as a good indication of the level of vegetation when comparing between different systems and climates.

Furthermore, vegetation may help quantify the climate of the DFS, as a proxy for precipitation. For example, dryland environments characterised by low precipitation are likely to have sparse vegetation coverage, and alternatively, tropical environments may be characterised by consistent precipitation enabling the coverage of dense vegetation. In this respect, vegetation coverage as a climate indicator is very generalised, when in reality, plant functional types are a more accurately reflect climate. Beyond the scope of this study, plant functional types are useful indicator of climate, whereby vegetation is categorised based on its physiological response to an environment, with remote sensing techniques being used to globally classify vegetation properties linked to climate (Ustin and Gamon, 2010). However, within the context of this study, a broad indicator of using NDVI to detect vegetation cover as a proxy for banks stability is suitable.

Catchment Area

Catchment area feeding the DFS has been extracted from HydroSHED's HydroBASIN (Lehner and Grill, 2013) data and used as a proxy for discharge entering each system, where larger catchment areas would expect to have higher discharge rates, and therefore produce wider channels. Comparing each system by catchment area can help identify if over-riding factors (other factors influencing sediment flux such as source rock lithology, climate etc.) cause variability in the medial zone.

2.2.7 Statistical Testing

The degree of variability observed in the medial zone for the studied distributive fluvial systems will be established within each system (downstream trends) and between the systems using the normalised widths and statistical testing.

Within Systems

While variations may be evident between DFS, downstream trends within the medial are also important to consider. As established previously, DFS are characterised by downstream decreases in the measured parameters from the proximal zone to the distal; detailed measurements of the medial zone may illustrate how much this varies within the system. To test this downstream relationship, Spearman's Rank correlation coefficient was used (R_s and P value), utilising a non-parametric test where the data does not require a normal distribution (Myers and Sirois, 2006). A linear regression trendline and R-squared value have also been used to gauge the significance of the downstream model. Finally, the coefficient of variance (CV) used as a measure of dispersion within the data, normalising the standard deviation.

Between Systems

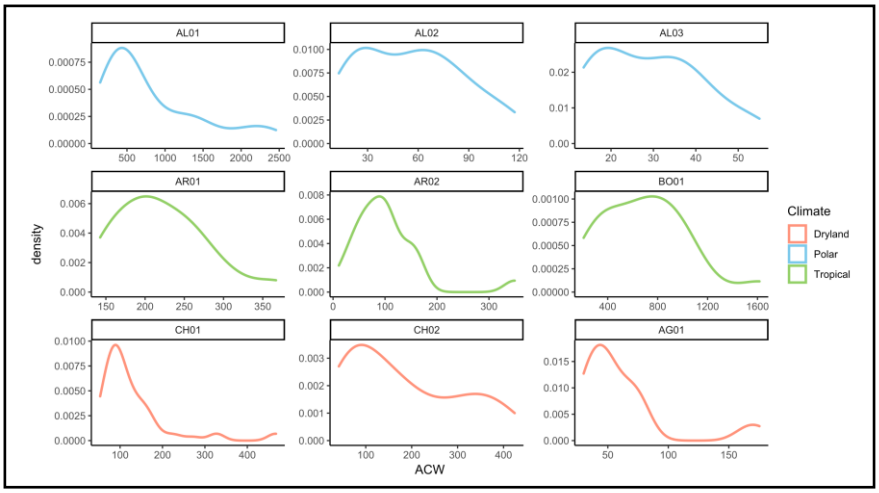

Figure 2.4: Distribution curves for active channel width (ACW) in metres, for each of the 9 measured medial DFS sites. Curves show that the data is not normal, skewing to the left.

Due to a range of climatic settings, catchment sizes, vegetation coverage, variability between the systems is expected. Quantifying and understanding the variability between the systems was undertaken using the non-parametric Kruskal-Wallis Test, the alternative to the normal distribution one-way ANOVA (McKight and Najab, 2010; Hecke, 2012). This is necessary as the data collected is not normally distributed, skewing to the left, as shown in **Figure 2.4**. If a statistically significant result (P value < 0.05) was identified in the Kruskal-Wallis test, a pairwise Wilcoxon test (Wilcoxon, 1945) was performed identifying DFS pairs that have a statistically significant difference or not.

Kruskal-Wallis Hypotheses:

H_1 (alternative hypothesis): If $p < 0.05$ mean ranks between each group (e.g. individual DFS, climate group) are statistically different and not all equal.

H_0 (null hypothesis): If $p > 0.05$ the mean ranks between each group are equal and therefore there is **no** statistically significant difference between the data groups.

Wilcoxon Hypotheses:

H_1 (alternative hypothesis): If $p < 0.05$ the medians between the tested pair statistically differ and are not equal

H_0 (null hypothesis): if $p > 0.05$, the medians between the tested pair are equal and have no statistical difference.

Other trends between the systems have been analysed, based on other factors including catchments size and relative vegetation coverage, again using Spearman's Rank Correlation Coefficient to outline any patterns.

2.2.8 Data Normalisation

Between each of the systems in this study, the magnitude of catchment area, river length, among other features, vary considerably. Strahler (1957) discussed the importance of dimensionless numbers, such as a ratio, when comparing systems of different scales, particularly those that are dynamically and geometrically similar (Strahler, 1968). Accounting for the size differences of each system, the width measurements taken (channel belt width and active channel width) were normalised to create dimensionless values for statistical comparison:

$$\frac{ACW_x}{ACW_{max}} = aW^*$$

$$\frac{CBW_x}{CBW_{max}} = cW^*$$

Where aW* is the normalised active channel width (ACW), and cW* is the normalised channel belt width (CBW). *X* and *max* refers to a singular width measurement in the dataset, and the maximum width of the dataset respectively.

By dividing by the maximum measurement, a 0 to 1 scale ratio is created without excluding or squashing outliers, which when measuring variability within and between systems is important to consider. Normalised values of 1 are indicative of the widest measurement of each system, and 0 the smallest.

Despite the importance of dimensionless and normalised data, absolute values were also plotted and statistically tested. While each system varied in size, which can have an effect on channel size based on relative discharge, the absolute widths of the active channel and channel belt should be considered when quantifying variation in such parameters across various DFS. Comparing the absolute and normalised will further show if catchment size truly has an impact on widths for the study areas. Furthermore, statistical testing of this data can determine if absolute channel widths significantly differ between systems.

2.3 Study Area

2.3.1 Site Selection Methods

In choosing suitable DFS study areas, the database provided by Hartley *et al*., (2010) was reviewed and filtered using pivot tables to find sites that covered a range of climatic settings, within the temporal constraints of the project. These include basin climates of polar, tropical, and dryland – chosen because variability may arise based on the precipitation/channel discharge and vegetation coverage associated with each climatic zone. Furthermore, while climatic zone differed, tectonic setting for each system were kept the same (foreland basins). This was to limit the number of external factors that may drive variation in these systems and avoid creating overly complex comparisons.

In constraining the medial zone, a sample of nine systems were chosen (three for each climatic zone). However upon further study, two of these sites were deemed unsuitable (within tropical and polar climates), as before the system can naturally run through to the distal zones, they are truncated by axially draining rivers. Therefore, certain axial river terminations were avoided. In some cases, such as the Bermejo (AR01_TROP), the channels run through the distal zone extensively before terminating at the axial river. This allowed for identifying and constraining the full extent of each DFS zone.

To expand the data set, a further three DFS were selected upon measuring the medial zone in detail and the removal of AF01_DRY (a dryland site that provided hosted imagery with a resolution too low for analysis). These extra sites were chosen through the previously described selection process, with the medial zone defined based on common geomorphic elements and characteristics found in the DFS used for medial constraint. **Figure 2.5** shows a map indicating the global positions of the systems studied.

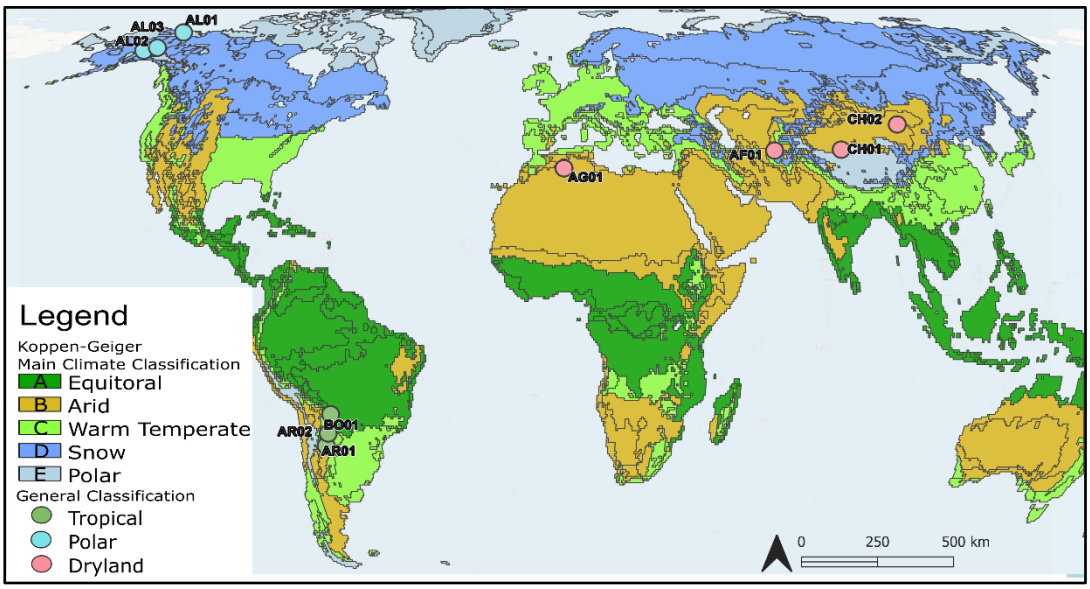

Figure 2.5: Map illustrating the geographic locations of each of the studied systems, with the first two characters indicating the region (e.g. AL = Alaska, USA). Koppen-Geiger Climate Classification as been applied using the Main Climate Class (A-E). In the context of this study, a more general classification of tropical, dryland and polar are used.

2.3.1.2 *Study Site Nomenclature*

Each induvial DFS in this study has assigned a code for ease of reference, using the first two characters of the country/region the DFS is situated (avoiding duplications), a number separating where DFS are in the same locality, and an abbreviation referring to the climatic setting. Where 'TROP', 'DRY', and 'POL' refer to tropical, dryland, and polar climates respectively.

E.g. AR01_TROP = Argentina, 1st Argentinian DFS studied, Tropical setting

This is provided in the table below, alongside other information about each system and summary percentages of the results discussed below.

2.3.2 Study site Information

The following tables provide summary information for the sites used in constraining the medial zone, as well as the extra three DFS included for measuring the medial zone in more detail, as well as how each system is named with respect to location and climate.

DFS	Climate catchment	Climate Basin	Tectonic Setting	Location	Location coordinates	Channel Planform	Total Channel length (km)	Apex – Toe Distance (km)	Catchment area (km^2)	Medial Channel length (km)	Termination Type	River Name	References
AF01_DRY	Dryland	Dryland	Foreland	Afghanistan	36.706, 64.907	Meandering	73	54	12872	29	Into dune field	Andkhui	Lehner and Grill, 2013; Hartley et al., 2010
AL01_POL	Polar	Polar	Foreland	Alaska, USA	69.851, -146.461	Braided, bifurcating	49	37	4724	18	Into ocean	Canning	Lehner and Grill, 2013; Hartley et al., 2010
AL02_POL	Polar/ Continental	Polar/ Continental	Foreland	Alaska, USA	62.749, -152.993	Braided to single meandering	37	31	99	9	Becomes contributary then runs into axial river after a while	Little Tonzona	Lehner and Grill, 2013; Hartley et al., 2010
AR01_TROP	Polar/ Subtropical	Tropical	Foreland	Argentina	-23.293, -64.074	Braided to meandering	1256	704	34316	505	Axial River	Bermejo	Lehner and Grill, 2013; Hartley et al., 2010
AR02_TROP	Subtropical	Tropical	Foreland	Argentina	-22.208, -63.612	Braided to single thread	122	97	2974.4	1343	Becomes somewhat unconfined, running as a tributary of the Bermejo	Itiyuri	Lehner and Grill, 2013; Hartley et al., 2010
CH01_DRY	Polar/ dryland	Dryland	Foreland	China	37.249, 84.417	Braided, bifurcating	44	53	2410	20	Into dune field with one channel continuing on	Unnamed	Lehner and Grill, 2013; Hartley et al., 2010
CH02_DRY	Dryland	Dryland	Foreland	China	40.996, 100.272	Braided	178	165	22103	83	Into desert	Ruo Shui	Lehner and Grill, 2013; Hartley et al., 2010

Table 2.3: Summary information for each DFS site used in constraining the medial zone and/or measuring variation within the proposed medial zone. Location and climate basin used in the naming process for each DFS to be referred to as. Information primarily sourced from Hartley et al., 2010 DFS database, with catchment areas from Lehner and Grill, 2013

DFS	Climate catchment	Climate Basin	Tectonic Setting	Location	Location coordinates	Channel Planform	Total Channel length (km)	Apex – Toe Distance (km)	Catchment area (km^2)	Medial Channel length (km)	Termination Type	River Name	References
AG01_DRY	Dryland	Dryland	Foreland	Algeria	32.2, 2.3	Meandering	59	42	7539	26.8	Into dune field and lake	Que del Mehaigu ene	Lehner and Grill, 2013; Hartley et al., 2010
AL03_POL	Polar/ continental	Polar/ continental	Foreland	Alaska, USA	64.062, -147.246	Meandering	127	78	5350	42	Axial System	Dry Creek	Lehner and Grill, 2013; Hartley et al., 2010
BO01_TROP	Dryland/ Subtropical	Tropical	Foreland	Bolivia	-20.022, -63.189	Braided	203	175	7514	68	Becomes contributary then dies out	Parapeti	Lehner and Grill, 2013; Hartley et al., 2010

Table 2.4: Summary table for the additional systems added to the study of variability within the medial zone, with the climate basin and location used for naming the system in text. Information primarily sourced form Hartley et al., 2010 DFS database, with catchment areas from Lehner and Grill, 2013

Chapter 3: Defining the Medial Zone

As discussed in Chapter 1, the literature base for defining each zone of modern distributive fluvial systems is more limited than rock record deposits, where each zone is characterised by distinct fluvial architecture, grain sizes and facies proportions (Nichols and Fisher, 2007; Kjemperud *et al*., 2008; Rittersbacher *et al*., 2014; Owen *et al.*, 2015a, 2017, 2018; Martin *et al.*, 2021; Priddy and Clarke, 2021). It is imperative that a method for determining the zones on a modern DFS is established before characterising the medial zone. This chapter outlines the key results found that feeds into the determination of zones on a DFS, particularly the medial zone, the zone of interest in this study.

3.1 Results

3.1.1 Individual Site Observations

In using the criteria described in Chapter 2, prominent downstream patterns have been observed within each of the 7 systems studied, discussed individually below. **Figures 3.1 and 3.2** summarise the data collected for each of the measurable criteria per DFS. By plotting and evaluating patterns in the graphs, the proximal – medial transition, and the medial – distal transition have been proposed, shaded in the light and dark grey boxes. **Figure 3.2** outlines the elevation of each system's channel with the change in slope angle extracted and plotted alongside.

AR01_TROP – Bermejo River, Argentina

The Bermejo DFS (**Figure 3.3**) consists of a single channel, the largest system to be studied in this collection (500 km apex to toe), situated within the Andean foreland basin, and extends from the Andes into the Chaco Plain. The Bermejo lies within a tropical climate, with generally consistent precipitation and discharge rates year round, with variation controlled by the monsoon season. Active channel and channel belt width are both widest at the start of the system: maximum widths of approximately 3000 m and 5000 m respectively. These parameters significantly decrease at around 20% downstream, corresponding with channel morphology changes from braided to meandering. Moreover, this transition occurs with a change in channel elevation, as see in **Figure 3.2**): the braided portion of the system has a channel slope of -7 to -6.4, which flattens to approximately -2 upon transitioning to meandering. Farther downstream, the active channel width and channel slope remain relatively constant. However, at ~65% downstream the channel belt width narrows further. At this interval, the ACW/CBW ratio increases with a moderate positive correlation (+0.44), where channel belt becomes a similar width to active channel. Channel belt width slightly increases upon reaching the toe, where the system terminates into the axial Paraguay River.

AR02_TROP – Itiyura River, Argentina

AR02_TROP, the Itiyuri River, Argentina, is also located within the Andean foreland basin, as well as resides within the same climatic regime as the Bermejo, it is therefore expected to show similar trends with regards to sediment dynamics and discharge rates. Furthermore, AR02_TROP shows a similar trend to AR01_TROP, in that channel morphology transitions from braided to meandering around 20 – 30% downstream, coincident with the change in channel slope gradient from -3.6 to 1.6. There is a general decrease downstream, supported by a strong statistically significant Rs of -0.81 and -0.82 (**Table 3.1**), in both active channel and belt widths, however there is not a large decrease corresponding with the change in channel morphology and slope, as there is with AR01_TROP. Further downstream, at approximately 75% downstream, the ACW:CBW becomes 1, where the channel belt

width equals active channel width, where the corresponding widths are both 0 m and the channel becomes unconfined.

AL01_POL – Canning River, Alaska, USA

The Canning River, or AL01_POL in this study, consists of multiple braided channels extending radially due to downstream bifurcation, extending from the Brooks Range, within a foreland basin tectonic regime and terminating into the Arctic Ocean. Climate within this region is largely seasonal, with discharge and sediment supply controlled by glacial melt. Therefore, it can be considered discharge rates to be highest during the summer season, and thus its channel morphology is a product of high sediment concentrations. Channel bifurcation of the measured channels occurs continuously downstream with the most bifurcation points present at 20 – 35% (**Figure 3.5**), however channel complexity, related to the onset of bifurcation, drives a widening of belt widths between 25 – 45 % downstream, before narrowing as expected. Due to this fluctuation in widths, the ACW has no statistically significant correlation between width and distance downstream. Alternatively, CBW and ACW/CBW ratio are much more statistically significant in their downstream trends. ACW/CBW ratio has a strong positive correlation of 0.709; channel belt and active channel become similar in size. Qualitatively, these trends are seen where channels become distinctly separated by overbank (**Figure 3.5a**).

Channel slope gradient remains consistent throughout the system (~-1.8), alongside the braided nature (**Figure 3.2)**. However, gradient flattens from -1.4 to 0 beyond 80% downstream, towards the toe of the DFS. This corresponds to where the channel becomes more sinuous upon termination at the ocean. Within this similar distal area, 75 – 80% downstream, the abundance of ponding increases.

AL02_POL – Little Tonzona River, Alaska, USA

Another single channel DFS, extending from the Alaskan Range and terminating within an axial draining system, AL02_POL shows many similarities to AR01_TROP and AR02_TROP, in that it exhibits a braided to meandering/more sinuous transition, coupled with a minor change in channel gradient approximately 35 – 45% downstream, -6.4 to -3.2. Furthermore, it may differ from the Canning River in that it may not exhibit such extremes in annual discharge rates. While the system is glacially fed, its locality and vegetation cover suggests frequent precipitation events, therefore, sediment concentrations are likely much lower. However, Significant active channel decreases are also observed at this margin downstream, with widths of ~170 m at 35%, and <100 m beyond this point. A similar trend is found for channel belt widths where from 35 – 45% downstream widths are <200m. Further significant active channel and belt narrowing is observed at approximately 55 – 65% downstream: channel belt decreases to values <200m, along with a decrease in active channel width (50m), alongside a further channel gradient decrease to approximately -1.8.

Despite distinct and strong negative correlations between widths and distance downstream (**Table 3.1**), the ratio between the two parameters exhibits no apparent significant correlation. By assessing ACW/CBW in **Figure** 3.**1**, the ratio starts high and decreases downstream until 20%, where channel belt starts to become wider than active channel, generally continuing to increase downstream.

AF01_DRY – Andkhui, Afghanistan

One of the smaller systems in this study, AF01_DRY is a single thread meandering DFS situated over Andkhui in northwest Afghanistan, terminating as splay into dune fields. As with other dryland environments, or systems controlled by large seasonality, infrequent but high magnitude precipitation events are characteristic in this region. However, based on the single meandering channel planform,

the system is likely fed by continuous flow sourced from the upper catchment, and is not shaped by high energy flood events. **Figure 3.1** shows how the channel belt width in this system is highest closest to the apex (>100 m) and significantly decreases between 20 – 30% downstream (<30 m). This is marked by a bifurcation point at approximately 20% downstream (**Figure 3.7**). However, while ACW has a more consistent decrease in downstream width, both width parameters have significantly strong negative correlations (ACW: -0.83, CBW -0.89). Alternatively, the ACW/CBW ratio has a significantly strong increase / positive correlation, where the channel belt and active channel narrow to similar widths, this ratio becomes almost 1 beyond 60 – 70% downstream. Similarly to AR02_TROP, observations from satellite imagery shows how beyond 60 – 70% distance downstream, the primary channel bifurcates considerably, surrounded by a large splay area (**Figure 3.7**). Interestingly, channel elevation and gradient behave differently to the other systems, where here the more proximal part of the system gently slopes downstream (-0.4) before steepening beyond approximately 40% downstream (~-1.8).

CH01_DRY – Unnamed, China

This system runs similarly to AL01_POL, with the characteristic radial fan shape, and multiple bifurcating braided channels, terminating into the Tarim Basin. Similarly to AL01_POL, channel planform is likely formed due to infrequent, high energy flood events with a high sediment concentration, linked to the dryland nature of this region. Both active channel and channel belt decrease downstream, with active channel decreasing considerably at approximately 30% downstream, corresponding with the bifurcation points observed in **Figure 3.8**. These trends are supported by statistically significant R_s values, indicating a very strong negatively correlating trend (**Table 3.1**). CBW further decreases upon 70% downstream where it remains relatively constant. Despite the consistent downstream decreases for ACW and CBW, the ratio between the two parameters is limited, fluctuating downstream. Here the R_s value indicates no downstream relationship with the ratio. Furthermore, slope gradient remains constant downstream from apex to toe, averaging -6.84.

CH02_DRY – Ruo Shui, China

The Ruo Shui DFS, or CH02_DRY, is a braided system located in Northern China, sourced from the Qilian Mountains, in a foreland basin tectonic setting, before terminating on the Juyan Lake Basin, within the Gobi Desert. Also, a dryland system, seasonality is expected to influence annual discharge rates, with higher precipitation in the upstream catchment supplying the DFS with generally constant sediment and water, and sporadic high magnitude events potentially driving significant channel migration within the DFS, due to high discharge rates and sediment concentrations. While predominantly of a braided channel, minimal bifurcation occurs at the apex, and the active channel displays a general downstream decrease in width, with maximum values of 500 m towards the apex to <100 m upon reaching the toe. From between 0 – 15% downstream, the active channel rises, however proceeds to decrease further downstream. A similar trend follows for CBW, where overall the system narrows from maximum values of >1500 m to <100 m wide at the toe. Statistically, these widths have a moderately significant negative correlation and downstream decrease. Alternatively, the downstream ACW/CBW ratio slightly increases downstream, with a moderate positive correlation, particularly increasing after 75% downstream, coinciding with further narrowing of the active channel and channel belt. Channel slope remains quite constant from apex to toe, averaging -1.5. Furthermore, similar to AF01_DRY and through observing the satellite imagery, 65 – 75% downstream marks where the primary channel bifurcates more and splays into the desert upon termination, with slope gradient flattening to -0.2 (**Figure 3.9**).

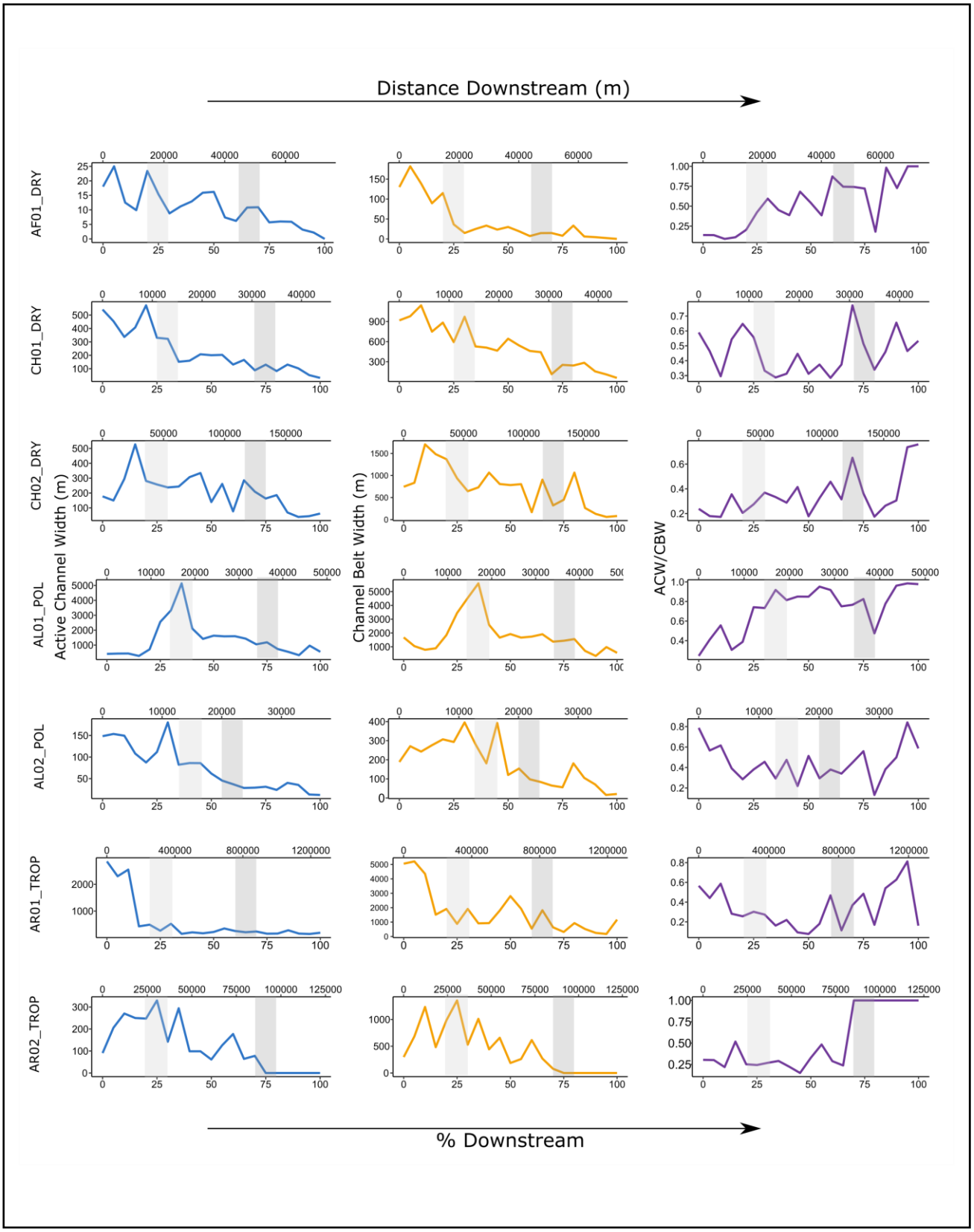

Figure 3.1: Downstream plots of active channel width (ACW), channel belt width (CBW) and the ratio of active channel / channel belt. Shaded areas indicate the proposed proximal – medial zone (light grey) and the medial – distal zone (grey).

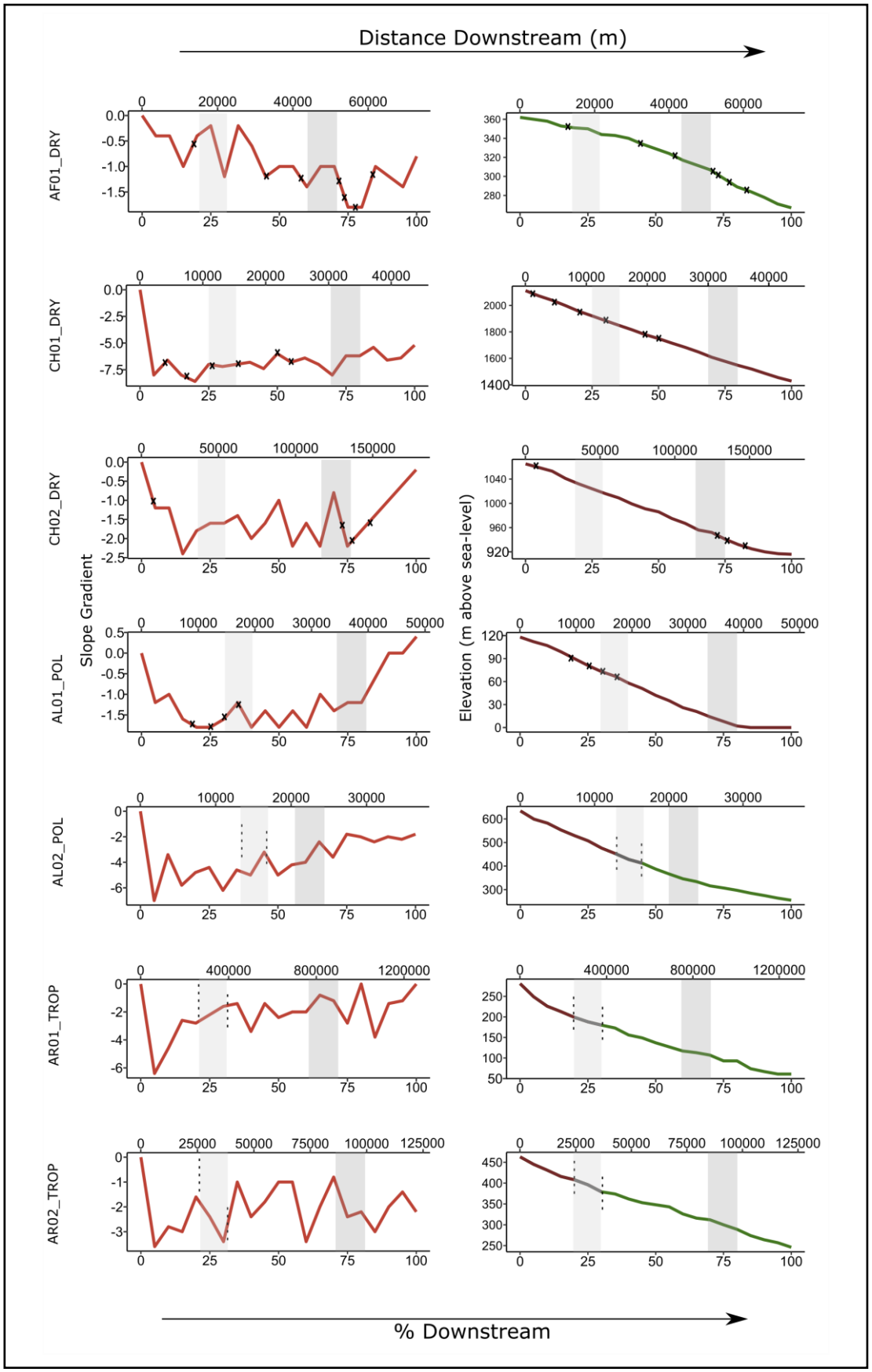

Figure 3.2: Downstream plots for channel elevation for each studied DFS and the change in slope angle downstream. Shaded areas indicate the proposed proximal – medial zone (light grey) and the medial – distal zone (grey).

Sites	Spearman's Rank					
	ACW		CBW		Ratio	
	R_s	P	R_s	P	R_s	P
AR01_TROP	-0.72	**1.09e-04**	-0.71	**1.6e-05**	0.441	**2.3e-02**
AR02_TROP	-0.81	**3.595e-07**	-0.82	**2.46E-06**	0.643	**8.3e-04**
AL01_POL	0.02	0.462	-0.40	**3.7e-02**	0.709	**1.6e-04**
AL02_POL	-0.92	**2.0e-09**	-0.78	**1.27E-05**	-0.013	0.478
AF01_DRY	-0.83	**1.867e-07**	-0.89	**2.41E-08**	0.928	**6.77E-10**
CH01_DRY	-0.93	**4.5e-10**	-0.94	**2.66E-10**	0.081	0.364
CH02_DRY	-0.59	**2.6e-03**	-0.68	**3.7e-03**	0.458	**1.8e-02**

*Table 3.3: Spearman's Rank Correlation Coefficient to determine nature of downstream trend for each of the DFS where the medial zone can be constrained. R_s values 0.70 – 1 suggest a strong correlation (- negative/ + positive), 0.40 – 0.69 moderate correlation, 0 – 0.39 a weak correlation. P values **< 0.05** are statistically significant; accept the alternative hypothesis "There is a significant relationship between channel width and distance downstream", these values are formatted as bold and blue, otherwise, the values are red.*

3.2 Medial Position

Due to the dynamic nature of these systems, and to avoid abruptly marking changes that are not visually apparent, approximate transition zones for the start and end of the medial have been proposed – 'proximal-medial transition' and 'medial-distal transition'. For each system these constitute as a 10% proportion of the downstream channel distance, illustrated in **Figures 3.3 – 3.9** and **Table 3.2**. These zones for each of the DFS studied are proposed based on the results outlined in 3.1, discussed below and outlined in **Table 3.2**.

3.2.1. Indiviudual Sites

AR01_TROP – Bermejo River, Argentina

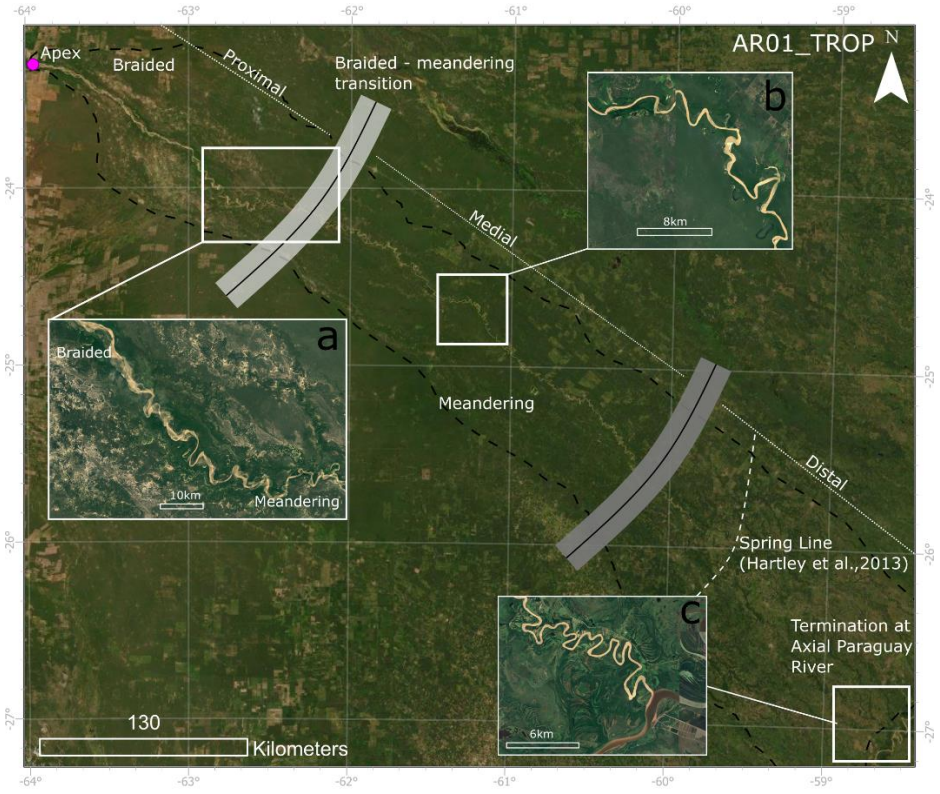

Figure 3.3: Site map of Bermejo DFS (AR01_TROP) indicating the margin for the proximal – medial transition (light grey), and the medial – distal transition (dark grey), annotated with key geomorphic features. Imagery from Landsat 8 and Google Earth Pro.

The proximal – medial transition for AR01_TROP has been proposed based on the distinct geomorphic changes seen through the sudden decrease in active channel and belt width, the channel planform, and channel elevation change, all occurring at approximately 20% downstream. Therefore, considering these factors, the proximal – medial transition zone was presumed to be 20 – 30% downstream. Active channels are generally much wider in the proximal zone, where water discharge and supply are highest near the source – the DFS apex (Weissmann *et al.*, 2013). In ancient DFS, proximal zone deposits are characterised by wide, very amalgamated channel bodies (Owen *et al.*, 2017; Führ Dal' Bó *et al.*, 2019), where the system has the energy, and narrower area, for lateral migration and avulsion, reworking into older channel and overbank deposits as the basin area is limited. Here, channel belts are expected to be wider corresponding to higher flows and wider channels, thus a decrease in active channel and belt widths can mark the end of the proximal zone.

Furthermore, the proximal zone can be characterised by steep channel gradients, in order to maintain the energy and sediment supply from the apex (Davidson *et al.*, 2013), a feature also observed across the gravel sand transition (Dingle *et al.*, 2021). This observation is often associated with channel morphology (Parker and Cui, 1998); the Bermejo DFS initiates as a multi-threaded braided system with a steeper channel gradient, when the slope flattens, energy and bedload decreases, transitioning the system into a meandering channel. The zone before this transition in planform can be considered the proximal zone, whereas downstream the system becomes medial. To add, Weissmann *et al*. (2015) notes that from 140 km from the apex (approximately 20 – 30% in this study) a significant change in sinuosity is observed, 1.08 average sinuosity in the upper portion to 1.64 below this, coincident with

other observations made, further supporting the proposed proximal – medial margin. However this has not been linked to the change in gradient.

Alternatively, when assessing the medial – distal zone, there are fewer distinct features that aid in interpreting the transition from medial to distal. However, while the active channel was observed to remain constant further downstream, channel belt width narrowed, increasing the ratio between ACW and CBW. This may suggest less lateral migration of the meandering channels, introducing the presence of narrow, isolated ribbon channels, a geomorphic feature familiar with the distal zone in ancient distal deposits (e.g. Kumar *et al.*, 1999; Gibling, 2006; Nichols and Fisher, 2007; Owen *et al.*, 2015a). As this trend can be observed 60 – 70% downstream, the medial – distal transition is interpreted to be here.

AR02_TROP – Itiyura River, Argentina

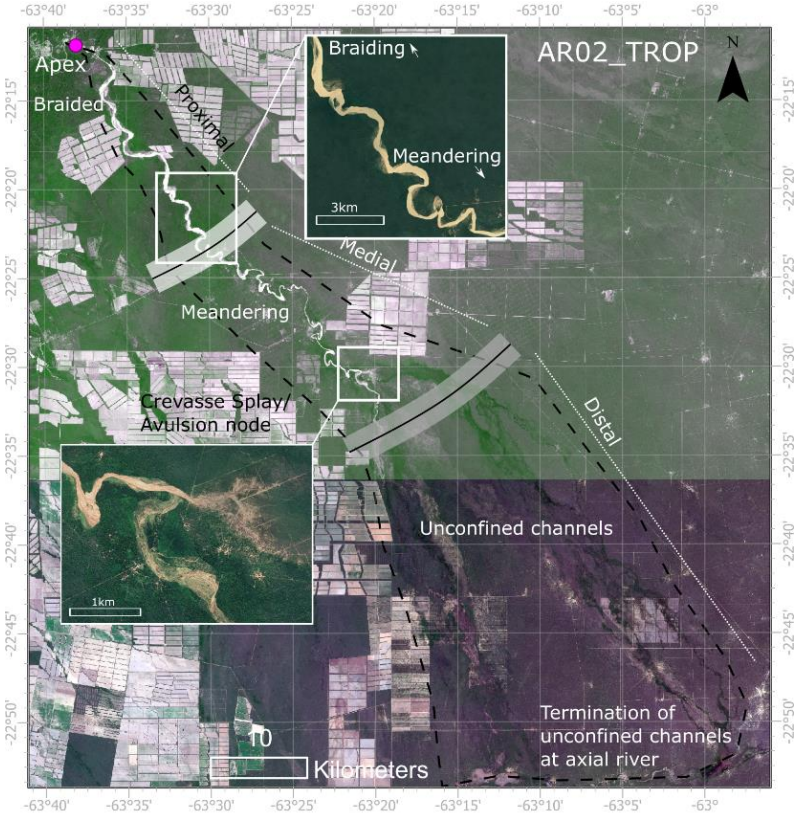

Figure 3.4: Site map of DFS AR02_TROP indicating the margins for the proximal – medial transition (light grey), and the medial – distal transition (dark grey), annotated with key geomorphic features. Imagery from Sentinel 2 and Google Earth Pro.

AR02_TROP displays similar upstream trends as its larger counterpart AR01_TROP, where a braided to meandering morphological change takes place coincident with a change in gradient. While there is no distinct decrease in widths, further indicating a change in processes and stream power, as seen in AR01_TROP, channel planform change can be indicative of the proximal – medial transition. Channel gradient is often steeper and braided in the proximal region (Davidson *et* al., 2013). Beyond the gravel – sand transition, channel morphology shifts into a narrower single meandering channel in the medial zone (Dubille and Lavé, 2015). Thus, occurring at 20 – 30% these processes assume that the medial zone lies beyond this margin.

Furthermore, where channels experience a loss of energy downstream, related to sediment and water discharge, channels are much more likely to become unconfined, often in the form of terminal splays.

For AR02_TROP, this can be observed where active channel and channel belt widths are 0, and as seen in satellite imagery, sheet-like deposits are observed (**Figure 3.4).** These observations are characteristics of distal zone in the DFS rock record (Fisher *et al*., 2007; Cain and Mountney, 2009; Nichols and Fisher, 2012), and in modern systems (Tooth, 2000; 2005). Thus at 70 – 80% downstream, the medial – distal transition can be inferred where the active channel begins to become unconfined.

AL01_POL – Canning River, Alaska, USA

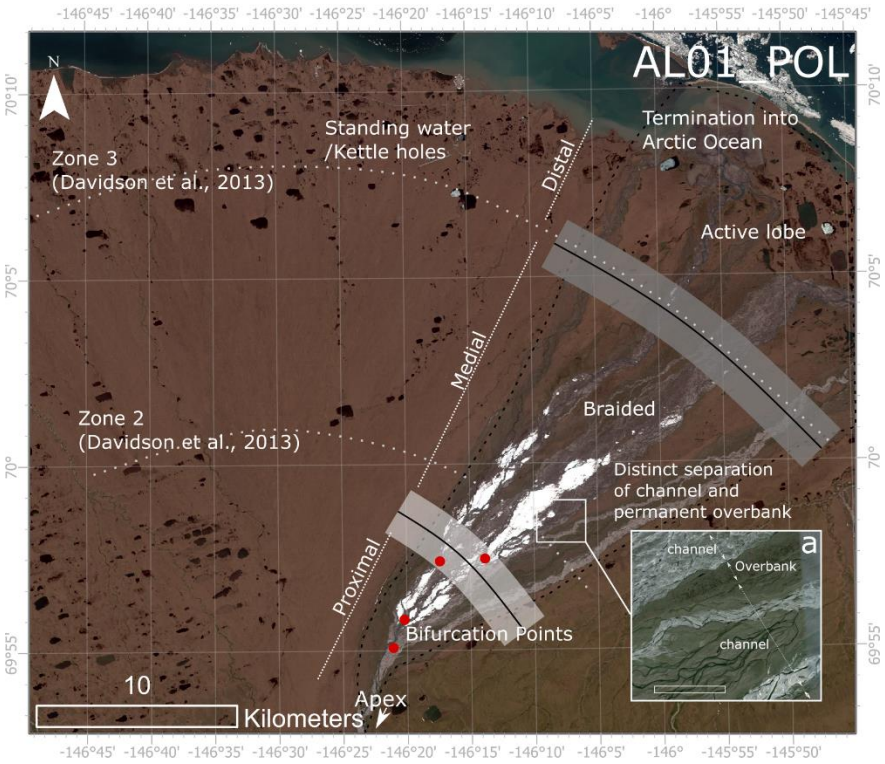

Figure 3.5: Site map of DFS Al01_POL indicating the margins for the proximal – medial transition (light grey), and the medial – distal transition (dark grey), annotated with key geomorphic features. Imagery from Sentinel 2 and Google Earth Pro.

In AL01_POL, the decrease in active channel and belt width observed at approximately 40% downstream, coinciding with the bifurcation of the active channels (**Figure 3.5**). Where this occurs, bifurcated channels begin to become laterally separated by floodplain deposits, similar to what is seen in ancient deposits. Within the rock record, the medial deposits are characterised by distinct channel bodies, separated by floodplain deposits (Owen *et al.*, 2017; Chesley and Leier, 2018). Therefore, the 30 – 40% margin is inferred to be the start of the medial zone in this system. Other studies have worked to constrain the various DFS in the Canning River; Davidson *et al*. (2013) marks the medial zone at a similar position to the one proposed in this study: Zone 2, as well as attributing the proximal zone increase in channel belt width to channel complexity driven by bifurcation. Conversely, the active channel and belt width increase could be attributed to an alternate apex position to the one proposed in the Global DFS database (Hartley *et al.*, 2010), where the apex has prograded northwards, incising (and narrowing) the initial 15% of the system.

The medial – distal zone is assumed to be 70 – 80 % downstream, based on the flattening of the channel slope gradient and some increased sinuosity of the channel. This flatter and distal portion of the system has a higher abundance of ponding and kettle holes, relating to the downstream prevalence of impermeable soils and limited infiltration (Hartley *et al.*, 2013), characteristic of the distal zones fine grained deposits.

AL02_POL – Little Tonzona River, Alaska, USA

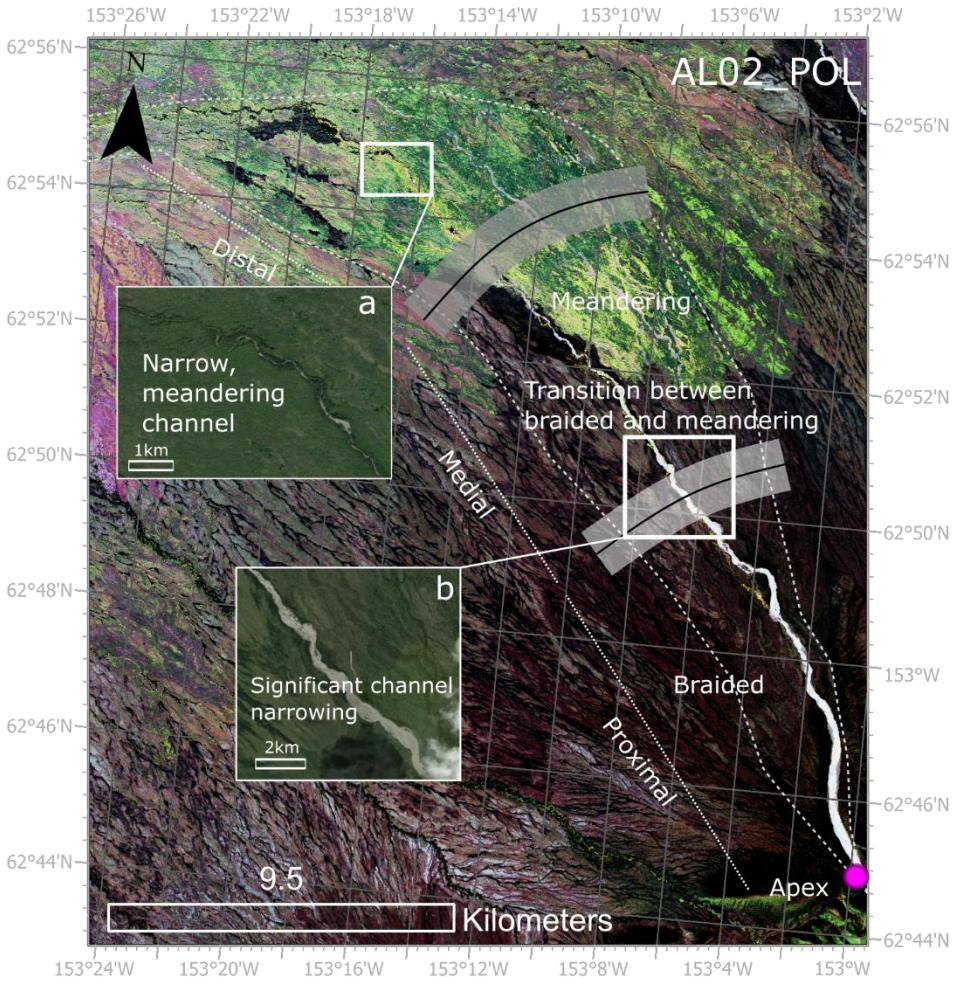

Figure 3.6: Site map of DFS AL02_POL indicating the margins for the proximal – medial transition (light grey), and the medial – distal transition (dark grey), annotated with key geomorphic features. Imagery from Sentinel 2 and Mapbox.

While AL02_POL differs in climate to the tropical DFS used in this study, the systems share several similarities, which have been used in defining the downstream position of the medial zone. For instance, AL02_POL displays a downstream braided to single channel thread, meandering transition paired with a minor change in channel gradient, indicative of changes in stream power and sediment and water supply as previously stated for AR01_TROP and AR02_TROP. Furthermore, the significant narrowing of active channel and belt is coeval with the other stated morphological changes, suggesting the proximal – medial zone to be 35 – 45% where these changes and characteristics are observed.

Additionally, when channel belt width decreases downstream, and the ratio of active channel to channel belt increases, it may suggest a decline in the extent of lateral migration, producing channels with few lateral accretion sets and instead a ribbon channel morphology: a single sandbody within the rock record. Similarly, lateral migration of channels has been linked to sediment flux and discharge (Wickert *et al.*, 2013; Bufe *et al.*, 2019), so with decreasing downstream supply, migration should decrease. Statistically, the R_s value for AL02_POL indicates a decrease in the ratio as an overall downstream trend. However, **Figure 3.1** for AL02_POL shows the system undertakes a decrease in ratio (so an increase in lateral migration), before an increase at 55% downstream, where lateral migration ceases/reduces. Therefore, the medial – distal zone could be assumed to be 55 – 65 %

downstream in this instance, where channel belt width and active channel width are almost the same; the ratio between these gradually increasing from this point.

AF01_DRY – Andkhui, Afghanistan

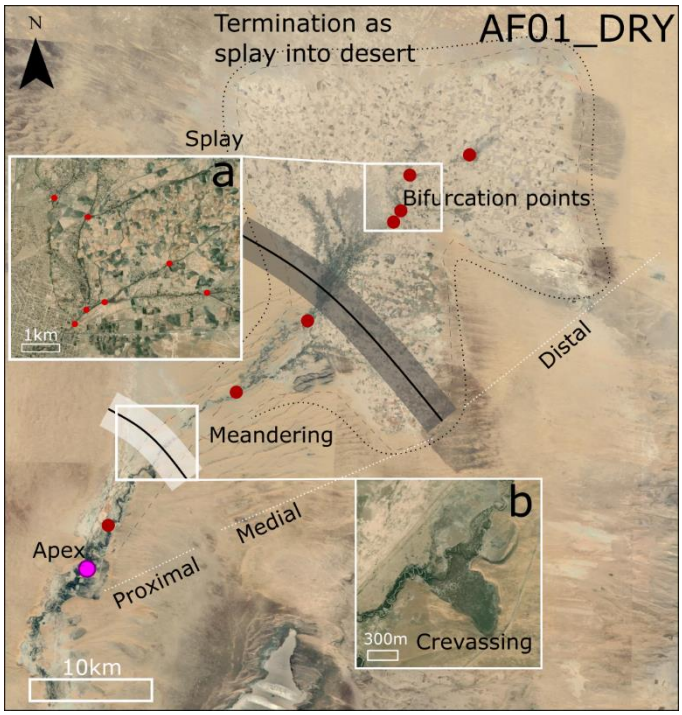

Figure 3.7: Site map of DFS AF01_DRY indicating the margins for the proximal – medial transition (light grey), and the medial – distal transition (dark grey), annotated with key geomorphic features. Imagery from Google Earth Pro and Mapbox.

The medial position for AF01_DRY is constrained by a significant decrease in active channel and channel belt width, attributed to a loss of energy downstream from the apex. This takes place approximately 20 – 30% downstream.

While active channel width continues to decrease downstream, channel belt width remains relatively stable and low beyond the proximal – medial transition. This enables the ratio to increase downstream, where active channel almost equals channel belt width (at approximately 60 – 70% downstream), producing the characteristic distal ribbon channels. Bifurcation is most prevalent at 70%, and according to the satellite imagery (**Figure 3.7**), alongside a large terminal splay. Moreover, as the distal zone is associated with finer grain size, and therefore more impermeable deposits, soils are expected to be better developed (Hartley *et al.*, 2013), better suited for agricultural practices, which are abundant beyond the 70% interval in the satellite imagery (**Figure** 3.**7**). However, these soils are still likely to be weak and undeveloped due to the dryland climate. Instead, as the channel flow velocity decreases downstream, channels become unconfined 'floodouts' (Tooth, 2000), producing large splays (**Figure** 3.**7**). The distal bifurcation seen in this system can be attributed to the downstream steepening of channel gradient, triggering channel avulsion, alongside periods of diminishing flow, where unconfined flows can become channelised (Fisher *et al.*, 2007).

CH01_DRY – Unnamed, China

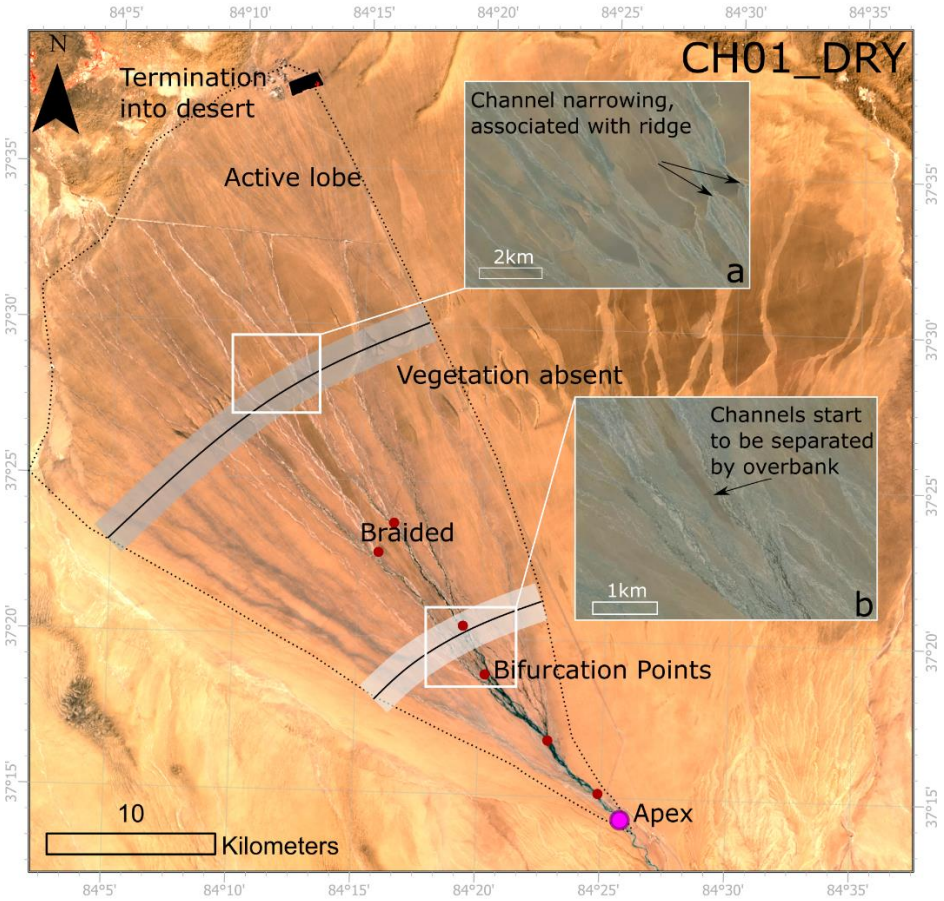

Figure 3.8: Site map of DFS CH01_DRY indicating the margins for the proximal – medial transition (light grey), and the medial – distal transition (dark grey), annotated with key geomorphic features. Imagery from Sentinel 2 and Mapbox.

A significant decrease in active channel width and the onset of bifurcation occurs at 25 – 35% downstream, similar characteristics observed in AL01_POL. These observations are due to processes that are characteristic of the proximal zone, where sediment supply and stream power are much higher. Therefore, the proximal – medial transition zone can be constrained to the 25 – 35% downstream for this system.

For the medial – distal transition zone, there are fewer obvious indicators that may help constrain this zone; active channel width decreases further downstream at a constant rate, and the ACW/CBW ratio is quite variable downstream, despite a general increase from 60% downstream. However, from 70% downstream, channel belt width considerably narrows, driving a peak in the ratio between ACW and CBW. At this interval, the channel slope increases slightly, where a small ridge extends across the DFS, this may drive the onset of the channel narrowing (**Figures 3.2 and 3.8a**). Thus, 70 – 80% downstream is interpreted to mark the onset of the distal zone for this system.

CH02_DRY – Ruo Shui, China

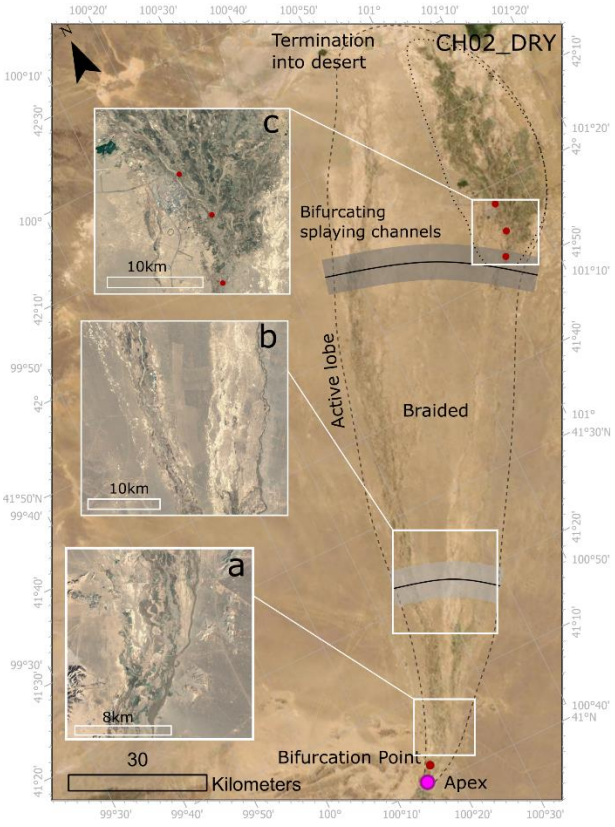

Figure 3.9: Site map of DFS CH02_DRY indicating the margins for the proximal – medial transition (light grey), and the medial – distal transition (dark grey), annotated with key geomorphic features. Imagery from Sentinel 2 and Google Earth Pro.

Despite initially having a narrow width nearest the apex, the primary active channel in CH02_DRY (alongside the channel belt) significantly decreases in width between 20 – 30 % downstream (having increased downstream from the 5% interval), based on a reduction in downstream discharge associated with downstream DFS trends (Hartley *et al.*, 2010; Weissmann *et al.*, 2010). As there are no other planform or elevation changes, the proximal – medial transition is proposed to be at this 20 – 30% margin. On the contrary, as active channel and belt profile remain quite constant downstream, other geomorphic features are considered for constraining the medial – distal zone. At 65 – 75% downstream, the main active channel bifurcates into multiple channels that splay out (**Figure 3.9**) characteristic of some distal terminations (Tooth, 2005; Davidson *et al.*, 2013). This is also coupled with the flattening of the channel gradient, indicative of the channel energy decreasing. Therefore, 65 – 75% is the proposed medial to distal transition zone.

3.2.2 Discussion: Medial Zone Position

DFS	Proximal – Medial	Medial – Distal	Catchment Area (km²)	DFS Area (km²)	Catchment / DFS	Total Channel Length (km)	Medial Length/ Total Length
AR01_TROP	20 – 30%	60 – 70%	34316	43,428	0.78	1255.8	0.44
AR02_TROP	20 – 30%	70 – 80%	1343	1473	0.90	121.9	0.44
AL01_POL	30 – 40%	75 – 80%	4724	1089	4.30	48.5	0.36
AL02_POL	35 – 45%	55 – 65%	99	305	0.32	36.5	0.24
AF01_DRY	20 – 30%	60 – 70%	12872	725	1.77	72.9	0.40
CH01_DRY	25 – 35%	70 – 80%	2410	1841	1.30	43.715	0.45
CH02_DRY	20 – 30%	65 – 75%	22103	13706	1.60	178.1	0.47
Average	**25 – 35%**	**65 – 75%**					

Table 3.4: Summary table for the proposed downstream transition zones for the proximal – medial, and medial – distal for each of the studied distributive fluvial systems.

In general, each DFS followed a trend where the medial zone constitutes as approximately 40% (**Table 3.2**) of the system, with each system displaying a clear downstream decrease in active channel width. This was expected where discharge decreases downstream due to bifurcation, evapotranspiration and infiltration (Hartley *et al.*, 2010; Weissmann *et al.*, 2010), with some variation due to different climatic settings. However, variation between systems is apparent. It is thus difficult to establish a 'one size fits all' approach for defining the medial zone of modern distributive fluvial systems. Despite this, broad trends can be observed and based on the criteria and proposed zones, averages of each zone's downstream percentage could be used for systems not included in this study (25 – 35% downstream proximal – medial; 65 – 75% downstream for medial – distal). It is important to recognise that variations can be present from this general trend, as seen in AL02_POL. It is therefore recommended, that where possible, when studying the zones of modern DFS using satellite imagery, that an analysis should be done, of which a tested methodology of how to distinguish the different zones has been established in this study.

By using the ratio of catchment area to DFS area (**Table 3.2**), a relative assessment on how much the catchment area contributes towards the DFS can be conducted. Ratios less than 1, indicate that the catchment area is less than the DFS area. Therefore, the catchment is likely to provide high amounts of sediment and water, contributing to the larger DFS area. The ratios for AR01_TROP and AR02_TROP are 0.78 and 0.90, where the DFS area and catchment are almost similar in size, however AL02_POL has a ratio of 0.32, where the catchment area is notably smaller than the DFS area, implying a high sediment load contributing to the DFS area. Alternatively, catchment to DFS area ratios above 1 are indicative of systems where the catchment area is much larger than the DFS area, and therefore material in the catchment contributes to the development of the DFS, this is seen in AL01_POL, CH01_DRY, CH02_DRY and AF01_DRY. This is likely related to the dryland environment most of these systems sit in, where sediment and discharge rates are controlled by infrequent precipitation events. It is important to note that other factors can influence the DFS area, including the system zones positions, such as the bedrock geology of the catchment, tectonics, and perhaps anthropogenic activity within the catchment area.

The difference in zone position for AL02_POL may be attributed to the downstream channel gradient change. Between 0 and 5% downstream, the very start of the proximal zone, the channel slope gradient is one of the steepest of the studied systems and remains steeper than the other systems

downstream despite a gradual downstream flattening. When channel slope is steep this can be indicative of high sediment loads, sourced from the catchment beyond the apex (Weissmann *et al.*, 2013). This may allow for the transportation of bedload sediment further downstream, thus making the proximal – medial margin, where channel morphology significantly changes, also further downstream. Furthermore, as discussed above, the sediment load in this system is suspected to be quite high, based on catchment area to DFS area ratio. To add, AR01_TROP is similar where the 0 to 5% interval gradient is -6.4, yet there is a flattening of the slope and proximal – medial transition occurs at the 20 - 30% margin, suggesting a lower sediment flux than AL02_POLs'. Alternatively, CH01_POL has a much steeper channel gradient, remaining consistent downstream, suggesting catchment sediment loads to also be high, but the proximal – medial position (25 – 35%) is more similar to the other systems. However it should be considered that the arid nature of this system means that while sediment loads are high, events that deposit these are less frequent, whereas the climate associated with AL02_POL are much more suited to continuous sediment and water discharge. Therefore, these conditions may allow for the progradation of the proximal – medial transition zone in AL02_POL, placing it further downstream than the other systems studied.

Across every system studied, wide active channel and belt widths are seen in the proximal zone, only limited in some systems where the channels have been confined near the apex. Wide braided and belt systems characterise most of the proximal zones in these systems, a consequence of the large extent of reworking associated with this portion of distributive fluvial systems (Weissmann *et al.*, 2013; Owen *et al.*, 2015a). The transition zone between proximal and medial is characterised primarily by a significant decrease in active channel and belt width, with some systems featuring further morphological changes in the planform present such as a transition from braided to meandering, alongside a slope break. Furthermore, the downstream trends in channel planform and slope, can be attributed to the relative grain size trends downstream (related to sediment/water discharge), and may therefore control the position of the medial zone in DFS, as described for the differences seen in AL02_POL. Testing this would require ground truthing grain sizes for each DFS, beyond the constraints of this project.

In the upstream/proximal portion of DFS, avulsions occur where channel instability is driven by higher sediment discharges (Jones and Schumm, 1999; Slingerland and Smith, 2004; Chakraborty *et al.*, 2010). This triggers a switch (avulsion) in channel direction from a nodal point, a fixed position of the channel (Weissmann *et al.*, 2015). In braided bifurcating systems (e.g. CH01_DRY and AL01_POL), the avulsion node is positioned furthest upstream between 8 – 10% downstream (Davidson *et al.*, 2013), whereas it has been found between 15 - 20% downstream for single threaded sinuous systems in this study. These node point positions found in Davidson *et al*. (2013) occur in the proximal zone defined in this study, which has been represented in **Figure 3.10**. Bifurcation occurs here where the old channel has not been abandoned upon avulsing. Avulsion is observed throughout the systems, however the mechanisms that drive this differ where conditions change (Makaske *et al.*, 2012).

After the proximal – medial zone has been delineated, the medial zone is generally characterised by distinct channels separated by floodplain and overbank (in systems where there are multiple bifurcated channels). Whether this portion of the system varies will be explored later in this study. **Figure 3.10** reflects the medial zone characteristics seen in each system, including a narrowing downstream pattern in channel width, increased sinuosity, and the distinct separation between channels.

The medial to distal transition in **Figure 3.10** has been illustrated where the relationship between channel belt and active channel changes. Channel belts narrow becoming equal to active channel as lateral migration reduces. Avulsion through crevasse splay events becomes more abundant

downstream (Jones and Schumm, 1999), driven by sediment deposition/supply and overbank flooding (Tooth, 2005). Crevassing has been identified in some sites where sandy coloured deposits are present in the satellite imagery, e.g. AR02_TROP, associated with low gradients in the distal reaches of channels upon termination (Li *et al*., 2019), e.g. CH02_DRY and AF01_DRY. Within this zone, further medial – distal nodal avulsion and bifurcation can occur (e.g. AF01_DRY), as channel gradient decreases downstream and channel flow attempts to be diverted (Davidson *et al.*, 2013). Channels gradient lowers downstream, coinciding with a decrease in stream power that inhibits the transportation of bedload material and enables the deposition of fines, as a result, the distal zone is characterised by deposits with low permeability and porosity – leaving areas of standing water (Hartley *et al.*, 2013).

While these systems are incredibly dynamic, variability arises in each, all driven by a number of autogenic and allogenic factors. Primarily, morphological differences have been observed between systems of different climatic settings. For instance, AR01_TROP, AR02_TROP, and AL02_POL are downstream meandering channels beyond the high energy proximal zone, as well as have a much higher abundance of vegetation coverage than all the dryland sites, and AL01_POL, most of which are all braided/multi-thread channels. This suggests a link between channel planform, channel stability and vegetation. However, the downstream positions of the proximal, medial, and distal do not differ too much across each system and different climatic zone.

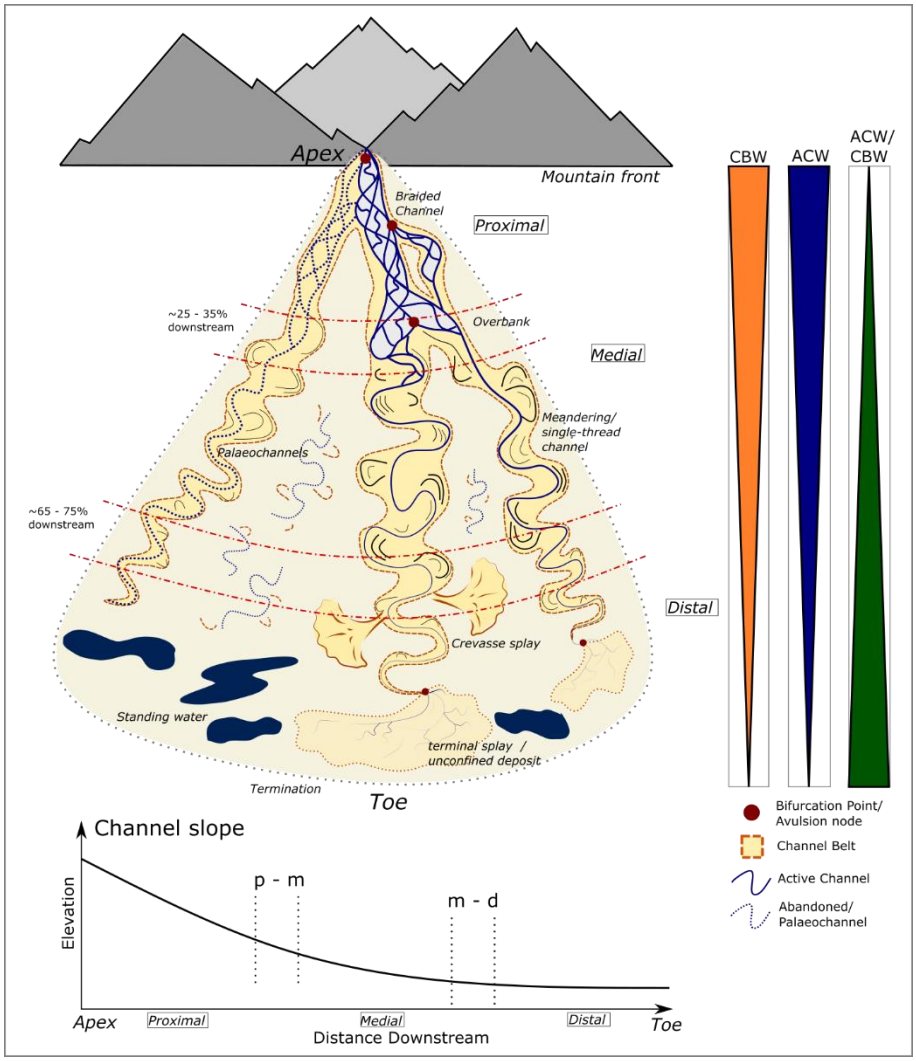

Figure 3.10: Summary diagram illustrating the key observations from constraining distributive fluvial systems into proximal, medial, and distal zone. ACW: Active channel width, CBW: Channel belt width, ACW/CBW: active channel width and channel belt width ratio. P – M: Proximal – Medial transition, M – D: Medial – Distal transition.

Once the position of the medial zone has been defined, a detailed study into the medial zone characteristics and variability can be undertaken, which follows in Chapter 4.

Chapter 4: Medial Variation Results

This chapter outlines the main results from measuring the various parameters in the medial zone, as described in Chapter 2 (active channel width, channel belt width, and proportion of active channel: channel belt: overbank). Particular attention will be given to understanding downstream trends in the medial zone within each system (4.1), and those between the different systems (4.2).

4.1 Individual System Results

DFS Code	ACW							CBW							ACW/CBW						
	R_s	R^2	CV %	Trend (+ or -)	Min	Max	Mean	R_s	R^2	CV %	Trend (+ or -)	Min	Max	Mean	R_s	R^2	CV %	Trend (+ or -)	Min	Max	Mean
AR01_TROP	**-0.64**	0.39	26.0	-	142	367	221	**-0.60**	0.3	54.6	-	380	3641	1831	**+0.37**	0.097	66.9	+	0.05	0.50	0.16
AR02_TROP	**-0.68**	0.43	68.7	-	11	349	102	**-0.59**	0.31	73.7	-	11	709	255	0.09	0.003	48.7	0	0.14	1.0	0.50
BO01_TROP	**-0.68**	0.40	49.1	-	207	1616	700	**-0.84**	0.62	45.4	-	733	4535	2476	0.03	0.009	26.1	0	0.18	0.50	0.29
AL01_POL	**-0.54**	0.35	77.2	-	147	2458	845	**-0.86**	0.37	76.1	-	482	6228	2046	-0.12	0.005	32.9	0	0.10	0.90	0.50
AL02_POL	**-0.86**	0.75	55.3	-	13	117	57	**-0.85**	0.67	54.6	-	32	396	177	0.12	0.01	34.8	0	0.12	0.52	0.35
AL03_POL	**-0.62**	0.33	42.2	-	13	55	30	-0.12	0.003	30.7	0	239	797	461	**-0.42**	0.23	46.6	-	0.02	0.13	0.07
CH01_DRY	**-0.74**	0.48	65.0	-	53	468	130	**-0.88**	0.52	52.6	-	8	1027	362	0.1	0.01	24.6	0	0.10	0.80	0.39
CH02_DRY	-0.28	0.09	65.9	0	41	424	185	-0.03	<0. 01	32.6	0	184	1060	594	-0.18	0.09	31.9	0	0.10	0.70	0.30
AG01_DRY	**-0.54**	0.35	62.5	-	30	175	62	**-0.41**	0.26	77.4	-	151	1426	383	0.06	<0.01	56.3	0	0.06	0.49	0.20
Mean					11	2458	319.1					11	6228	999					0.02	1.00	0.34

DFS Code	Normalised Proportion														Absolute Proportion									
	Active Channel %							Channel Belt %							Active Channel				Channel Belt				Overbank			
	R_s	R^2	CV %	Trend (+ or -)	Min	Max	Mean	R_s	R^2	CV %	Trend (+ or -)	Min	Max	Mean	R_s	R^2	CV %	Trend (+ or -)	R_s	R^2	CV %	Trend (+ or -)	R_s	R^2	CV %	Trend (+ or -)
AR01_TROP	-0.18	0.08	27.2	0	2.0	5.6	3.1	**+0.47**	0.20	18.7	+	17.0	33.3	21.3	0.15	0.001	30.7	0	**0.5**	0.24	29.0	+	0.27	0.16	16.0	0
AR02_TROP	-0.36	0.11	55.1	0	1.0	8.3	3.2	**-0.47**	0.17	53.7	-	4.0	29.4	14.0	0.05	0.00 04	50.0	0	-0.14	0.025	42.6	0	**0.90**	0.87	24.0	+
BO01_TROP	**-0.84**	0.74	49.7	-	1.0	7.8	4.0	**-0.84**	0.93	56.9	-	0.1	64.3	28.6	**-0.78**	0.55	42.6	-	**-0.86**	0.83	52.6	-	**0.89**	0.03	29.3	+
AL01_POL	**-0.96**	0.89	28.7	-	27.5	71.5	44.2	**-0.96**	0.90	20.0	-	41.5	88.0	61.4	**-0.50**	0.28	8.8	-	**0.45**	0.20	9.3	+	**0.98**	0.97	50.2	+
AL02_POL	-0.12	0.002	36.8	0	0.4	2.1	1.2	-0.2	0.03	31.1	0	2.7	8.5	5.0	-0.02	0.00 03	39.1	0	-0.12	0.026	31.0	0	**0.48**	0.19	2.8	+
AL03_POL	**-0.46**	0.15	44.4	-	0.1	0.8	0.4	**-0.82**	0.70	42.9	-	3.3	27.1	14.9	0.00	0.002	40.4	0	**-0.46**	0.29	36.6	0	**0.81**	0.60	22.6	+
CH01_DRY	**-0.66**	0.43	15.7	-	15.7	31.0	24.1	**-0.63**	0.43	25.0	-	20.4	49.9	42.7	0.10	0.02	13.7	0	0.21	0.00 04	16.4	-	**0.94**	0.99	23.8	+
CH02_DRY	**-0.86**	0.62	46.7	-	2.1	10.1	4.0	**-0.85**	0.75	58.1	-	9.0	44.3	20.2	**-0.46**	0.24	22.0	-	**-0.72**	0.47	25.1	-	**0.98**	0.85	29.3	+
AG01_DRY	**-0.51**	0.30	55.6	-	0.2	1.5	0.6	**-0.78**	0.65	41.7	-	6.2	28.7	16.9	**-0.54**	0.37	60.2	-	**-0.85**	0.73	44.2	-	**0.43**	0.60	7.3	+
Mean					0.1	71.0	9.5					2.7	88.0	25.4												

*Table 4.1: Summary table of key statistics measured in each system: Active channel width (ACW), Channel belt width (CBW), ACW/CBW, and active channel: channel belt: overbank proportions (normalised and absolute). Rs = Spearman's rank correlation coefficient, **Bold and Blue** values indicate a statistically significant result (P Value < 0.05), values in red indicate where the Rs is not statistically significant (P value > 0.05). R^2 = Linear Regression R-Squared value. CV = Coefficient of variation as a %. +/- indicates if there is a positive or a negative correlation, cells with zero indicate no correlation.*

4.1.1 AL01_POL: *Canning River, Alaska, USA*

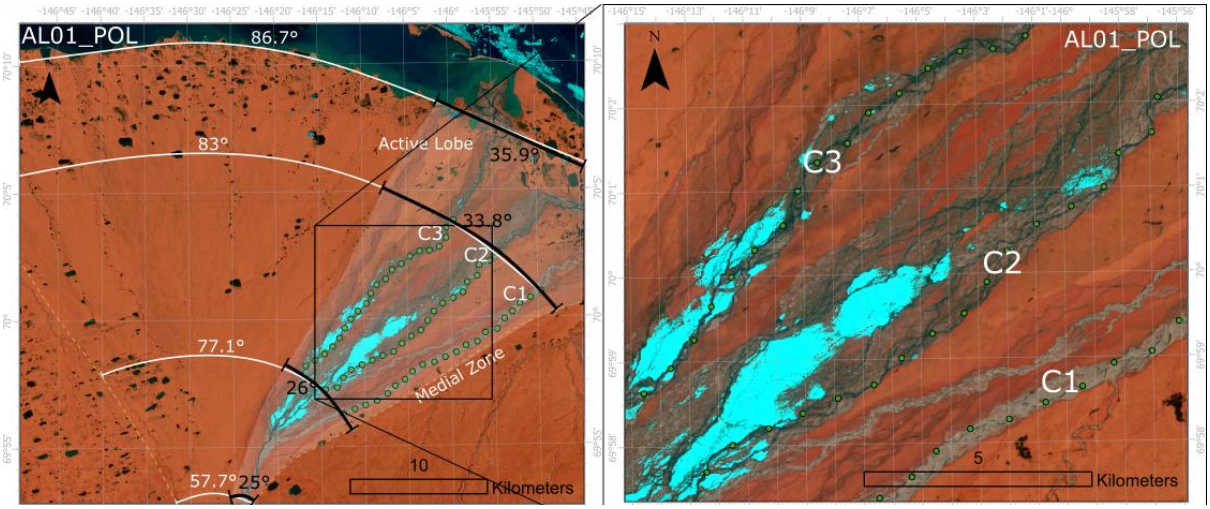

Figure 4.1 Whole DFS area of AL01_POL with sweep angles annotated in sequence of proximal, start of medial, end of medial, and fan toe. Highlighted area indicates the active lobe of the DFS where measurements took place. Studied medial zone outlined with the three active channels labelled (C1, C2, C3).

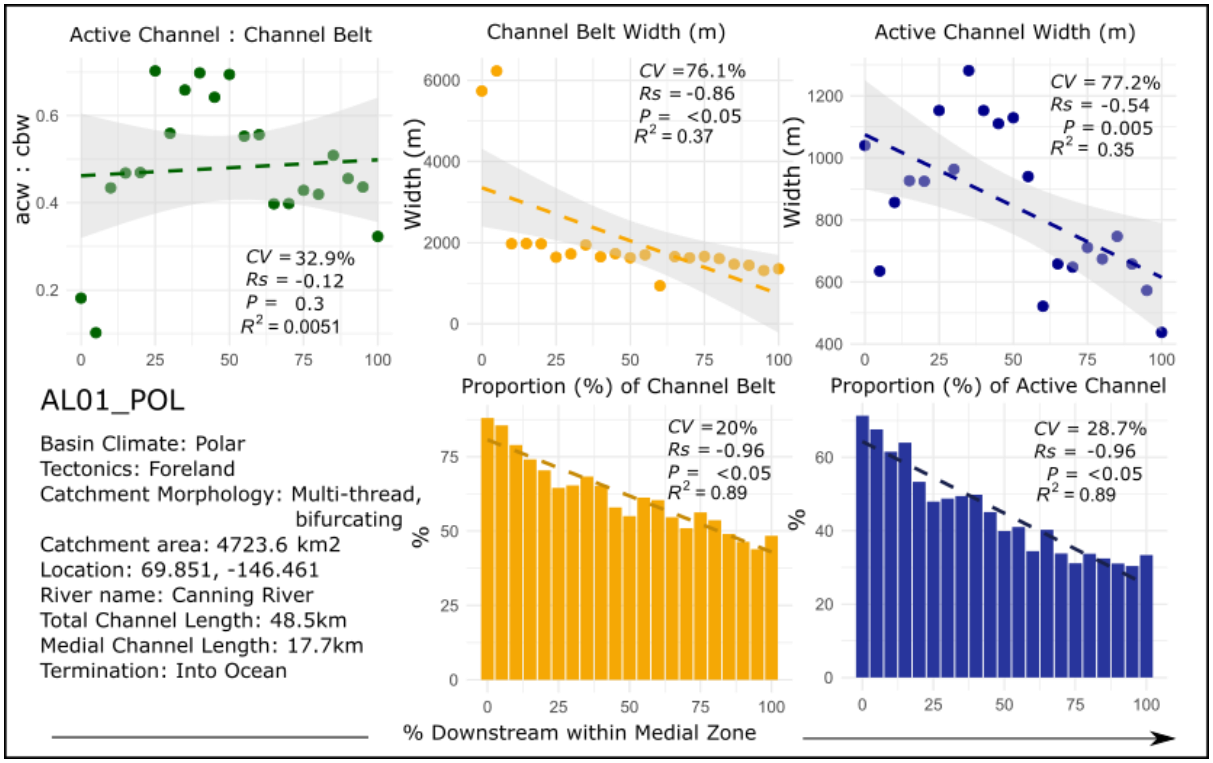

Figure 4.2: Plots summarising the primary results for AL01_POL with contextual information from the study area. Individual plots for the mean active channel width / channel belt downstream ratio, the mean channel belt width, mean active channel width, and the individual proportions of channel belt and active channel across the active lobe of the medial zone.

Active Channel Width (ACW)

The ACW plot in **Figure 4.2** shows the mean of the three channels combined plotted against distance downstream. This average width has a moderate downstream decrease with a negative correlation (Rs -0.54). There is a high degree of downstream variance (CV of 77.2%), and a weak R^2 value (0.35). In this dataset (average of all 3 channels), the minimum mean is 437.4 m and the maximum 1281.6m (mean 844.9 m).

When analysing each channel individually (**Figure 4.3**) distinct downstream trends are observed which accounts for the high variance in **Figure 4.2**. Channel 1 has a range of widths between 197.3 m to 681.8 m (mean: 417.6 m), with a low CV (28.9%), moderate to weak negative correlation (-0.38), and a weak R^2 (0.18). Channel 2 is the primary active channel in this system with the widest ACW (maximum: 2457.7 m, minimum: 524.7 m, mean: 1613.5 m) and has a CV of 34.5%. This channel widens downstream until the 35% interval where it decreases. Therefore, there is an insignificant negative correlation (R_s -0.32, P Value 0.08), and a very weak R^2 (0.14). However, channel 3 widths (maximum: 1001.6 m, minimum: 147.4 m, mean: 503.6 m) has a moderate CV (48.9%), the highest compared to the other channels in this system, a strong negative correlation (R_s -0.73) and moderate R^2 (0.47).

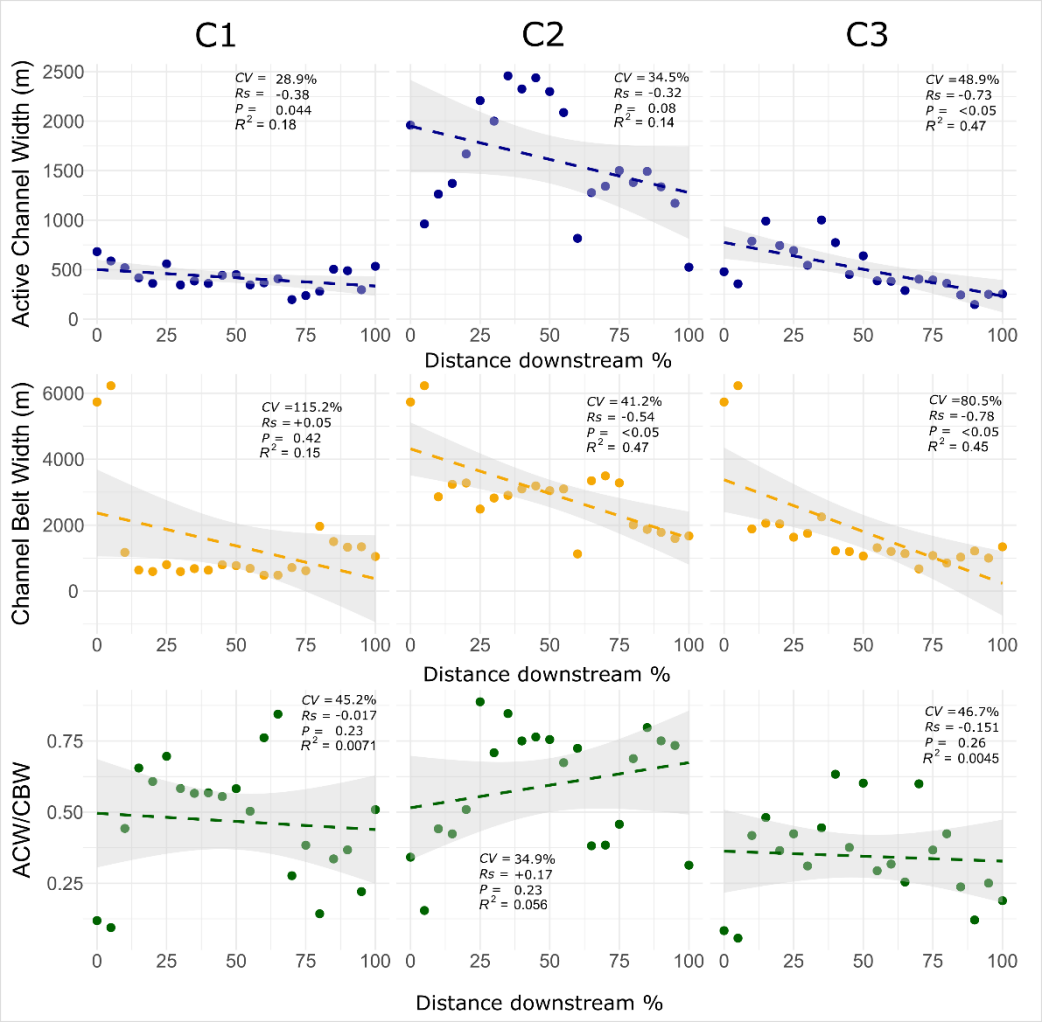

Figure 4.3: Individual plots for active channel width (ACW), channel belt width (CBW), and ACW/CBW ratio for the three channels that make up the averages in Figure 3, corresponding to the channels labelled in Figure 2 (C1, C2, C3). Statistics annotated on graphs include Linear Regression (trendline and R^2), coefficient of variation (CV), and Spearman's Rank Correlation Coefficient (Rs and P value).

Channel Belt Width (CBW)

Mean CBW for the dataset that combines the three measured channels (**Figure 4.2**) also shows a very high variance (CV 76.1%) and a weaker R^2 (0.37). The mean CBW has maximum mean value of 6228.2 m at 5% downstream but significantly narrows at the 10% interval (minimum mean width 937.8 m). There is a strong significant negative correlation (R_s -0.86).

The individual CBW for channels 1, 2, and 3 have the same width (maximum 6228.2 m) from 0 – 5% downstream before the decrease from 10% downstream (**Figure 4.3**). Channel 1 narrows to a minimum width of 481.5 m, however beyond the 10% interval, little change is observed as indicated by a R_s +0.05 (P value 0.42) and a very weak R^2 (0.15). The CV is exceptionally high (115.2%). Channel 2 has a moderately significant negative correlation (R_s -0.54), decreasing downstream with a minimum belt width of 1127.3 m. Channel 2 has a lower variance (CV 41.2%), and a moderate R^2 (0.47). Channel 3 follows a similar pattern to the others (minimum 673.5 m), where the belt narrows from the 10% interval, but differs due to a decrease as shown by a strong negative correlation (R_s -0.78). The CV is also high (80.5%) and there is a moderate R^2 (0.45).

Active Channel / Channel Belt Width (ACW/CBW)

The mean ACW/CBW ratio for the whole dataset (**Figure 4.2**) and for the individual channels (**Figure 4.3**) shows very little in way of statistically significant downstream patterns, with the mean plot (**Figure 4.2**) having a moderate CV of 32.9%, but no significant correlation (R_s -0.12, P Value 0.3) and a very low R^2 (0.0051). Similar trends are observed for the individual channel ratio plots, each with a moderate variance (CV for channel 1 - 3: 45.2%, 34.9%, 46.7%). There are no significant correlations for each channel (C1: R_s -0.017 P value 0.23, C2: R_s 0.17 P value 0.23, C3: R_s -0.151 P value 0.26), coupled with very weak R^2 (C1: 0.0071, C2: 0.056, C3: 0.0045).

Active Channel: Channel Belt: Overbank

When considering just the active channel percentage across the active DFS lobe (**Figure 4.2**), a significantly strong negative correlation (Rs -0.96) is observed; the proportion decreasing from ~65% to ~30% within the medial zone. This trend is coupled with a high, and significant regression (R^2 0.89) but low CV (28.7%). The channel belt proportion (CV 20%) follows a similar pattern (R_s -0.96 and R^2 0.89), yet proportions decrease from ~75% to 50%.

Figure 4.4b shows the data as absolute values (cumulative widths for active channel and channel belt taken across each transect downstream) and, upon review, true downstream decreases in the proportion of active channel and belt are absent or less significant compared to the normalised dataset (**Figure 4.2** and **4.4b**). Overbank deposits become more abundant downstream (**Figure 4.4b**), while the cumulative widths of channel belt and active channels remain constant. There is a significant strong positive correlation for overbank deposits (R_s +0.98, R^2 0.97), coupled with a moderate variation coefficient of 50.2%, compared with the absolute active channel and channel belt proportions, which have a very low CV of 8.8% and 9.3%. Cumulative active channel width has a moderate negative correlation (R_s -0.5), much weaker than the normalised percentages, however still indicating a slight downstream decrease. However, absolute channel belt widths have a moderate positive correlation (R_s +0.45), increasing downstream, the opposite to what was seen with the normalised data. When compared against the extremely low CV, it can be assumed that the proportion of active channels and channel belt reduce very little downstream in the medial zone for AL01_POL.

Sweep Angle (SA)

The sweep angle (**Figure 4.1**) across the whole DFS surface shows a downstream increase in angle. The SA at the proximal zone (5284 m downstream) starts at 57.5° and expands to 77.1° upon the start of the medial zone (11 km downstream). At the end of the medial zone (27.3 km), the SA is 83° and further expands to 86.7° upon reaching the toe (29.7 km) of the DFS numerically highlighting a radial shape to the system.

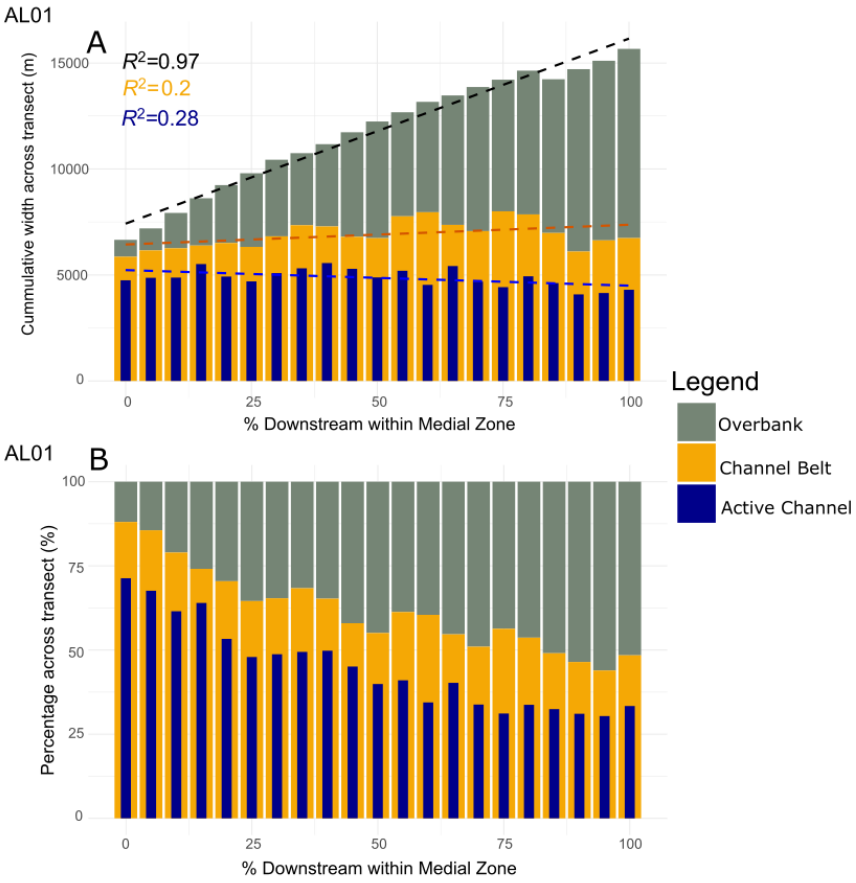

Figure 4.4: Stacked bar plots for the absolute proportion of overbank, channel belt and active channel on the surface of the active medial zone for AL01_POL (A), based on the cumulative widths taken across transects, with regression lines and R^2. And (B) the percentage proportion of overbank, channel belt, active channel for the across the transects for the active medial zone.

The SA of the active lobe surface (**Figure 4.1**) followed a similar trend, with a downstream increase in angle from proximal (25°), to the start (26°) and end (33.8°) of the medial, and on termination at the toe (35.9°).

4.1.2 AL02_POL: *Dry Creek, Alaska, USA*

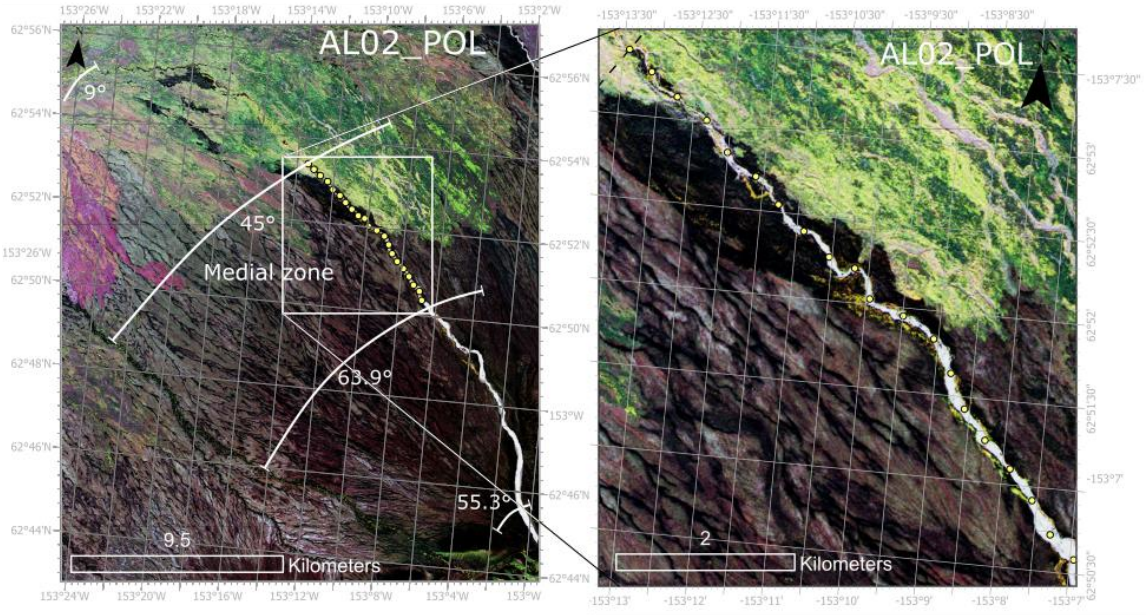

Figure 4.5: Whole DFS area of AL02_POL with sweep angles annotated in sequence of proximal, start of medial, end of medial, and fan toe.

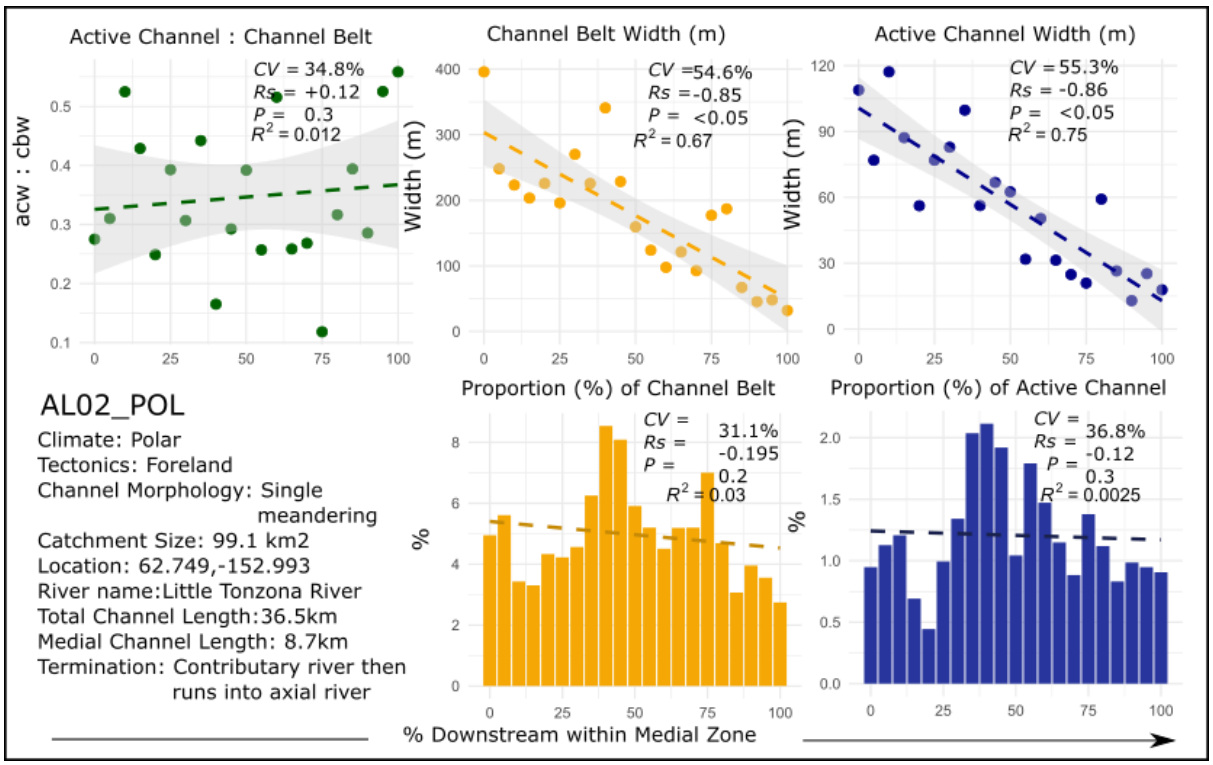

Figure 4.6: Plots summarising the primary results for AL02_POL with contextual information from the study area. Individual plots for the active channel width / channel belt downstream ratio, the channel belt width, active channel width, and the individual proportions of channel belt and active channel across the active lobe of the medial zone.

Active Channel Width (ACW)

The ACW plot in **Figure 4.6** comprises of data from a single channel and shows that there is a significant strong negative correlation in width (R_s -0.86) with a strong fit to the trendline (R^2 0.75), where there is a downstream decrease from maximum of 117.2 m to a minimum of 13 m (mean of 56.8 m). There is a moderate level of variance for ACW (CV 55.3%).

Channel Belt Width (CBW)

CBW for AL02_POL (**Figure 4.6**) also has a significantly strong negative correlation (R_s -0.85, R^2 0.67) and moderate CV (54.6%), where the maximum value is 395.8 m wide and the minimum 32 m (mean 176.6 m), demonstrating a downstream decrease in CBW.

Active Channel / Channel Belt Width (ACW/CBW)

The ratio of ACW/CBW (**Figure 4.6**) shows no statistically significant correlation (R_s 0.12, P value 0.3), and no overall trend (R^2 0.012), however CV is moderate to low (34.8%) where ratio values range from 0.56 (maximum) to 0.12 (minimum).

Active Channel: Channel Belt: Overbank

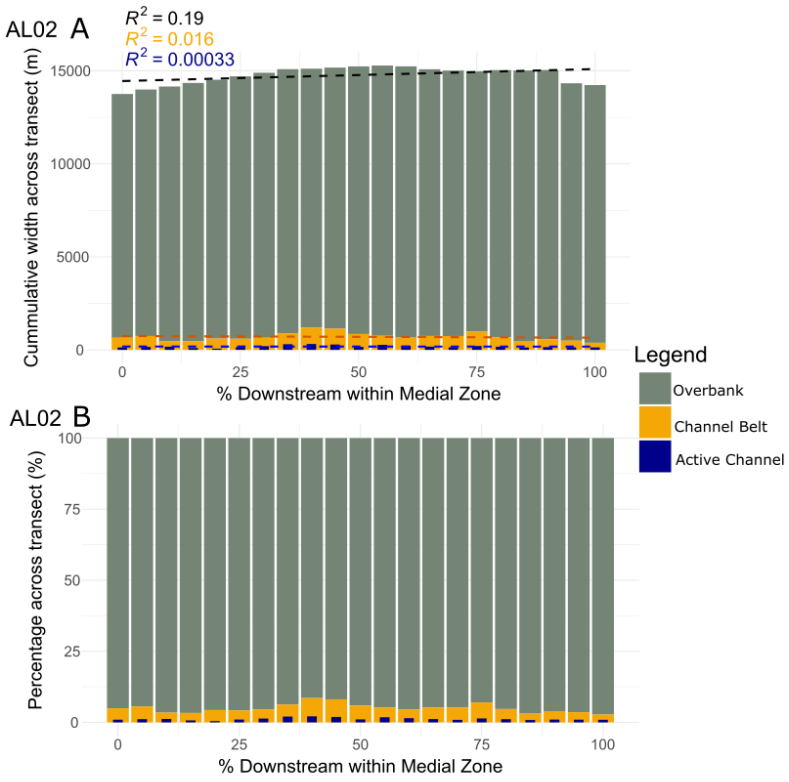

Figure 4.7: Stacked bar plots for the absolute proportion of overbank, channel belt and active channel on the surface of the active medial zone for AL02_POL (A), based on the cumulative widths taken across transects, with regression lines and R^2. And (B) the percentage proportion of overbank, channel belt, active channel for the across the transects for the active medial zone.

The individual proportions of active channel and channel belt (**Figure 4.6**) have moderate to low CV (AC 36.8%, CB 31.1%). The percentage of channel belt fluctuates downstream (maximum: 8.5%, minimum: 2.7%, mean: 5%), but overall has no statistically significant correlation (R_s 0.2, P value 0.2, and R^2 0.03). A similar trend is seen for the active channel percentage (R_s -0.12, P value 0.3, and R^2

0.0025), with a minimum of 0.4% and maximum of 2.1% (mean 1.2%). The proportion of overbank covers most of the medial zone of AL02_POL (downstream average 95%), seen in **Figure 4.7b.**

Furthermore, the absolute proportion using cumulative widths consists of a similar trend to the normalised percentages. Active channel (R_s -0.02, R^2 0.00033) and channel belt (R_s -0.12, and R^2 0.016) again have no statistically significant downstream trend, with moderate variation (CV 39.1% and 31%). However, overbank has a moderately strong positive correlation (0.48), but a very low variation (CV 2.8%) and R^2 (0.19). Overall, the proportions of active channel, channel belt, and overbank remain relatively constant downstream.

Sweep Angle (SA)

There is a small increase in sweep angle across the DFS (**Figure 4.5**). The SA at the proximal zone (2.5 km downstream) starts at 55.3° to 63.9° upon the start of the medial zone (11.3 km downstream). The SA remains relative constant within the medial zone, however tapers from the end margin of the medial (19.3 km downstream) 45° to 9° upon reaching the toe (30.1 km) of the DFS. This indicates that the system has a relatively narrow morphology. The measured area for the whole DFS surface covers the same area as the active lobe; image resolution and vegetation limits identifying the full extent of the whole DFS surface.

4.1.3 AL03_POL: *Little Tonzona River, Alaska, USA*

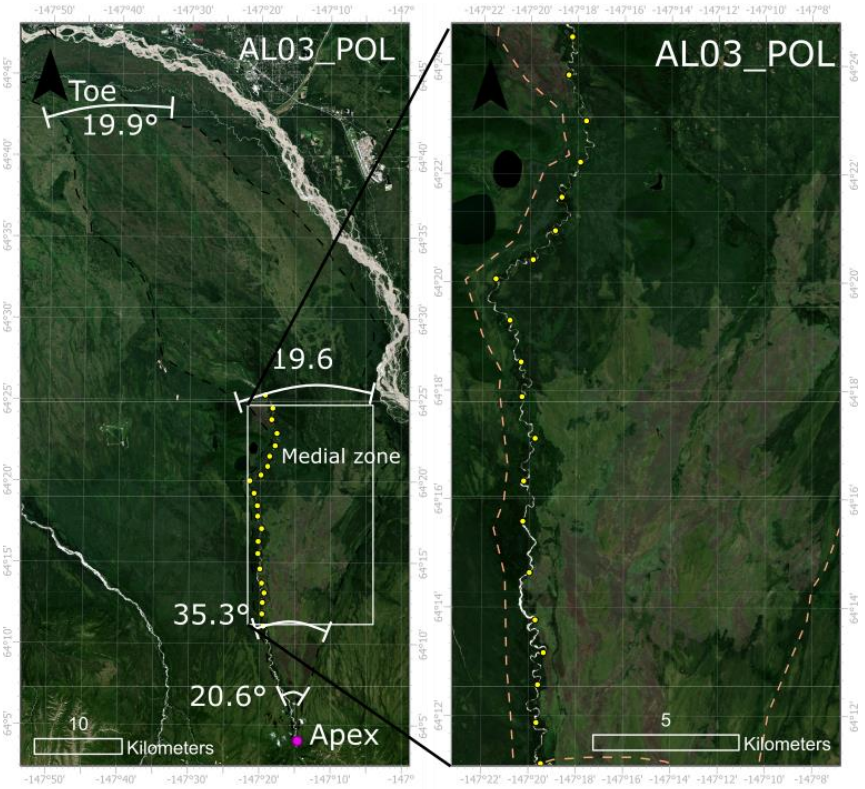

Figure 4.8: Whole DFS area of AL03_POL with sweep angles annotated in sequence of proximal, start of medial, end of medial, and fan toe.

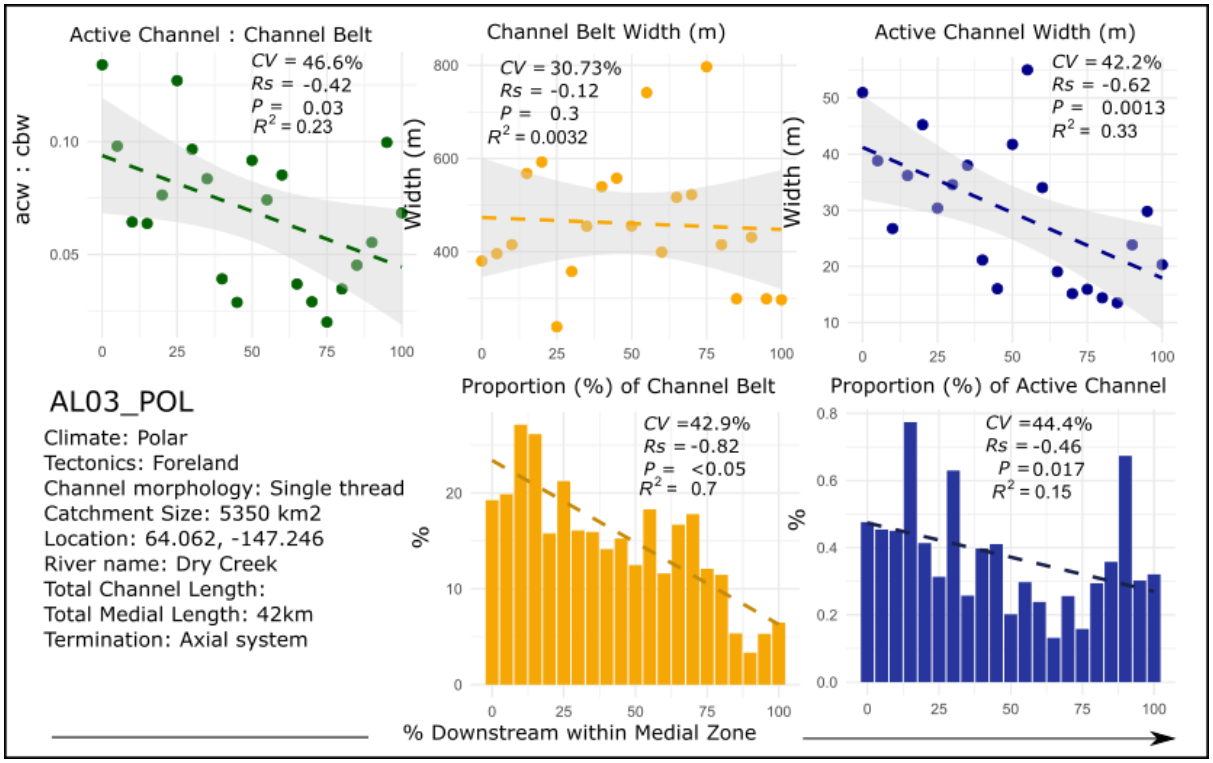

Figure 4.9: Plots summarising the primary results for AL03_POL with contextual information from the study area. Individual plots for the active channel width / channel belt downstream ratio, the channel belt width, active channel width, and the individual proportions of channel belt and active channel across the active lobe of the medial zone.

Active Channel Width (ACW)

ACW (**Figure 4.9**) has a moderately strong negative correlation (R_s -0.62), decreasing in width downstream (maximum: 55 m, minimum: 13.5 m, mean: 29.6 m). R^2 is moderate to weak (0.33) and the variability is moderate (CV 42.2%).

Channel Belt Width (CBW)

CBW for AL03_POL has no apparent correlation or downstream trends (R_s -0.12 and P value 0.3, R^2 0.0032), but a moderate to low variability (CV 30.73%) with widths ranging from 796.6 m (maximum) to 239.2 m (minimum), and a mean of 460.7 m.

Active Channel / Channel Belt Width (ACW/CBW)

The ratio of ACW to CBW has a slightly significant moderately strong negative correlation (R_s -0.42 and P value 0.03), and a weaker R^2 (0.23) alongside a moderately high variability (CV 46.6%). Ratio values are very low, ranging from minimum of 0.02 to maximum 0.13 (mean 0.07).

Active Channel: Channel Belt: Overbank

The downstream percentage of channel belt has a very strong negative correlation (R_s -0.82, R^2 0.7), highest proportions being near the start of the medial (27.1%) and lowest near the end (3.3%), with a mean of 27.1%. However, the percentage of active channel only has a moderate negative correlation (R_s -0.46) but weak R^2 (0.15), having decreased in proportion until 65% downstream where the percentage increases (maximum 0.77%, minimum: 0.13%). Active channel environments make up a very small proportion of the overall medial zone (mean: 0.37%), seen in **Figure 4.10**. Variability is moderate for both channel belt (CV 42.9%) and active channel (CV 44.4%).

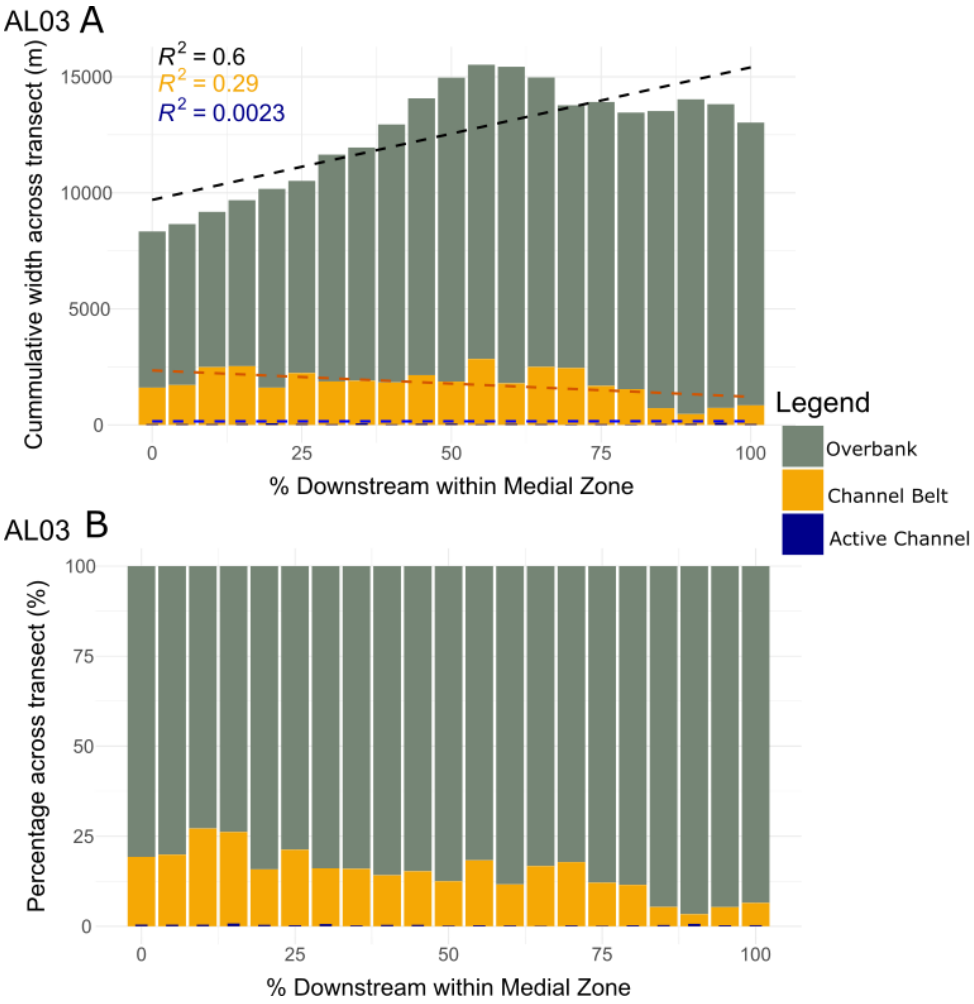

Figure 4.10: Stacked bar plots for the absolute proportion of overbank, channel belt and active channel on the surface of the active medial zone for AL03_POL (A), based on the cumulative widths taken across transects, with regression lines and R^2. And (B) the percentage proportion of overbank, channel belt, active channel for the across the transects for the active medial zone.

Figure 4.10a shows the absolute values used in calculating the percentages of **Figure 4.10b** and **4.9**. The cumulative widths for channel belt have a moderate negative correlation (R_s -0.46), however a weaker R^2 (0.29). However, absolute active channel widths have no significant downstream correlation (R_s 0, R^2 0.0023). Variability remains similar to the normalised percentages for channel belt (36.6%) and active channel (40.4%). However, the absolute widths of overbank environments have a strong positive correlation (R_s 0.81) and R^2 (0.6), alongside a low variability (CV 22.6%).

Sweep Angle (SA)

As expected for DFS, the SA or AL03_POL increases downstream from proximal (20° at 5 km directly downstream) to the start of the medial (35.3° 12.7 km downstream). However, the fan area narrows to 19.6° upon the end of the medial (40.4 km downstream) but the SA remains constant nearing the toe (80 km downstream). Therefore, the overall shape of this DFS is much narrower than others, such as AL01_POL, as the neighbouring systems and topography constrain it.

4.1.4 AR01_TROP: *Bermejo River, Argentina*

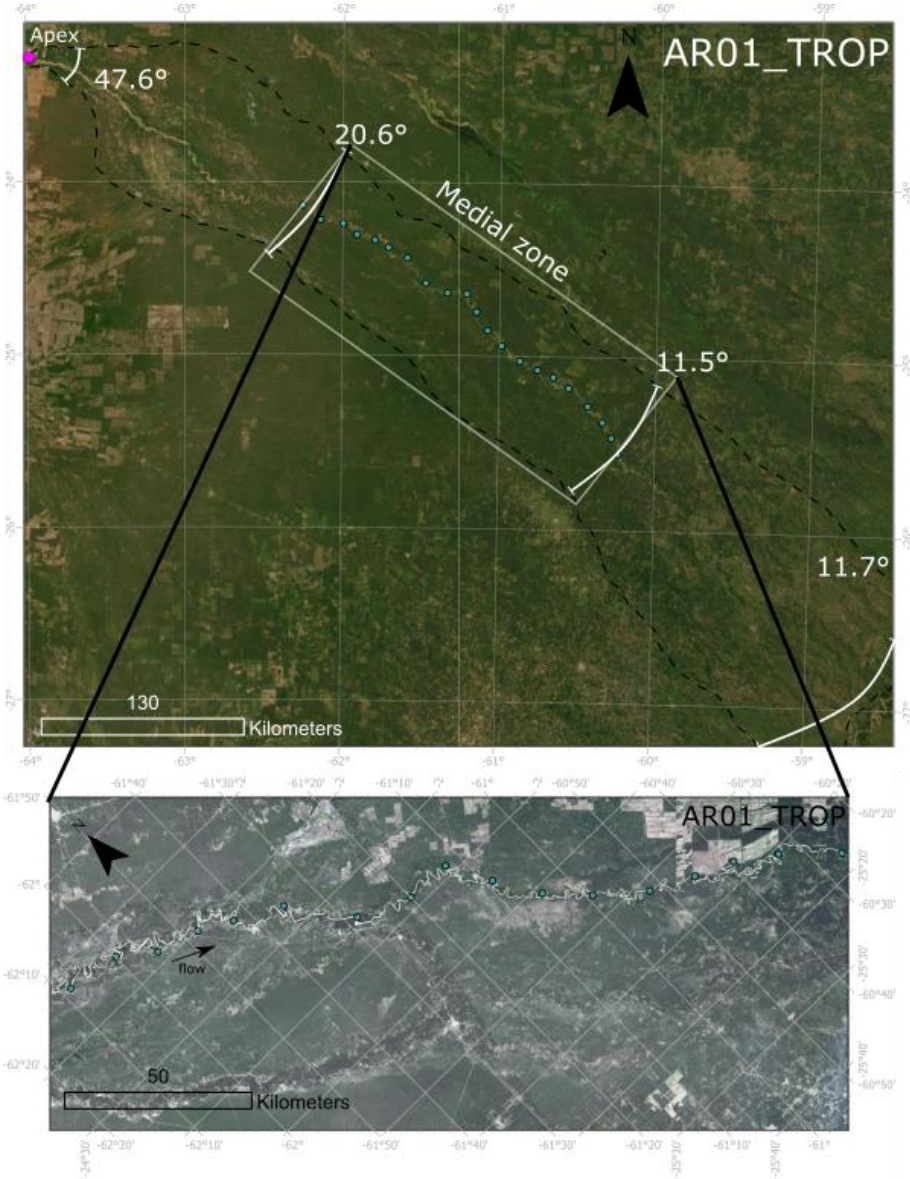

Figure 4.11: Whole DFS area of AR01_TROP with sweep angles annotated in sequence of proximal, start of medial, end of medial, and fan toe.

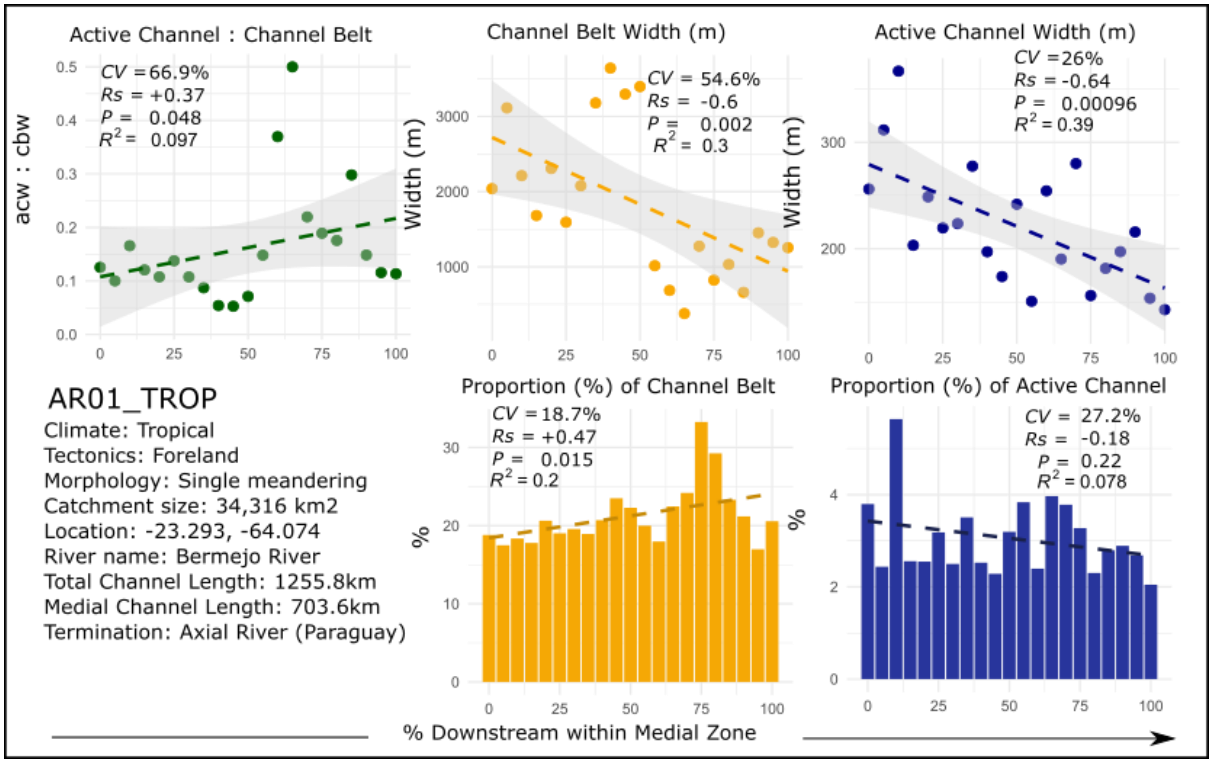

Figure 4.12: Plots summarising the primary results for AR01_TROP with contextual information from the study area. Individual plots for the active channel width / channel belt downstream ratio, the channel belt width, active channel width, and the individual proportions of channel belt and active channel across the active lobe of the medial zone.

Active Channel Width (ACW)

There is a general decrease in ACW (maximum: 355.9 m, minimum: 142.7 m, mean 221 m), with a moderately strong negative correlation (R_s -0.64) and a moderately low R^2 (0.39). However, variation is low (CV 26%).

Channel Belt Width (CBW)

A similar trend is observed for CBW (**Figure 4.12**), where there is a moderately strong negative correlation (R_s -0.6). However, the data fluctuates downstream: peaking at the 40% interval then decreasing (maximum: 3641.2 m, minimum: 380.4 m, mean: 1830.9 m), as a result, variation is overall high (CV 54.6%) and R^2 is relatively low (0.3).

Active Channel / Channel Belt Width (ACW/CBW)

ACW/CBW has a moderate to weak positive correlation (R_s 0.37, P value 0.048). However, the increase in the ratio downstream is very minor: maximum of 0.50 and a minimum of 0.05 (mean 0.16). Variation downstream is high (CV 66.9%) and as the data is well dispersed, the R^2 is very low (0.097). Therefore, they may not be any significant downstream trend.

Active Channel: Channel Belt: Overbank

The individually plotted channel belt percentage (**Figure 4.12**) has a moderate positive correlation (R_s 0.47, R^2 0.2) and a low variation (CV 18.7%); percentages range from 17% (minimum) to 33.3% (maximum), with a mean of 21.3%. The active channel percentage has a higher variation (CV 27.2%) but no significant correlation (R_s -0.18, P value 0.22, and R^2 0.078). Active channel makes up a low proportion of the medial zone (minimum: 2%, maximum: 5.6%, mean: 3.1%), whereas the overbank deposits cover a large area of the medial zone (**Figure 2.13b**).

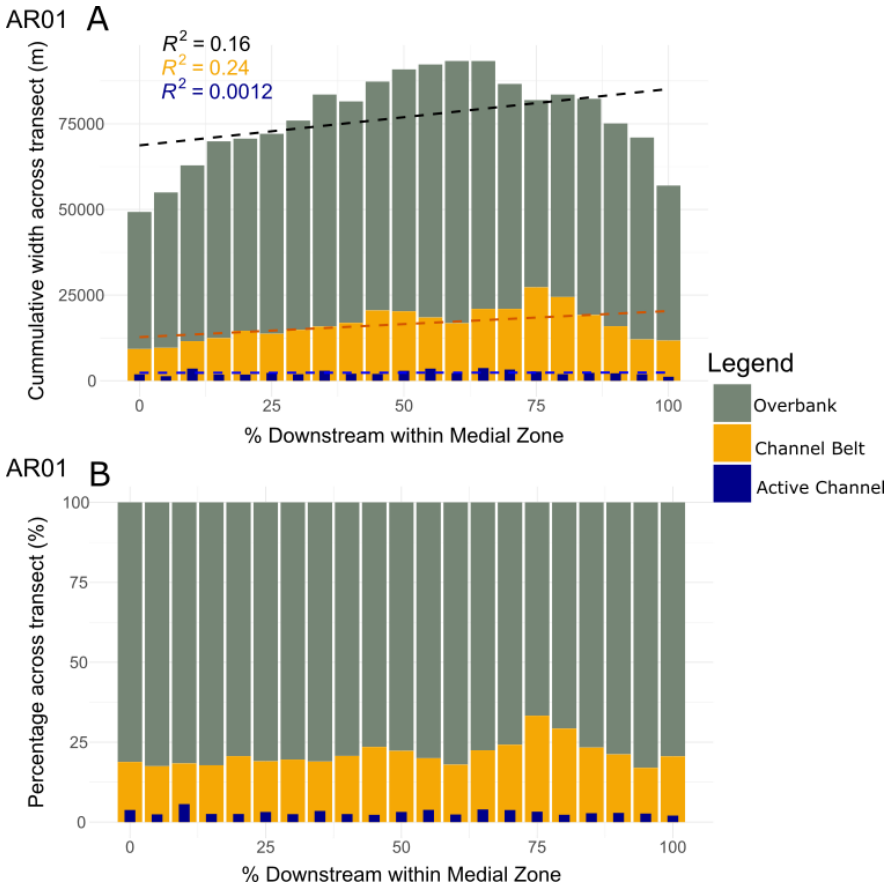

Figure 4.13: Stacked bar plots for the absolute proportion of overbank, channel belt and active channel on the surface of the active medial zone for AR01_TROP (A), based on the cumulative widths taken across transects, with regression lines and R^2. And (B) the percentage proportion of overbank, channel belt, active channel for the across the transects for the active medial zone.

Figure 4.13a shows the absolute proportions for channel belt, active channel, and overbank within the medial zone, with similar trends to the individual percentages (**Figure 4.12**). There is no downstream correlation for active channel cumulative width (R_s 0.15, R^2 0.0012) and variation similar to its corresponding percentage (CV 30.7%). Similarly, cumulative channel belt widths have moderate positive correlation (R_s 0.5, R^2 0.24), and moderate to low variation (CV 29%). Overbank deposits also has no correlation (R_s 0.26) and a weak R^2 (0.16), but low variation (CV 16%), as the system radiates downstream until approximately 50% where it narrows.

Sweep Angle (SA)

AR01_TROP SA starts (**Figure 4.11**) at the proximal zone radiating out to 47.6° (26 km direct distance downstream) but narrows downstream from the start (20.6° at 202.4 km downstream) to the end of the medial (11.5° at 457.7 km downstream). SA remains constant upon reaching the toe (11.7° at 601 km downstream). These SA indicate the shape of this DFS to be quite narrow, confined by neighbouring systems.

4.1.5 AR02_TROP: *Itiyui River, Argentina*

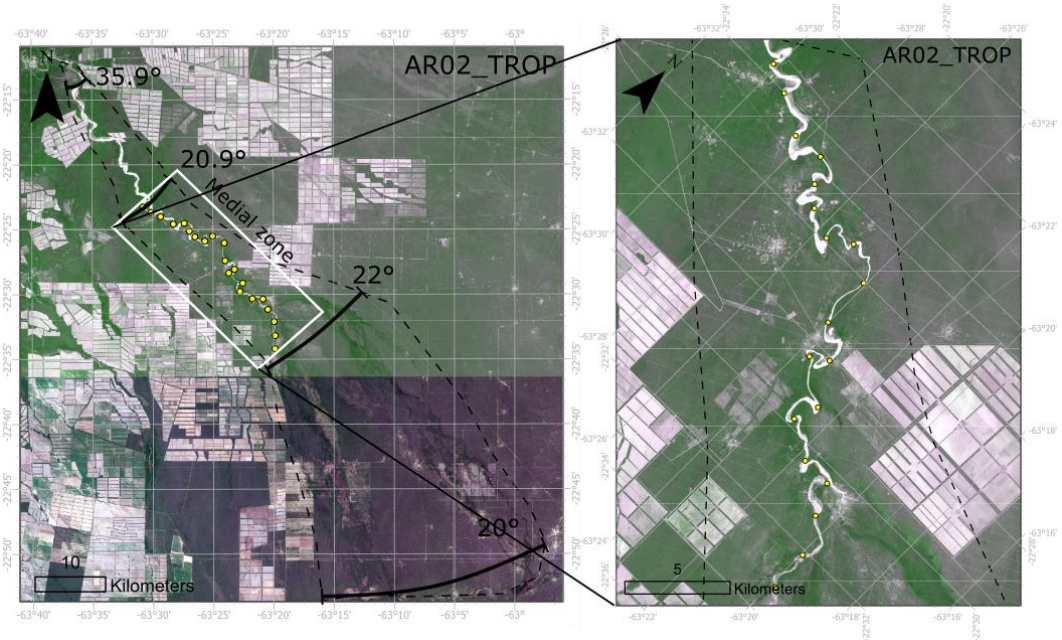

Figure 4.14: Whole DFS area of AR02_TROP with sweep angles annotated in sequence of proximal, start of medial, end of medial, and fan toe.

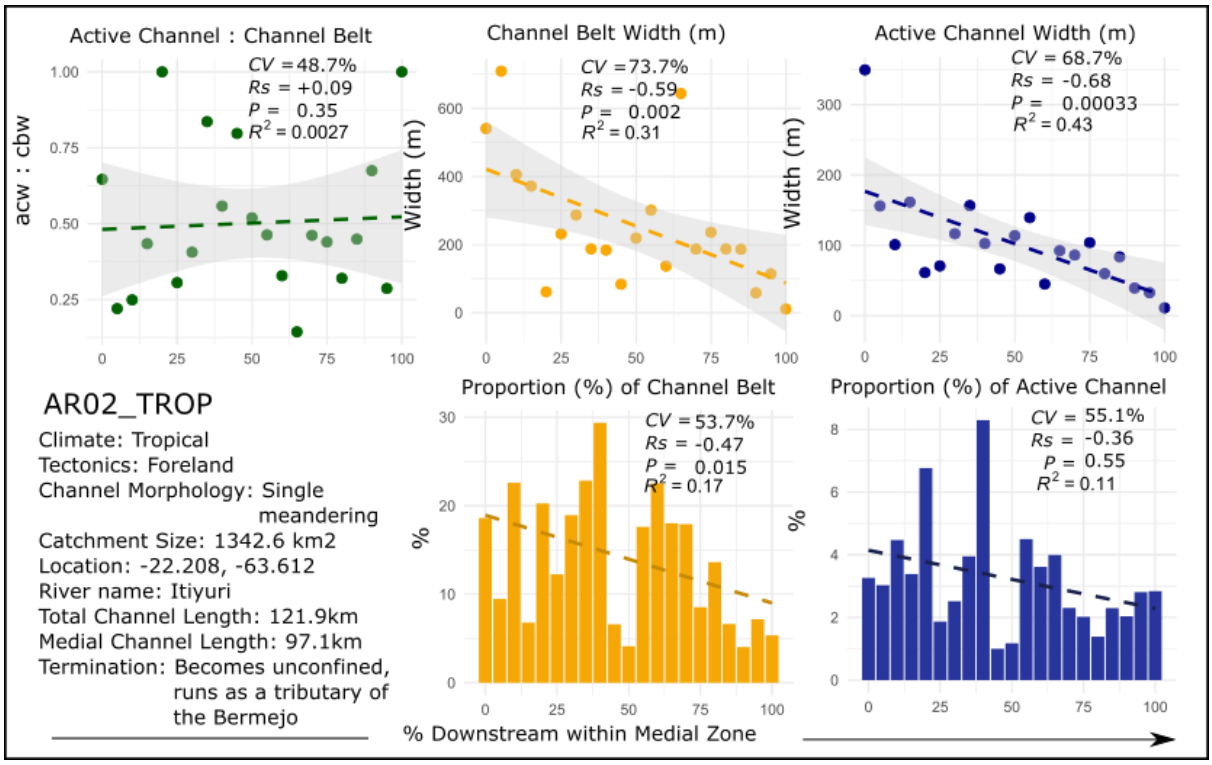

Figure 4.15: Plots summarising the primary results for AR02_TROP with contextual information from the study area. Individual plots for the active channel width / channel belt downstream ratio, the channel belt width, active channel width, and the individual proportions of channel belt and active channel across the active lobe of the medial zone.

Active Channel Width (ACW)

ACW (**Figure 4.15**) starts the medial zone at its widest (maximum 349.4 m) and has a strong downstream negative correlation (R_s -0.68), and a reasonably good fit to the trendline (R^2 0.43), however high variability is observed (CV 68.7%). The minimum width is 11.1 m with a mean of 102.4 m.

Channel Belt Width (CBW)

Similarly, CBW has high variability (CV 73.7%) and a moderate to strong negative correlation (R_s -0.59), however a weaker R^2 (0.31). The maximum widths at the start of the medial is 709.4 m and decrease to a minimum of 11.1 m at the end of the medial (mean of 254.5 m).

Active Channel / Channel Belt Width (ACW/CBW)

There are no apparent trends for the ACW/CBW ratio, as there is no significant correlation (R^s 0.09, P value 0.35) and a very weak R^2 (0.0027). The data is moderately variable (CV 48.7%), with a minimum ratio value of 0.14 to a maximum of 1.0 (mean 0.50).

Active Channel: Channel Belt: Overbank

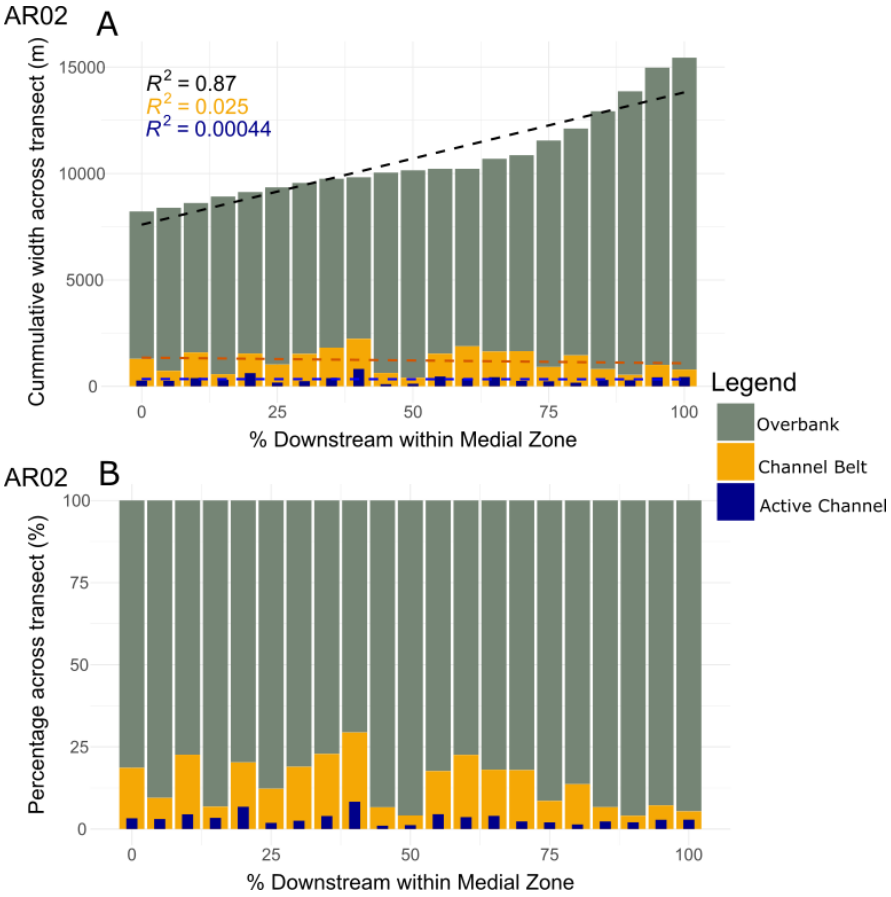

Figure 4.16: Stacked bar plots for the absolute proportion of overbank, channel belt and active channel on the surface of the active medial zone for AR02_TROP (A), based on the cumulative widths taken across transects, with regression lines and R^2. And (B) the percentage proportion of overbank, channel belt, active channel for the across the transects for the active medial zone.

The individual plots for the downstream percentages of channel belt and active channel (**Figure 4.15**) show some statistical downstream decreases. Channel belt has high downstream variability (CV 53.7%), a weak R^2 (0.17), yet a moderately strong negative correlation (R_s -0.47). The maximum

percentage is 14% and minimum 4% (mean 14%). Similarly, active channel proportion has a variability of 55.1%, and a moderate to weak negative correlation (R_s -0.36) and weak R^2 0.11. Maximum percentage is 8.3% and minimum 1% (mean 3.2%). Overall, overbank makes up the largest proportion within the medial across this system, averaging 96.8% (**Figure 4.16**).

In **Figure 4.16a**, the trends observed in the normalised dataset are absent for the cumulative widths. Variability is moderately high, however there is no significant correlation and very weak R^2 for channel belt (R_s -0.14, R^2 0.025, CV 42.6%) and active channel (R_s 0.05, R^2 0.0004, CV 50%). However, overbank has very strong positive correlation and R^2 (R_s 0.9, R^2 0.87), where the DFS area expands downstream (**Figure 4.14**), but a lower variability (CV 24%).

Sweep Angle (SA)

In **Figure 4.14**, SA is widest at the proximal zone (10km directly downstream) at 35.9° however narrows to 20.9° upon the start of the medial zone (25.2km downstream). This stays relatively constant with some very minor widening (22°) at the end of the medial zone (52.5km downstream) to the DFS toe (20°), 95.2km downstream. Therefore, the shape of the DFS is relatively narrow, constrained at the fan margins.

4.1.6 BO01_TROP: *Parapeti, Bolivia*

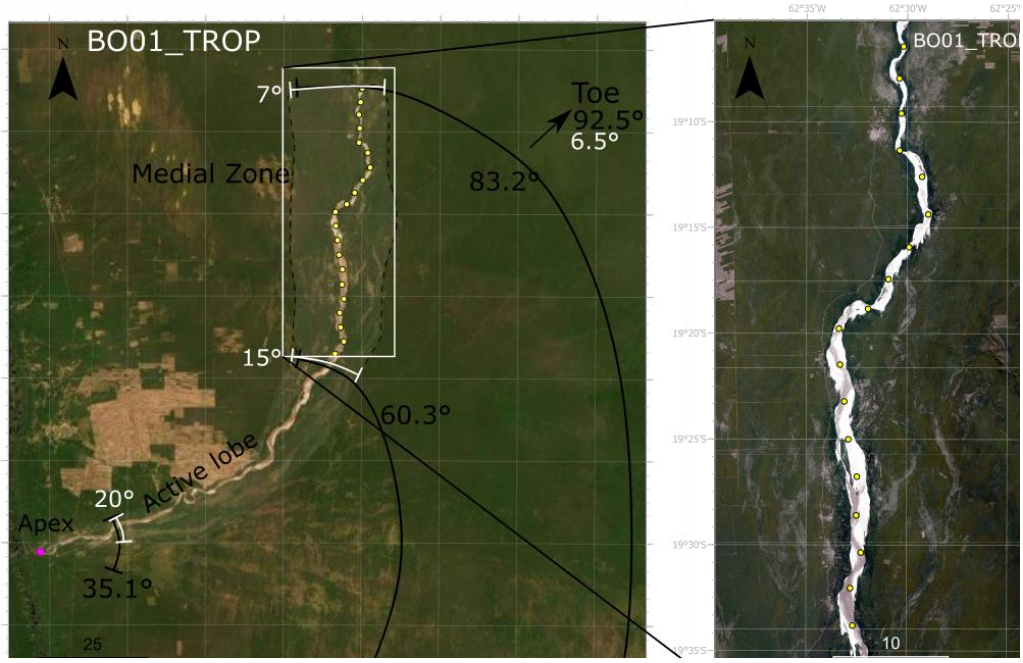

Figure 4.17: Whole DFS area of BO01_TROP with sweep angles annotated in sequence of proximal, start of medial, end of medial, and fan toe. Highlighted area indicates the active lobe of the DFS where measurements took place.

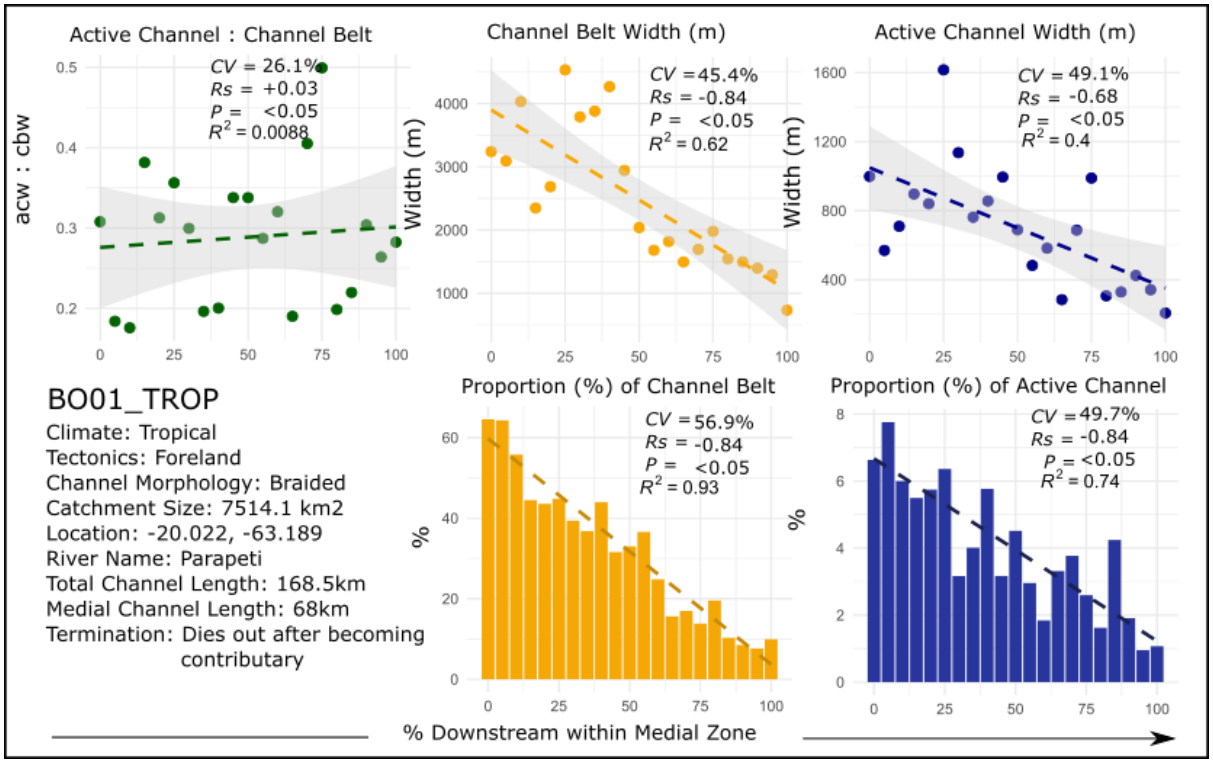

Figure 4.18: Plots summarising the primary results for BO01_TROP with contextual information from the study area. Individual plots for the active channel width / channel belt downstream ratio, the channel belt width, active channel width, and the individual proportions of channel belt and active channel across the active lobe of the medial zone.

Active Channel Width (ACW)

BO01_TROP (**Figure 4.18**) has a significantly strong negative correlation (R_s -0.68), where widest values are near the start of the medial zone (1615.8 m), narrowing downstream (minimum 207.1 m, mean 700.1 m). There is a moderately high variability (CV 49.1%) alongside a moderate to weak R^1 (0.4).

Channel Belt Width (CBW)

CBW has similar but stronger trends to ACW (**Figure 4.18**); there is a very strong negative correlation (R_2 -0.84) and a strong R^2 (0.62). Width decreases significantly downstream, with maximum width of 4535 m, a minimum of 733.2 m (mean 2476.4 m), and moderate variance (CV 45.4%).

Active Channel / Channel Belt Width (ACW/CBW)

Similar to the other systems, there are no statistically significant trends in the ACW to CBW ratio (**Figure 4.18**) of BO01_TROP (R_s 0.03 and P value 0.45, R^2 0.0088). The data is scattered downstream ranging between 0.50 and 0.18 (mean 0.29) but a lower CV of 26.1% is observed.

Active Channel: Channel Belt: Overbank

Individually, the proportion of channel belt and active channel both have very strong negative correlations (Both Rs -0.84) and strong fits to the linear regression (R^2 0.93, and 0.75) (**Figure 4.18**). Variability is also moderately high in both parameters. Channel belt percentage decreases from 64.6% to 7.6% (mean 31.7%) with a CV of 56.9%. Active channel percentage decreases from 7.8% to 1% (mean 4%), constituting a small proportion to the active medial lobe.

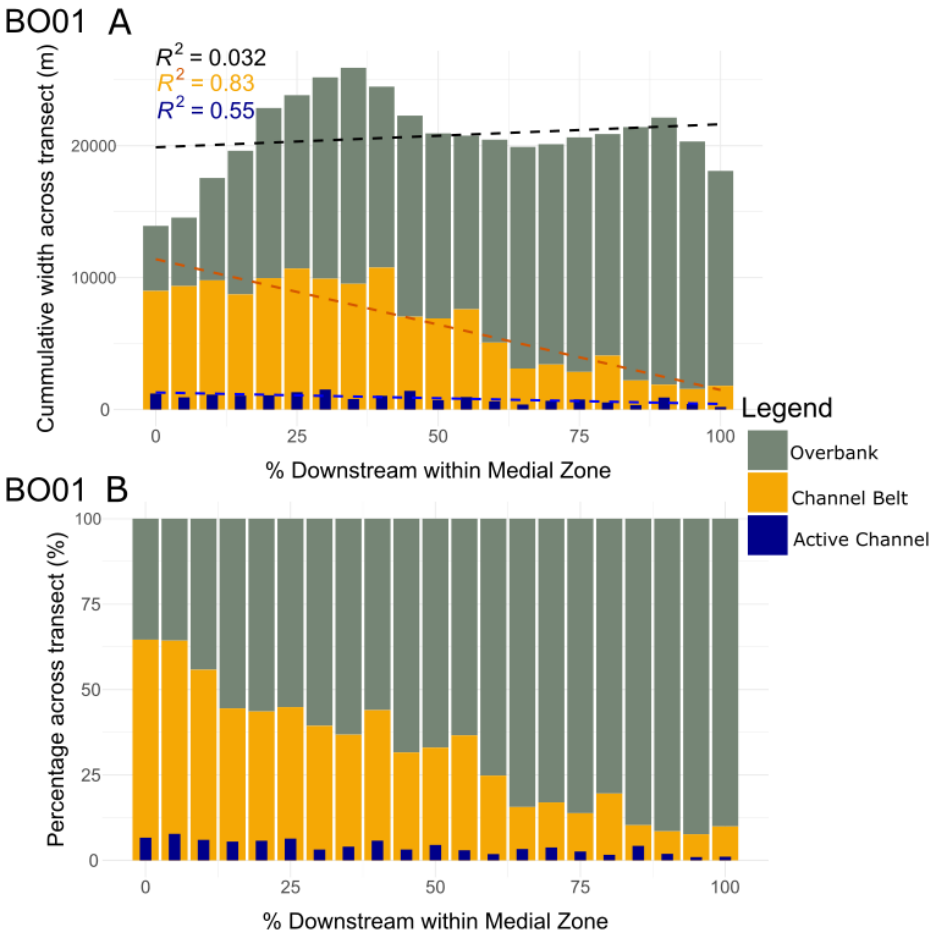

Figure 4.19: Stacked bar plots for the absolute proportion of overbank, channel belt and active channel on the surface of the active medial zone for BO01_TROP (A), based on the cumulative widths taken across transects, with regression lines and R^2. And (B) the percentage proportion of overbank, channel belt, active channel for the across the transects for the active medial zone.

Figure 4.19a shows similar trends to the normalised percentages. Channel belt and active channel cumulative widths decrease downstream indicated by a strong negative correlation (R_s -0.86 and -0.78), similar variance (52.5% and 42.6%) but slightly weaker R^2 (0.83 and 0.55). Alternatively, the proportion of overbank has a significantly strong positive correlation (R_s 0.89) but a weaker R^2 (0.55), and a lower CV (29.3%).

Sweep Angle (SA)

The SA for the over DFS surface for BO01_TROP (**Figure 4.17**) radiates downstream, starting at 35° (20km direct downstream) to 60.3° reaching the start of the medial zone (72km downstream). The surface radiates out further (83.2°) upon reaching the end of the medial zone (120.3 km) before terminating at the toe (160km downstream) at an angle of 92.5°. This DFS expands over a wide area,

similar to other systems that largely radiate out. Alternatively, the SA for the active lobe studied is much narrower, radiating from 20° to 15° from the proximal to medial, remaining consistently narrow from the end of the medial (7°) to toe (6.5°).

4.1.7 AG01_DRY: *Que del Mehaiguene, Algeria*

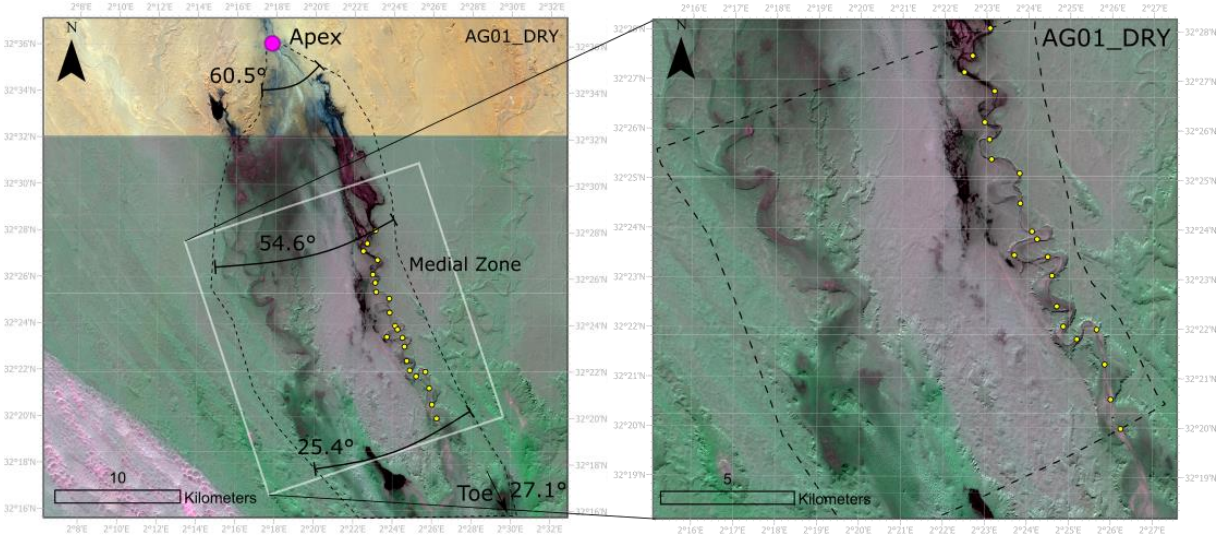

Figure 4.20 Whole DFS area of AG01_DRY with sweep angles annotated in sequence of proximal, start of medial, end of medial, and fan toe.

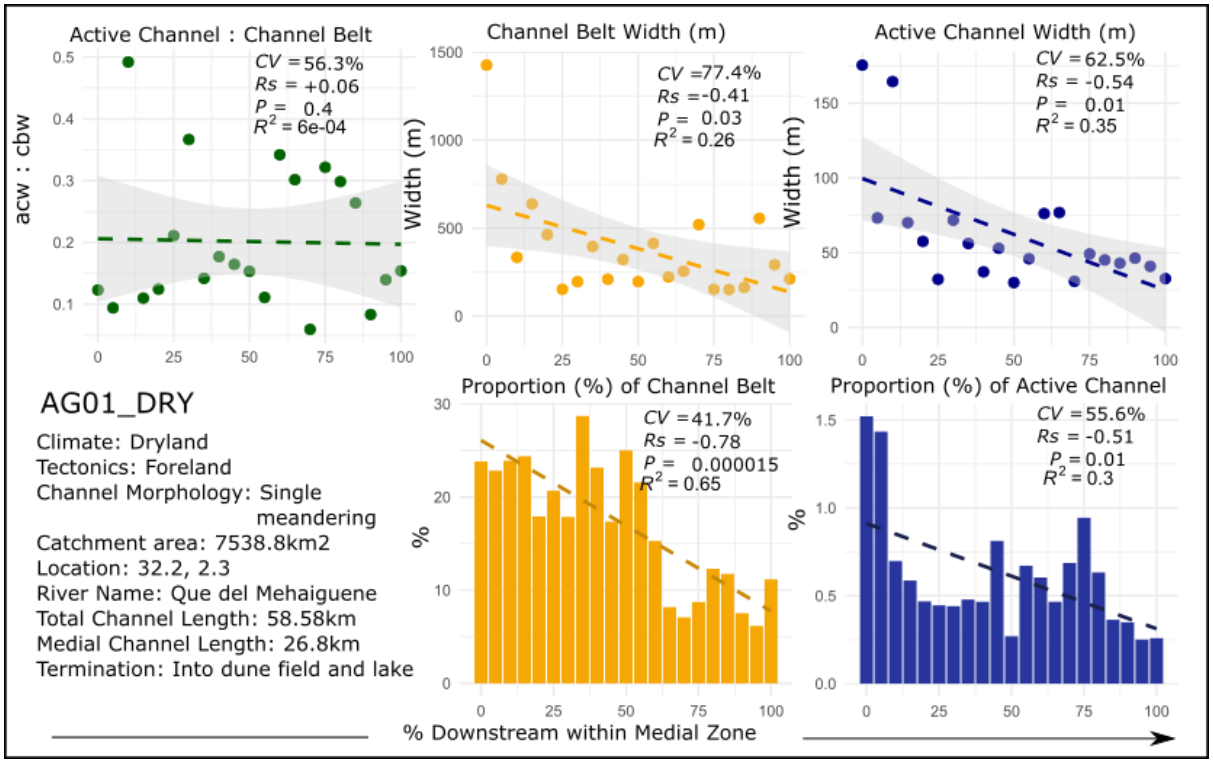

Figure 4.21: Plots summarising the primary results for AG01_DRY with contextual information from the study area. Individual plots for the active channel width / channel belt downstream ratio, the channel belt width, active channel width, and the individual proportions of channel belt and active channel across the active lobe of the medial zone.

Active Channel Width (ACW)

There is a moderately strong negative correlation for ACW in AG01_DRY (**Figure 4.21**) (R_s -0.54, R^2 0.35), where the active channel is widest before the 10% interval (maximum 175.4 m) where there is a large drop, followed by a general downstream decrease to a minimum of 30 m (mean 62.2 m), as a result, variability is high across the medial zone (CV 62.5%).

Channel Belt Width (CBW)

CBW also has moderate to weak negative correlation (R_s -0.41) and weak R^2 (0.26), where a similar drop in width occurs after the 5% downstream interval (**Figure 4.21**) (Maximum 1426.3 m). CBW continues to narrow downstream to a minimum of 151.1 m (mean 383.2 m). Similarly, variability is very high – CV of 77.4%.

Active Channel / Channel Belt Width (ACW/CBW)

There is no significant correlation observed in the ratio of ACW to CBW (R_s 0.06 and P value 0.4), plotted in **Figure 4.21**, as well as a very low, and therefore weak trend for the linear regression (R^2 0.0006). Ratio values range from 0.06 to 0.49 (mean 0.20), with moderately high variability (CV 56.3%)

Active Channel: Channel Belt: Overbank

Figure 4.21 and **4.22b** show the percentages of channel belt and active channel across the medial zone of AG01_DRY. Channel belt percentage has a very strong negative correlation (R_s -0.78) and high R^2 (0.65), percentages range from 28.7% to 6.2% (mean 16.9%) with a moderate variability (CV 41.7%). Active channel percentage follows a similar but weaker trend, R_s -0.51 and R^2 0.3, covering a very small proportion of the whole medial zone (mean 0.6%). Percentages range from 0.3% to 1.5%, with a CV of 55.6%.

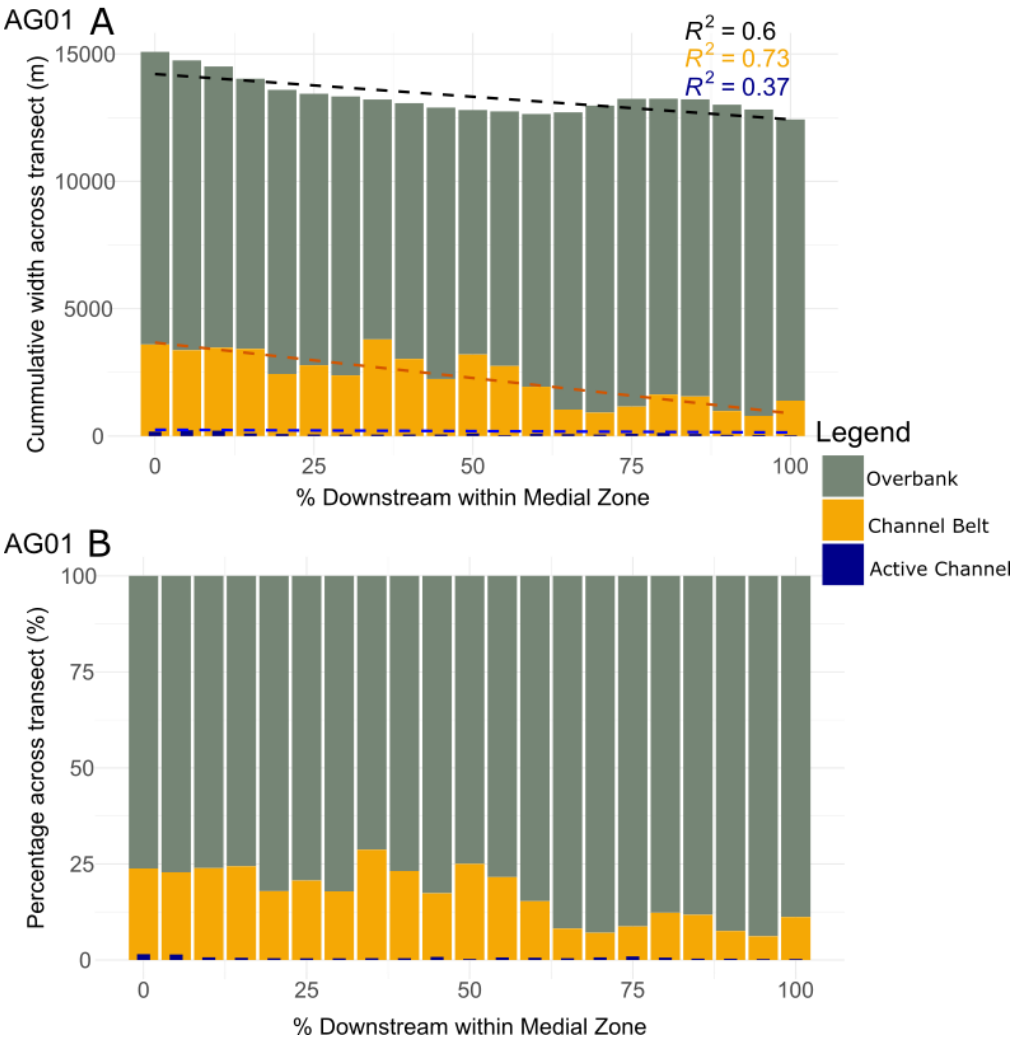

Figure 4.22: Stacked bar plots for the absolute proportion of overbank, channel belt and active channel on the surface of the active medial zone for AG01_DRY(A), based on the cumulative widths taken across transects, with regression lines and R^2. And (B) the percentage proportion of overbank, channel belt, active channel for the across the transects for the active medial zone.

Furthermore, **Figure 4.22a** shows similar downstream trends to the normalised percentages of active channel and channel belt. Cumulative channel belt width has a strong negative correlation (R_s -0.85, and R^2 0.73), and similar variability to the percentage proportion with CV 44.1%. Active channel width again makes up a very small proportion of the medial zone, but nonetheless has a moderate negative correlation (-0.54), weaker R^2 (0.37), and high variability (60.2%). The proportion of overbank appears to have a moderate positive correlation (R_s 0.43), however the linear regression trends negatively, with a strong R^2 (0.6). However, it is apparent from **Figure 4.22a** that the proportion of overbank does not vary much downstream, coupled with a low CV of 7.3%.

Sweep Angle (SA)

Figure 4.20 shows the downstream changes in SA. From the proximal (5.8km directly downstream) to the start of the medial (16.2km downstream), the SA decreases slightly from 60.5° to 54.6°, and again upon reaching the end of the medial (32.3km downstream) to 25.4°. Towards the toe (45km downstream) SA remains relatively constant at 27.1°. The shape of this system is consistently narrow downstream, possibly due to the small size of this system and limited migration of the active channel.

4.1.8 CH01_DRY: *Molcha, China*

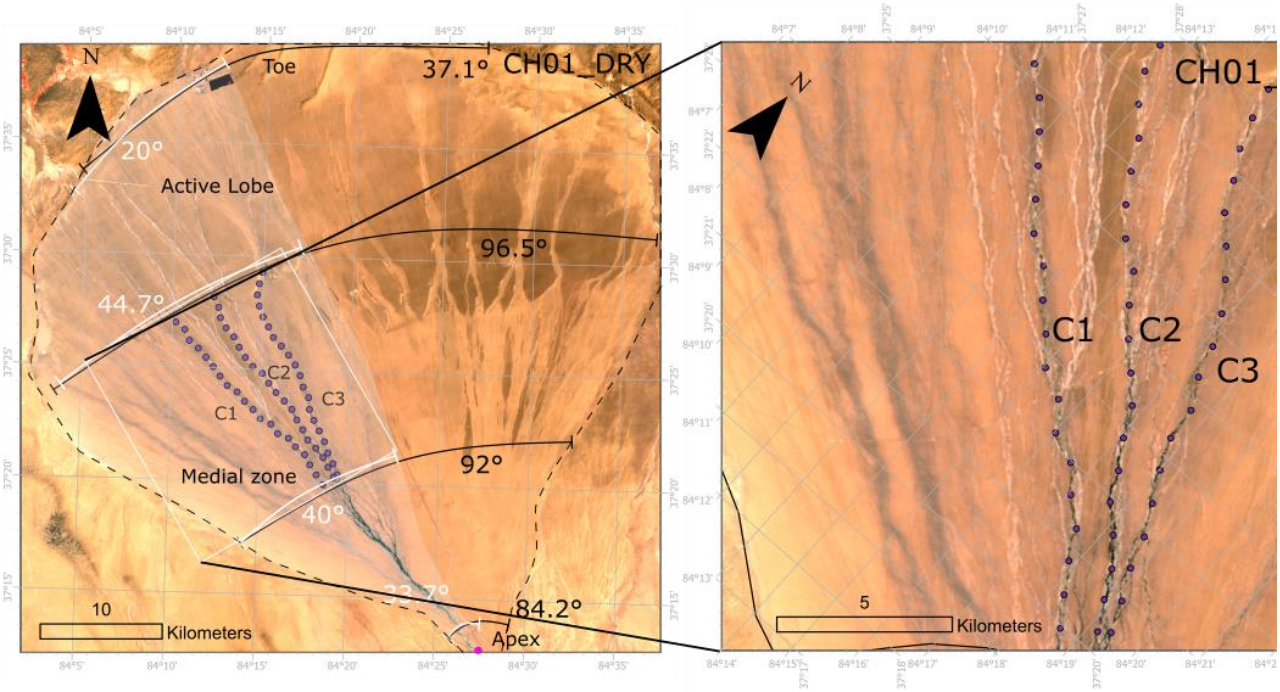

Figure 4.23: Whole DFS area of CH01_DRY with sweep angles annotated in sequence of proximal, start of medial, end of medial, and fan toe. Highlighted area indicates the active lobe of the DFS where measurements took place.

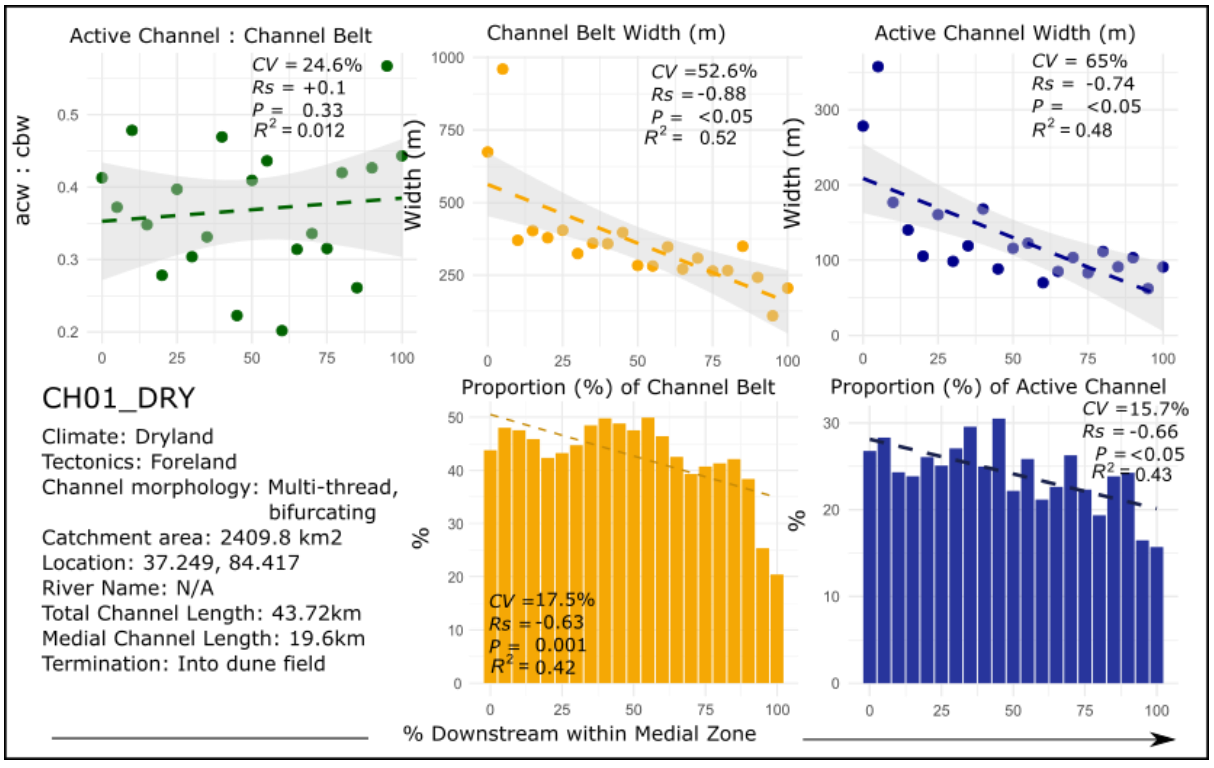

Figure 4.24: Plots summarising the primary results for CH02_DRY with contextual information from the study area. Individual plots for the average active channel width / channel belt downstream ratio, the average channel belt width, average active channel width, and the individual proportions of channel belt and active channel across the active lobe of the medial zone.

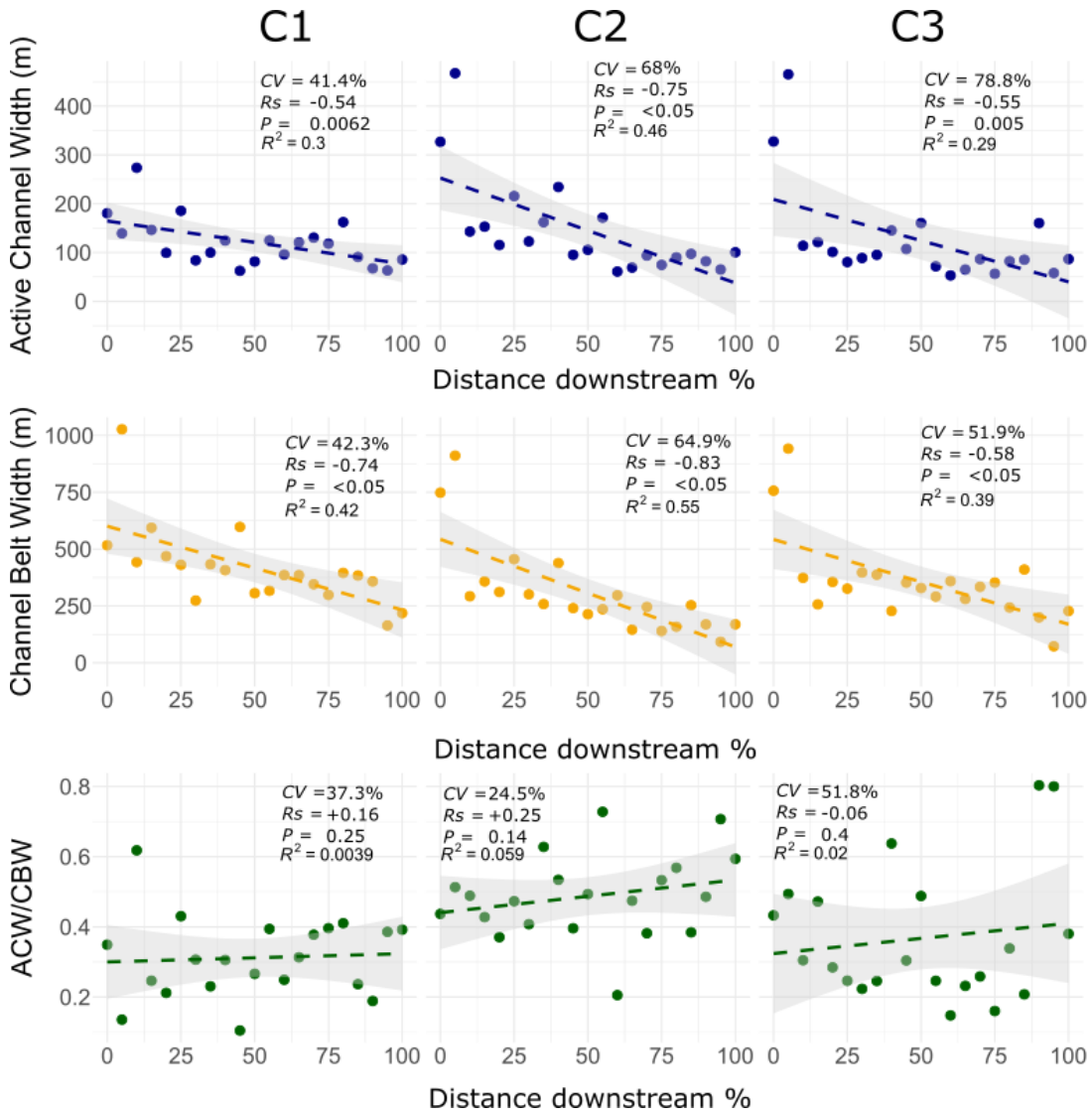

Figure 4.25: Individual plots for active channel width (ACW), channel belt width (CBW), and ACW/CBW ratio for the three channels that make up the averages in Figure 32, corresponding to the channels labelled in Figure 2 (C1, C2, C3). Statistics annotated on graphs include Linear Regression (trendline and R2), coefficient of variation (CV), Spearman's Rank Correlation Coefficient (Rs and P value).

Active Channel Width (ACW)

The ACW plot in **Figure 4.24** shows the average downstream ACW for the data set of the three channels measured in this system (C1, C2, C3 in **Figure 4.23**). There is a very strong negative correlation (R_s -0.74) and moderate R^2 (0.48). Mean width is highest near the start of the medial zone (maximum 467.6 m) and drops significantly at the 10% downstream interval, before decreasing to a minimum of 53 m (overall mean of 130.1 m), as a result, variability is high (CV 65%).

Each individual channel has distinct downstream trends observed in **Figure 4.25**, accounting for the high variance in **Figure 4.24**, similar to the trends observed in AL01_POL. Channel 1 (C1), has a moderate negative correlation (R_s -0.54, R^2 0.30) and widths ranging from 273.8 m to 62.5 m (mean 120.8 m). There is lower variance (CV 41.4%) than the mean dataset. Channel 2 has the strongest negative correlation between CH01_DRY's measured channels (R_s -0.75), and the highest R^2 (0.046). Variability is very high (CV 68%) with widths ranging between 467.6 m to 61 m (mean 145.1 m).

Channel 3 has a moderate correlation (R_s -0.55, R^2 0.29) similar to channel 1. However, variability is very high (CV 78.8%), and width ranges similar to channel 2 (maximum 465.3 m, minimum 53 m, mean 124.4 m). The high CV in channels 2 and 3 is attributed to the significant drop in widths occurring at the 10% interval, associated with bifurcation.

Channel Belt Width (CBW)

Mean downstream CBW (**Figure 4.24**) has a significantly strong negative correlation (R_s -0.88) and moderate R^2 (0.52). Variability is moderately high (CV 52.6%), where values range from 1027.2 m to 72.5 m (total mean 359.7 m).

Similar to ACW, the individual channels have their own downstream trends (**Figure 4.25**), with similarities in a significant decrease at the 10% downstream interval, related to bifurcation of the channels. Channel 1 has a strong negative correlation (R_s -0.74) but moderate CV (42.3%) and R^2 (0.42), with width ranging from 1027.2 m to 164 m (mean 416.7 m). Similarly, channel 2 has a very strong negative correlation (R_s -0.83, R^2 0.55), and a high CV (64.9%), values ranging from 911.2 m to 92.2 m (mean 306.4 m). Furthermore, channel 3 follows a similar trend, however with lower R_s (-0.58) and R^2 (0.39). Variability is moderately high (CV 51.9%), where widths range from 942 m to 72.5 m (mean 356 m).

Active Channel / Channel Belt Width (ACW/CBW)

Figure 4.24 shows average downstream ACW/CBW has no significant correlation (R_s 0.1 and P value 0.33, R^2 0.012) but low variability (CV 24.6%) with mean ratio values ranging from minimum of 0.20 to maximum of 0.57 (total mean 0.37).

The individual channels in the data set (**Figure 4.25**) all have no statistically significant correlations. Channel 1 (R_s -0.16 and P value 0.25, R^2 0.0039) has moderate to low variability (CV 37.3%) with ratios ranging between 0.10 to 0.62 (mean 0.31). Channel 2 (R_s 0.24 and P value 0.14, R^2 0.059) has a lower variance (CV 24.5%) and values ranging from 0.21 to 0.73 (mean 0.49). Channel 3 (R_s -0.06 and P value 0.4, R^2 0.02) has the highest variability (CV 51.8%) with values ranging from 0.15 to 0.80 (mean 0.37).

Active Channel: Channel Belt: Overbank

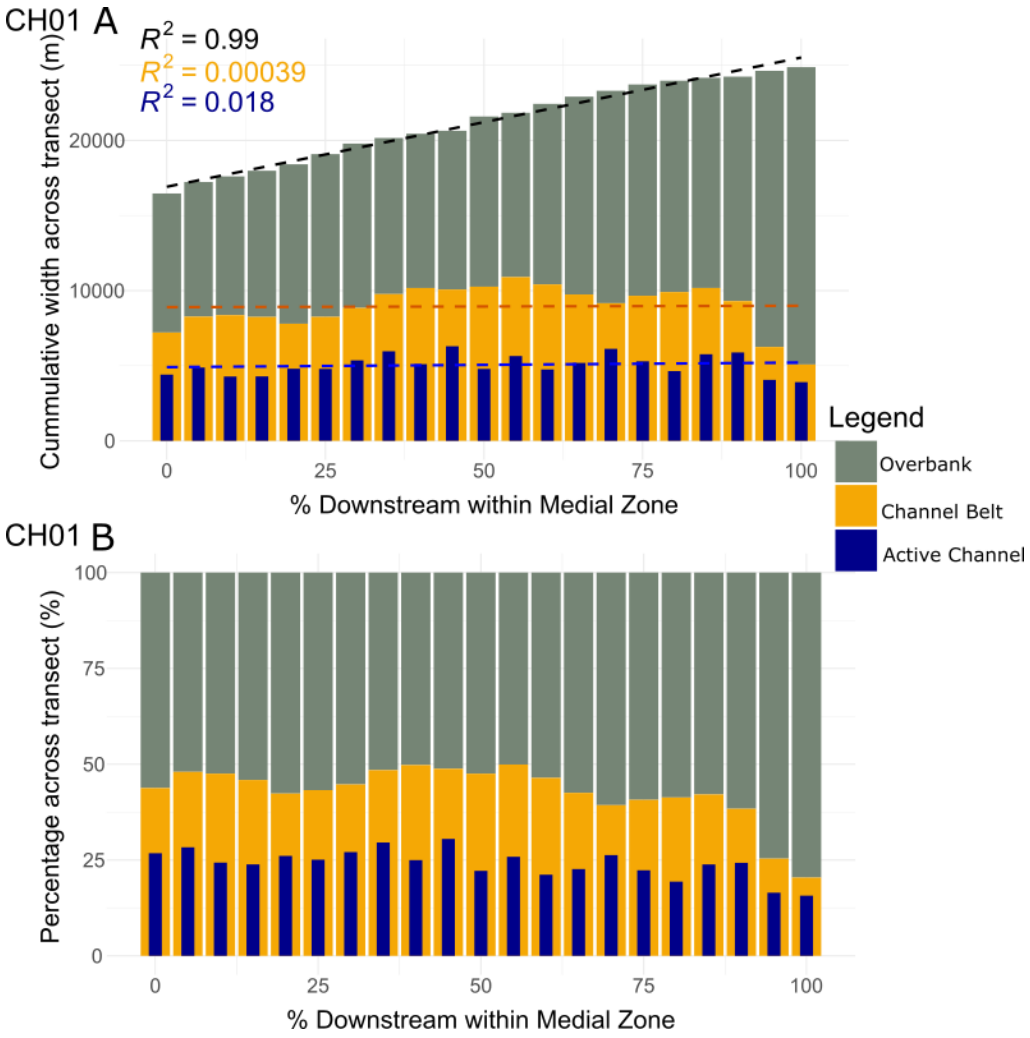

Figure 4.26: Stacked bar plots for the absolute proportion of overbank, channel belt and active channel on the surface of the active medial zone for CH01_DRY (A), based on the cumulative widths taken across transects, with regression lines and R^2. And (B) the percentage proportion of overbank, channel belt, active channel for the across the transects for the active medial zone.

Figure 4.24 shows that the proportion of channel belt and active channel both have moderately strong negative correlations (R_s -0.63 and -0.66), but moderately weak R^2 (both 0.43). Variance is low for both parameters; channel belt CV 25% with proportions ranging from 20.4% to 49.9% (mean 42.7%). Active channel CV is similar (15.7%), however makes up a smaller proportion (**Figure 4.26b**), ranging from 15.7% to 30.5% (mean 24.1%).

Alternatively, the absolute proportion of channel belt and active channel, using cumulative widths across the transects (**Figure 4.26a**), have no significant downstream trends with P values > 0.05. Cumulative channel belt width has an R_s 0.21 but an R^2 0.00039, similarly, active channel has R_s 0.1 and R^2 0.018. Variability is low for both channel belt (CV 16.4%) and active channel (13.7%), as both parameters remain relatively constant downstream. However, the absolute proportion of overbank has a significantly strong positive correlation (R_s 0.98) and very high R^2 (0.99), with a low variability (29.3%).

Sweep Angle (SA)

Figure 4.24 shows the SA for CH01_DRY. At the proximal zone (6 km downstream), SA is 84° and radiates to 92° at the start of the medial zone (16.2 km downstream). Towards the end of the medial the system expands slightly more to 96. 5° (33.5 km downstream) where it tapers to 37.1° upon reaching the toe (51 km downstream), indicative of the characteristic radial DFS shape. Similarly, the SA of the active lobe also radiates from proximal to medial (33° to 40° - 44°), before it narrows towards the toe (20°).

4.1.9 CH02_DRY: *Ruo Shui, China*

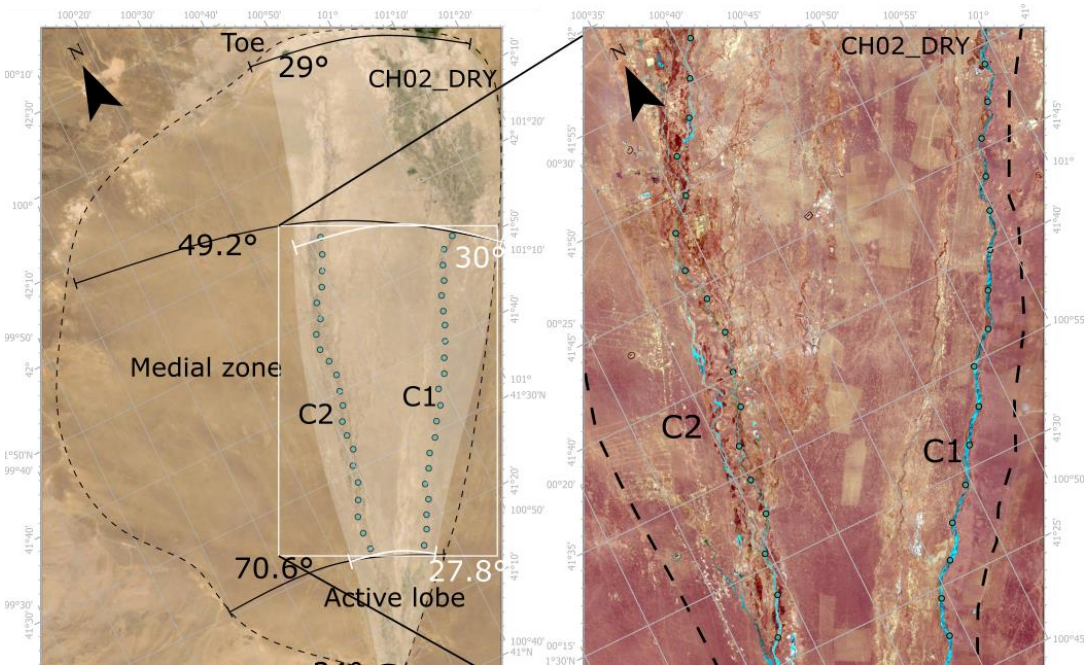

Figure 4.27: Whole DFS area of CH02_DRY with sweep angles annotated in sequence of proximal, start of medial, end of medial, and fan toe. Highlighted area indicates the active lobe of the DFS where measurements took place.

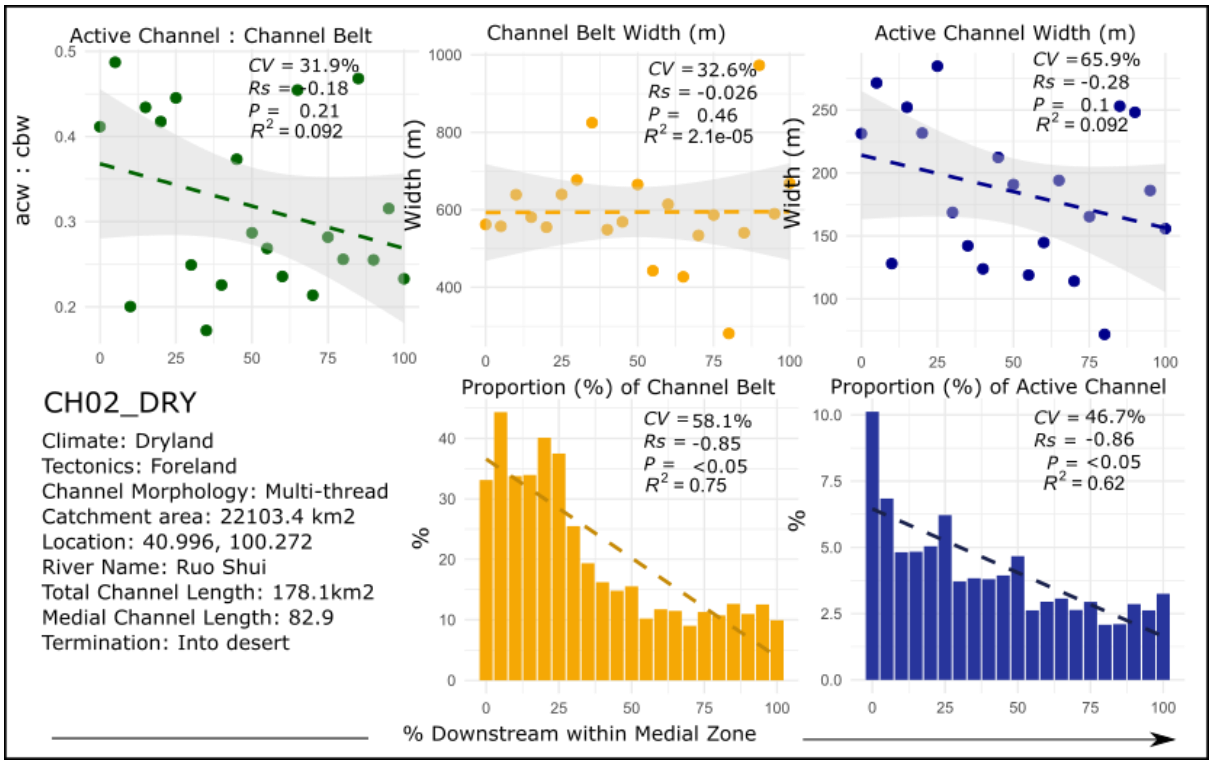

Figure 4.28: Plots summarising the primary results for CH02_DRY with contextual information from the study area. Individual plots for the average active channel width / channel belt downstream ratio, the average channel belt width, average active channel width, and the individual proportions of channel belt and active channel across the active lobe of the medial zone.

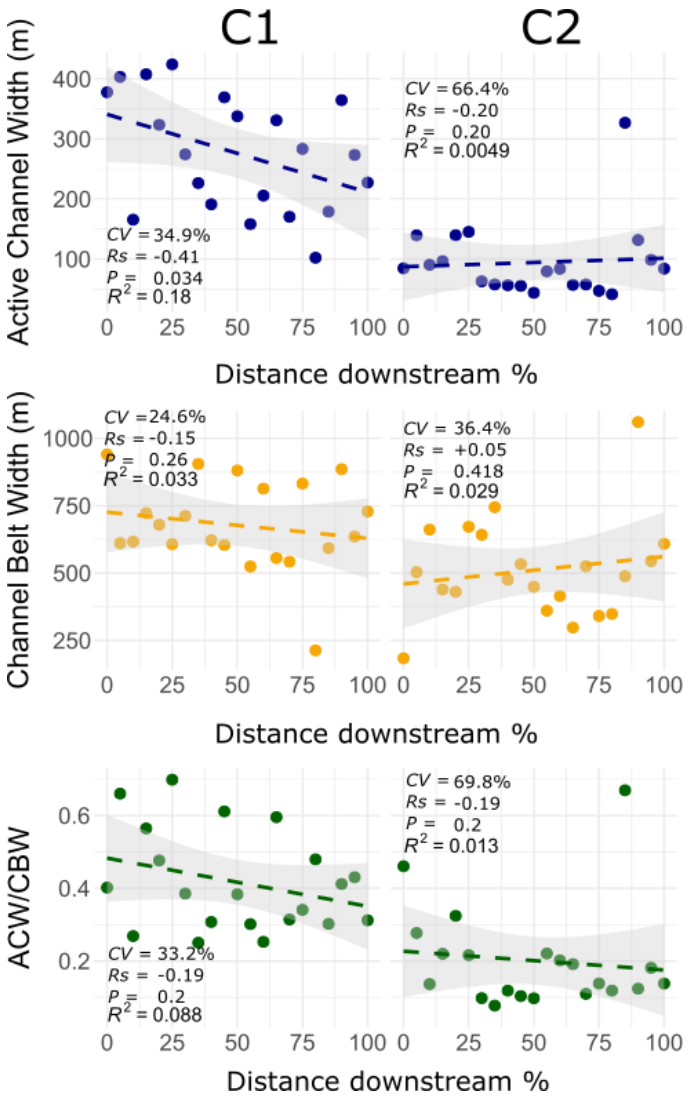

Figure 4.29: Individual plots for active channel width (ACW), channel belt width (CBW), and ACW/CBW ratio for the two channels that make up the averages in Figure 37, corresponding to the channels labelled in Figure 2 (C1, C2, C3). Statistics annotated on graphs include Linear Regression (trendline and R2), coefficient of variation (CV), Spearman's Rank Correlation Coefficient (Rs and P value).

Active Channel Width (ACW)

ACW plot in **Figure 4.28** consists of the downstream means of two channels (C1 and C2 **Figure 4.27**). Mean ACW has a weakly negatively correlating downstream trend (R_s -0.28 P value 0.1) with a very weak R^2 (0.092), alongside a high variance (CV 65.9%). Of this mean dataset, the maximum width is 284.8 m and minimum 71.8 m (total mean 185.2 m).

However, the high variance and weak statistical trends in the mean dataset can be understood better by assessing the individual channels (**Figure 4.29**). Channel 1 is much wider (maximum 424.2 m, minimum 102.3 m, mean 276.1 m) with moderate negative correlation (R_s -0.41) but weak R^2 (0.18), however the variance is much lower than mean dataset (CV 34.9%). Channel 2 is narrower but has no significant correlation (R_s -0.20 P value 0.2), high variance (CV 66.4%) and very weak R^2 (0.0049). Width ranges from maximum of 327 m to 41.4 m (mean 94.3 m).

Channel Belt Width (CBW)

Similarly, mean CBW (**Figure 4.28**) has no significant correlation (R_s -0.026 P value 0.46, R^2 0.000021). Variability is moderate to low (CV 32.6%) with a maximum mean width 972.9 m and minimum 280.8 m (total mean 594.1 m).

Both individual channel belts (**Figure 4.29**) have no significant correlation but differ in their variance. Channel 1 (R_s -0.15 and P value 0.026, R^2 0.033) has a lower variance (CV 24.6%) with width ranging from 940.2 m to 213.3 m (mean 677.4 m). Channel 2 (R_s 0.05 and P value 0.42, R^2 0.029) has a more moderate variance (CV 36.4%) and widths ranging from maximum 1060.3 m to 183.9 m (mean 510.8 m).

Active Channel / Channel Belt Width (ACW/CBW)

The mean ACW/CBW dataset is very scattered (**Figure 4.28**) and no significant correlation (R_s -0.18 and P value 0.21, R^2 0.092) is observed. However, a moderate to low variability is calculated (CV 31.9%) where ratio values range from 0.17 to 0.49 (mean 0.32).

The ratios for each channel, while both having no significant correlations (R_s -0.19 and P value 0.2), are highly variable (**Figure 4.29**). Channel 1 has a moderate variability (CV 33.2%) and weak R^2 (0.088), with ratios ranging from 0.25 to 0.70 (mean 0.42), whereas channel 2 has a high variability (CV 69.8%) and weak R^2 (0.013), ratios ranging between 0.08 to 0.67.

Active Channel: Channel Belt: Overbank

The percentages of channel belt and active channel have very strong negative correlations and downstream trends (**Figures 4.28** and **4.30b**), both with moderate levels of variance. Channel belt percentage (R_s -0.85, R^2 0.75) has a variance of 58.1% where the proportion starts the medial zone at a maximum of 44.3%, decreasing downstream to 9% (mean 20.2%). Active channel follows a similar trend (R_s -0.86, R^2 0.62), however consists of lower percentages, decreasing from 10.1% to 4.5% (mean 7.2%), producing a CV of 46.7%.

The absolute proportions of channel belt and active channel follow similar downstream trends to the normalised percentages. Cumulative channel belt width (**Figure 4.30a**) has a significant strong negative correlation (-0.72), however a weaker R^2 (0.47) than the percentage proportion, with low variability (CV 25.1%). Active channel again follows a similar but slightly weaker trend (Rs -0.46, R^2 0.24), and low variability (CV 22%). However, the absolute proportion of overbank deposits in the

medial zone significant increases downstream, evidenced by strong R^2 (0.85) and R_s (0.98), and low to moderate CV (29.3%).

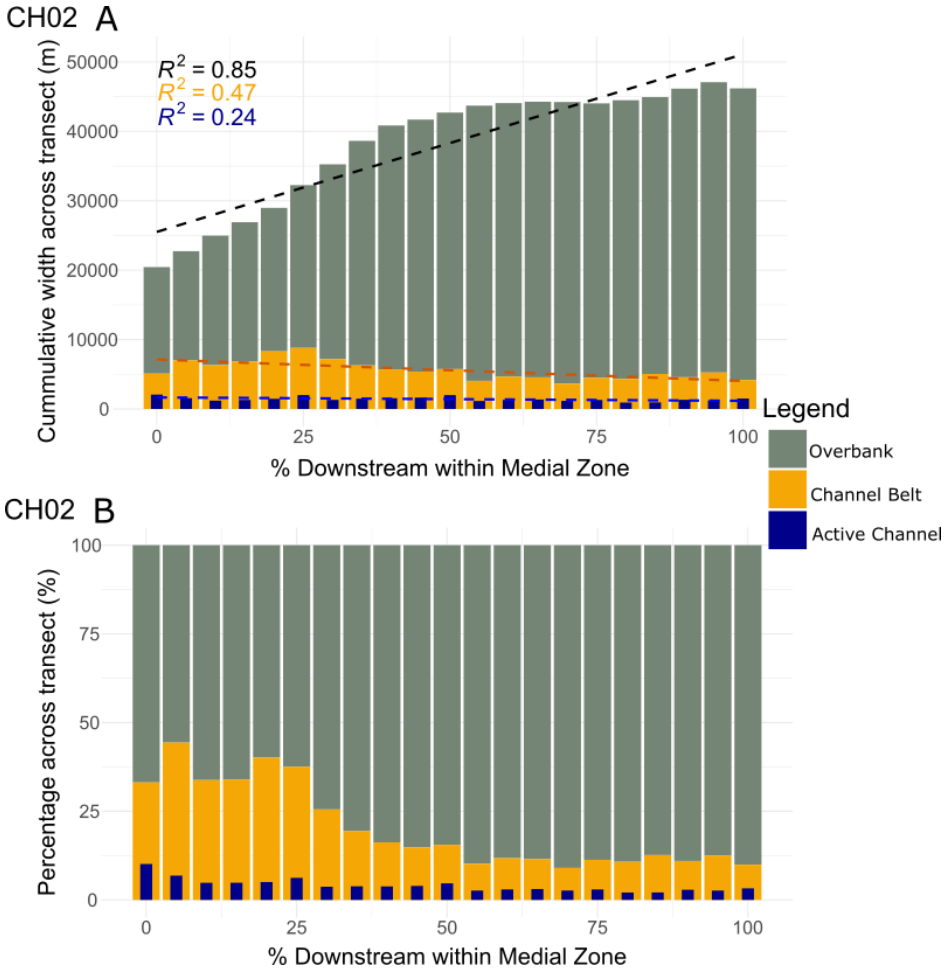

Figure 4.30: Stacked bar plots for the absolute proportion of overbank, channel belt and active channel on the surface of the active medial zone for CH02_DRY (A), based on the cumulative widths taken across transects, with regression lines and R^2. And (B) the percentage proportion of overbank, channel belt, active channel for the across the transects for the active medial zone.

Sweep Angle (SA)

SA for the whole DFS surface (**Figure 4.27**) starts at the proximal zone (16.3 km downstream) as 34.1° and expands to 70.6° at the start of the medial zone (41.8 km downstream). Limited by topography, the whole DFS SA at the end of the medial zone (118.1 km downstream) decreases to 49.2° and to 29° at the toe (165.2 km downstream). However, the active lobe in this system remains a consistent SA from proximal to medial (33.7° to 27.8°- 30°) to the distal toe (29°).

4.2 Comparison Results

It is apparent from section 4.1 that each of the studied DFS has their own downstream patterns, however it can be beneficial to compare these to understand where similarities and differences lie. To start, how the downstream trends associated with DFS compare across the studied systems can be analysed, and statistically test if there is significant variance between each system, using the Kruskal-Wallis test (P value labelled on each plot), and paired Wilcoxon (**Tables 4.2 – 4.8**). It is hypothesised that there is a downstream decrease in active channel width, channel belt width, and downstream increase in floodplain area on a DFS (Hartley *et al.*, 2010; Weissmann *et al.*, 2010).

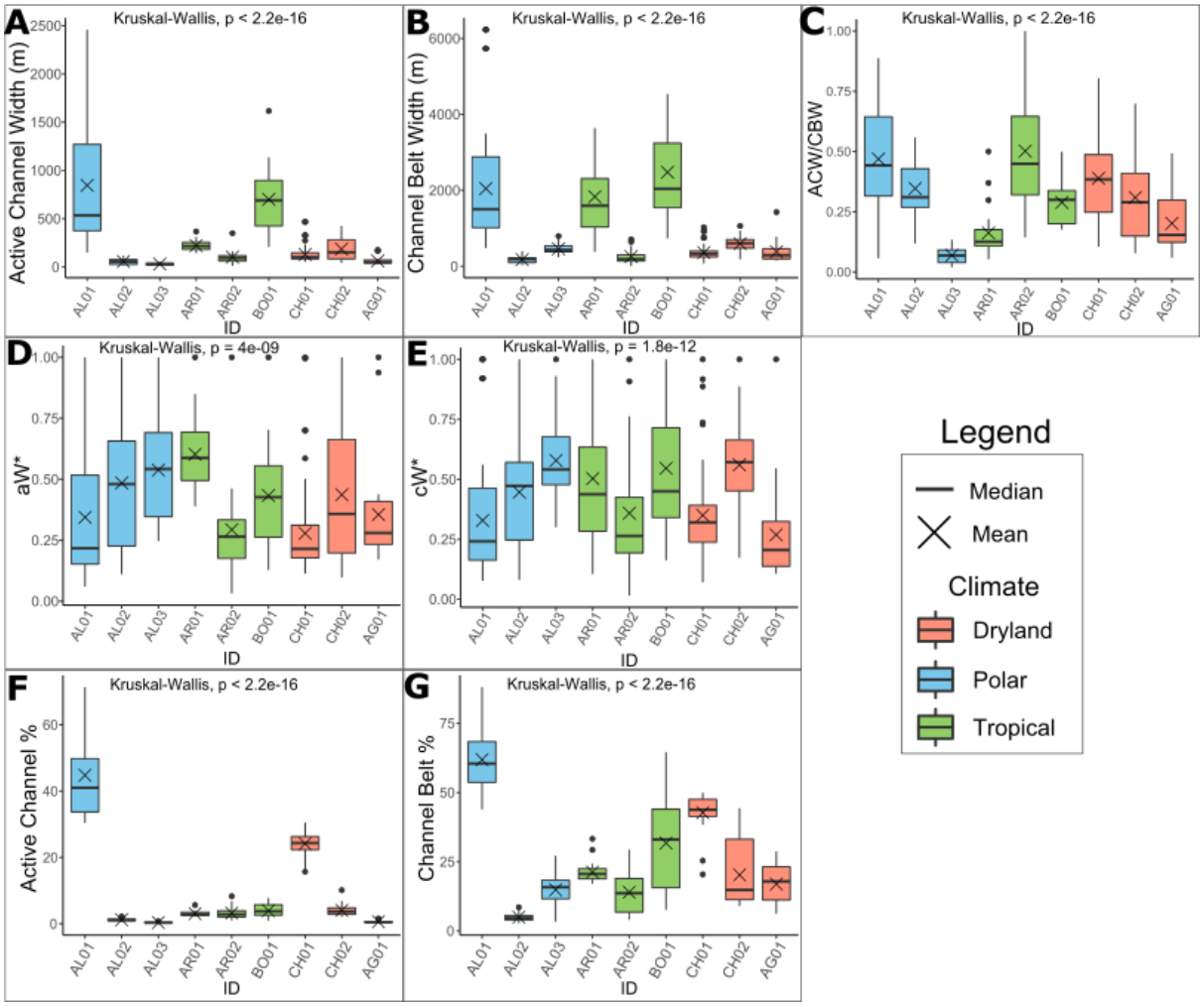

Figure 4.31: Boxplots comparing each system against the measured parameters: active channel width (ACW), normalised ACW (aW), channel belt width (CBW), normalised CBW (cW*), ACW/CBW, active channel %, channel belt %. Kruskal-Wallis test P value annotated, and values < 0.05 are statistically significant.*

Although variability exists in the ranges and means for each system, every system studied has a downstream decrease in ACW, reflecting the characteristic and hypothesised DFS downstream decrease in active channel width, losing width due to bifurcation, evapotranspiration, or infiltration (Hartley *et al.*, 2010; Weissmann *et al.*, 2010, 2011, 2013). Similarly, most systems studied have a downstream decrease in CBW, with AL03_POL and CH02_DRY as exceptions, as both have no apparent downstream decrease. CBW remaining constant downstream suggests there is no downstream change in the degree of channel mobility as possibly expected in DFS, possibly driven by high discharge and sediment supply. In general, each system follows similar trends with regards to ACW and CBW, however variation is present in the ranges of these widths, visualised in **Figure 4.31**, particularly AL01_POL and BO01_TROP which have the highest ranges in ACW and CBW. It is apparent that variability between each site is very high (e.g. a total CV for ACW of 141%), based on **Figure 4.31**, however the Kruskal-Wallis test is used to determine that variability between the sites is statistically significant; the P value is less than 0.05, and the Wilcoxon tests to observe what systems are statistically different or similar to others (**Tables 4.2 – 4.4**). However, the ACW to CBW ratio for most of the systems have no downstream trends, with variable and scattered downstream values; where there are no distinct trends in channel migration based on this metric, when a downstream increase in ratio values is expected.

ACW Wilcoxon Test P values									
	AL01	AL02	AL03	AR01	AR02	BO01	CH01	CH02	AG01
AL01									
AL02	8.6e-12								
AL03	8.6e-12	0.0037							
AR01	1.2e-09	3.7e-12	3.7e-12						
AR02	2.3e-11	0.0057	4.3e-07	1.6e-07					
BO01	1.0000	3.7e-12	3.7e-12	4.5e-09	7.1e-11				
CH01	< 2e-16	6.7e-07	9.2e-12	2.0e-07	0.1164	3.8e-11			
CH02	6.7e-14	1.1e-06	7.0e-15	0.0764	0.0150	7.4e-11	0.0860		
AG01	9.9e-12	0.9207	1.9e-05	3.6e-10	0.0100	3.7e-12	3.0e-07	3.1e-07	

Table 4.2: Pairwise Wilcoxon test for active channel width (ACW) where values < 0.05 are statistically significant and indicate a difference between the system pair.

CBW Wilcoxon Test P values									
	AL01	AL02	AL03	AR01	AR02	BO01	CH01	CH02	AG01
AL01									
AL02	8.6e-12								
AL03	1.0e-10	1.0e-09							
AR01	0.8042	7.4e-12	7.8e-09						
AR02	3.3e-11	0.2715	9.4e-05	1.1e-10					
BO01	0.0271	3.7e-12	1.5e-11	0.0553	3.7e-12				
CH01	< 2e-16	2.9e-06	0.0015	1.1e-10	0.0053	1.2e-11			
CH02	8.1e-13	5.3e-13	0.0034	1.6e-09	9.9e-08	4.9e-15	8.8e-09		
AG01	3.6e-10	0.0031	0.0182	5.9e-09	0.0739	4.5e-11	0.5770	5.3e-05	

Table 4.3: Pairwise Wilcoxon test for channel belt width (CBW) where values < 0.05 are statistically significant and indicate a difference between the system pair.

ACW/CBW Wilcoxon Test P values									
	AL01	AL02	AL03	AR01	AR02	BO01	CH01	CH02	AG01
AL01									
AL02	0.017								
AL03	7.1e-11	1.5e-11							
AR01	9.8e-08	4.9e-06	1.4e-05						
AR02	0.7645	0.0268	3.1e-08	1.8e-06					
BO01	0.0002	0.1682	3.7e-12	1.2e-05	0.00098				
CH01	0.0307	0.5286	9.9e-12	4.9e-08	0.0615	0.0072			
CH02	0.0002	0.2311	6.7e-13	0.00034	0.0015	0.9481	0.0126		
AG01	1.5e-06	0.00053	2.4e-07	0.17618	1.7e-05	0.0031	3.9e-06	0.0244	

Table 4.4: Pairwise Wilcoxon test for active channel width / channel belt width ratio (ACW/CBW) where values < 0.05 are statistically significant and indicate a difference between the system pair.

As a function of sediment supply and discharge, catchment area can influence the width of the active channel and channel belt. As each system varies in size, normalising (aW* and cW* in **Figure 4.31**) ACW and CBW creates dimensionless values that can be compared without catchment area size interfering with values, as a larger catchment with larger discharge is suspected to created wider rivers In **Figure 4.31**, the Kruskal-Wallis statistical test indicates that there *is* a significant difference between all the groups, however by normalising the data, outlying ranges cannot be observed, such as AL01_POL, seen in the raw data that provides more information about variability. Upon comparing individual systems with the Wilcoxon test in **Tables 4.5** and **4.6**, there are **no** significant differences

between many pairs (indicated by red in the table) that are statistically different when using the raw dataset (**Tables 4.2** and **4.3**).

Normalised ACW (aW*) Wilcoxon Test P values									
	AL01	AL02	AL03	AR01	AR02	BO01	CH01	CH02	AG01
AL01									
AL02	**0.0178**								
AL03	**0.00042**	0.359							
AR01	**2.9e-05**	0.116	0.263						
AR02	0.9959	**0.017**	**0.0005**	**2.7e-06**					
BO01	0.25	0.473	0.1159	**0.009**	**0.014**				
CH01	0.847	**0.0012**	**9.0e-07**	**5.2e-09**	0.646	**0.0008**			
CH02	0.0953	0.414	0.083	**0.0099**	0.0964	0.694	**0.0155**		
AG01	0.141	0.116	**0.0037**	**2.5e-05**	0.385	0.0943	**0.0274**	0.60	

Table 4.5: Pairwise Wilcoxon test for normalised active channel width (aW) where values < 0.05 are statistically significant and indicate a difference between the system pair.*

Normalised CBW (cW*) Wilcoxon Test P values									
	AL01	AL02	AL03	AR01	AR02	BO01	CH01	CH02	AG01
AL01									
AL02	0.227								
AL03	**5.3e-06**	0.054							
AR01	**0.0043**	0.642	**0.141**						
AR02	0.532	0.213	**0.0013**	0.0575					
BO01	**0.00028**	0.252	**0.40**	0.538	**0.008**				
CH01	0.0634	0.073	**1.3e-06**	**0.023**	0.595	**0.0007**			
CH02	**7.3e-08**	**0.041**	**0.873**	0.231	**0.0004**	0.630	**3.0e-08**		
AG01	0.39	**0.008**	**7.1e-06**	**0.002**	0.213	**0.0001**	**0.010**	**6.1e-07**	

Table 4.6: Pairwise Wilcoxon test for normalised channel belt width (cW) where values < 0.05 are statistically significant and indicate a difference between the system pair.*

Active channel and channel belt percentages decrease downstream for most of the systems in the study, exceptions being AL02_POL and AR01_POL, with the decreasing proportions corresponding with increasing DFS area. Absolute active channel proportions remain relatively constant downstream for each system where change is primarily driven by increasing proportion of overbank. Sites AL01_POL and CH01_DRY have the largest ranges in active channel percentage, as well as channel belt percentages, related to the bifurcation of these systems (**Figure 4.31)**. Similar to ACW and CBW, variability is also high between the systems, all with varying ranges, shown in **Figure 4.31** with the Kruskal-Wallis test indicating statistically significant variance, and Wilcoxon in Tables 7 and 8 indicating where these differences and similarities arise.

Active Channel % - Wilcoxon Test P values									
	AL01	AL02	AL03	AR01	AR02	BO01	CH01	CH02	AG01
AL01									
AL02	3.7e-12								
AL03	3.7e-12	1.7e-10							
AR01	3.7e-12	7.4e-12	3.7e-12						
AR02	3.7e-12	1.6e-07	3.7e-12	0.8228					
BO01	3.7e-12	2.9e-07	3.7e-12	0.1258	0.2202				
CH01	7.4e-12	3.7e-12	3.7e-12	3.7e-12	3.7e-12	3.7e-12			
CH02	3.7e-12	2.9e-07	3.7e-12	0.0358	0.0739	1.0000	3.7e-12		
AG01	3.7e-12	5.7e-06	0.0031	3.7e-12	1.1e-10	4.5e-11	3.7e-12	3.7e-12	

Table 4.7: Pairwise Wilcoxon test for active channel percentage, where values < 0.05 are statistically significant and indicate a difference between the system pair.

Channel Belt % - Wilcoxon Test P values									
	AL01	AL02	AL03	AR01	AR02	BO01	CH01	CH02	AG01
AL01									
AL02	3.7e-12								
AL03	3.7e-12	2.0e-07							
AR01	3.7e-12	3.7e-12	0.00015						
AR02	3.7e-12	3.0e-06	0.90098	0.00163					
BO01	3.6e-07	2.6e-11	0.00311	0.16049	0.00059				
CH01	2.1e-08	3.7e-12	7.1e-11	1.4e-09	7.1e-11	0.01081			
CH02	7.4e-12	3.7e-12	0.54986	0.08724	0.10244	0.05529	3.4e-08		
AG01	3.7e-12	3.6e-10	0.30580	0.11962	0.13893	0.00729	5.2e-10	0.58368	

Table 4.8: Pairwise Wilcoxon test for channel belt percentage, where values < 0.05 are statistically significant and indicate a difference between the system pair.

The summary table (**Table 4.1**) presents the key statistics for each system, including the overall minimum, maximum, mean, and CV for each measured parameter. The entire dataset is highly variable where the overall ACW ranges from 11.1m to 2457.7m (mean 319.1m). However there is a very high CV of 141% suggesting that most width measurements lie distantly from the mean. Similar high variability across the dataset from the other measured systems is also seen for overall CBW (11.1m to 6228.2m, mean 999.1m, CV 118%), ACW/CBW (0.02 to 1, mean 0.34, CV 60.5%), active channel percentage (0.13% to 71.3%, mean 9.5%, CV 158%) and channel belt percentage (2.7% to 88%, mean 25%, CV 75%). However, the percentage of overbank ranges from 12% to 97%, with a mean of 75% and a CV of 25.5%, suggesting much lower variability. Aside from overbank percentage, the other measured parameters are all highly variable, thus it is beneficial to evaluate different factors that cause DFS variability.

As dynamic natural systems, variability in fluvial systems is expected to arise due to the interplay of a number of different factors. These include climate (both basin and catchment) which influences sediment supply, discharge and runoff (Waters *et al.*, 2010), as well as DFS termination type (Hartley *et al.*, 2010), where DFS with low discharge are likely to die out within the basin. Furthermore, as climate controls discharge rates and sediment supply, there is an inherent effect on channel geometry (Blum and Törnqvist, 2000), and therefore variability within the medial zone. These groups are compared as climate has a significant impact on variability in fluvial systems. For example, in dryland climates, fluvial systems are often ephemeral and shaped by intermittent but flashy floods, bringing high sediment supplies and discharge that shape the channel (Hartley *et al.*, 2010), and are characteristically devoid of vegetation, meaning channel stability is weaker. Therefore, it may be expected that active channel width is wider in systems where discharge rates are high, and where

sediment concentrations are high and composed of coarser material, a braided morphology is observed (Mueller and Pitlick, 2013). Alternatively, tropical climate fluvial systems are formed continuous year-round discharge and sediment supply, with some seasonal variability during the monsoon seasons, and are much richer in vegetation. Therefore, bank stability is likely to be high affecting the channel widths and mobility (Nichols and Fisher, 2007). Polar systems may be more variable where some systems are fed through glacial melt, and others with more constant supplies. Also linked to climate, and a proxy for precipitation, vegetation cover can impact channel mobility and planform, leading to distinct characteristics in fluvial systems found in dry and vegetation sparse settings (Vandenberghe, 2003), as opposed to highly vegetated systems with increased bank stability. Another factor included is tectonics, which also influences sediment supply (e.g. via earthquake triggered landslips, exposure of local geology), and first order controls on fluvial planform related to the rates of basin subsidence (e.g. sediment fining rates which influences downstream channel morphology) and slope (where coarse sediment produces steeper slopes), as well as generating accommodation space for DFS accumulation and preservation. In this study, the chosen sites are all within the same tectonic setting (foreland), aiming to negate the effect of tectonics when comparing variability. However, it is important to note that the rate of activity can still vary at each site.

As discussed, these factors influence sediment supply and discharge rates, the major influence of channel planform, however there are other factors that have not been considered in this study, such as source rock lithology and weathering rates, impacting the available sediment supply and grain sizes. Finally, catchment area can serve as a proxy for sediment supply and discharge, as the fluvial system scales with increasing catchment size (Burgers *et al*., 2014), variations from this trend may indicate unexpectedly high or low sediment concentrations, influenced by other factors. Therefore, channel planform, such as river style and the number of channels in the system, and catchment area are useful to consider in trying to understand variability between DFS, as proxies for sediment supply and discharge. Thus, the following work compares the dataset, grouped by different factors that may account for the variability within the dataset, to see if any distinct trends appear.

4.2.1 Climate Comparisons

In section 4.2, a comparison has been conducted of each individual system and its measured parameters to identify if any differences and similarities arise statistically. However, as seen in Tables 2 – 6, internally within a climate group most systems are statistically different from each other. However, as previous studies have observed distinct differences in fluvial characteristics between different climates (Vandenberghe, 2003; Hartley *et al.*, 2010; Mescolotti *et al.*, 2021), the dataset has been grouped by climate category (polar, tropical or dryland) to determine if, despite internal variations, variability in the medial zone of DFS occurs between different climates. Therefore, these three groups have been plotted in **Figure 4.32**, and use the Kruskal-Wallis test to determine statistically significant difference between the groups as a whole, and the Wilcoxon test, for difference between each group (e.g. Tropical and Polar, Tropical and Dryland, and Dryland and Polar).

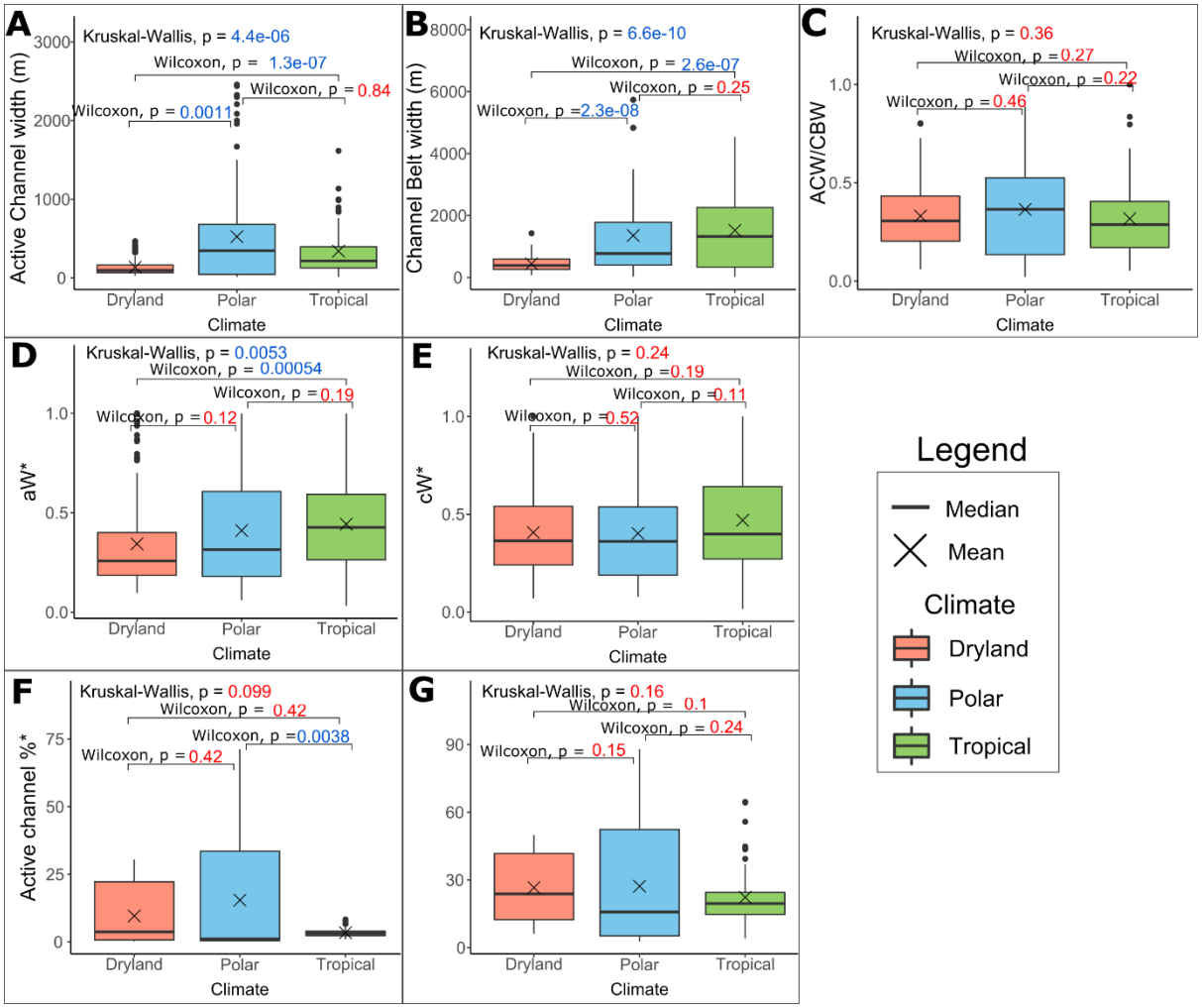

Figure 4.32: Boxplots comparing the three climate groups for the systems (tropical, polar, dryland) against the measured parameters: active channel width (ACW), normalised ACW (aW), channel belt width (CBW), normalised CBW (cW*), ACW/CBW, active channel %, channel belt %. Kruskal-Wallis test P values with Wilcoxon test pairs annotated, and values < 0.05 are statistically significant.*

Active Channel Width (ACW)

Normalised ACW (aW*), **Figure 4.32d**, shows a distinct difference in aW* between the three climate groups, with Tropical and Polar having the widest normalised active channels, and dryland the smallest. Wilcoxon testing between each climate group shows that Tropical and Dryland are the only pair with any statistical differences (P = 0.00054).

Alternatively, absolute ACW, **Figure 4.32a**, shows that Polar climates have the widest channel widths, and the largest range (minimum: 13.0 m, maximum: 2457.7 m, mean: 524.2 m). Statistically, Tropical and Polar have no difference in the means (P = 0.84), yet Dryland, with the smallest ACW range (30 m to 467.6 m, mean: 137.2 m) is statistically different to both Polar (P = 0.0011) and Tropical (P = 1.3e-07).

Channel Belt Width (CBW)

Normalised CBW (cW*), **Figure 4.32e**, shows the ranges for each climate group to be very similar, with Kruskal-Wallis (P = 0.24) and Wilcoxon tests identifying no statistically significant differences. However, the absolute CBW (Figure 31B) shows much more variability. The Dryland climate has the smallest ranges and mean (72.5 m to 1426.3 m, mean: 441.8 m), with significant differences to Polar (P = 2.3e-08) and Tropical (P = 2.6e-07). CBW then increases from Polar to Tropical, however there is no statistical difference between these (P = 0.25)

Active Channel Width / Channel Belt Width (ACW/CBW)

The ratio of ACW to CBW has no apparent trends when considering the climate group of the studied systems, with each systems having similar ratios: Dryland (0.05 to 0.80, mean: 0.33), Tropical (0.05 to 1, mean 0.32), and Polar (0.02 to 0.89, mean: 0.36). Furthermore, there are no statistical differences, based on the Wilcoxon tests (**Figure 4.32c**).

Active Channel : Channel Belt : Overbank

The percentage of active channel and channel belt in the medial zone of the three climates varies in the ranges of values, however there is no apparent statistical difference based on the Wilcoxon P values (**Figure 4.32f** and **g**). Tropical has the smallest proportions for both active channel (1% to 8.3%, mean: 3.4%), and channel belt (4% to 64.6%, mean: 26.6%), whereas Polar and Dryland are similar in their proportions. Drylands has a minimum active channel percentage of 0.25% to maximum 30.5% (mean 9.6%) and Polar 0.13% to 71.3% (mean 15.4%). For channel belt percentage, Dryland ranges from 6.2% to 50% (mean 26.6%), and Polar from 2.7% to 88% (mean 27.2%).

4.2.2 Morphology Comparisons

Similarly to climate, the measured parameters for each system can vary due to differences in channel morphology, including channel style and the number of channels in the systems, and may be a proxy for understanding sediment supply and discharge in a system. For example, braided and bifurcating channels, such as AL01_POL and CH01_DRY, form through high sediment supply and discharge (Davidson *et al.*, 2013), whereas more sinuous systems are driven by lower flows and sediment supply. Thus, it is expected that braided systems are characterised by wider channels and meandering characterised by narrower. Furthermore, DFS with bifurcating channels, and therefore multiple measurable channels, will have a higher proportion of active channel and channel belt, based on higher frequency of channels in the medial area.

Therefore, the studied systems have been grouped by channel morphology (dominantly braided or meandering), and the number of measured channels (1, 2, or 3), plotted with each measured parameter in **Figure 4.33** and **4.34**. Moreover, Kruskal-Wallis followed by pairwise Wilcoxon tests have been used to determine any statistical differences between the different groups. P values less than 0.05 indicate a statistical difference between the groups, implying high variability.

River Style

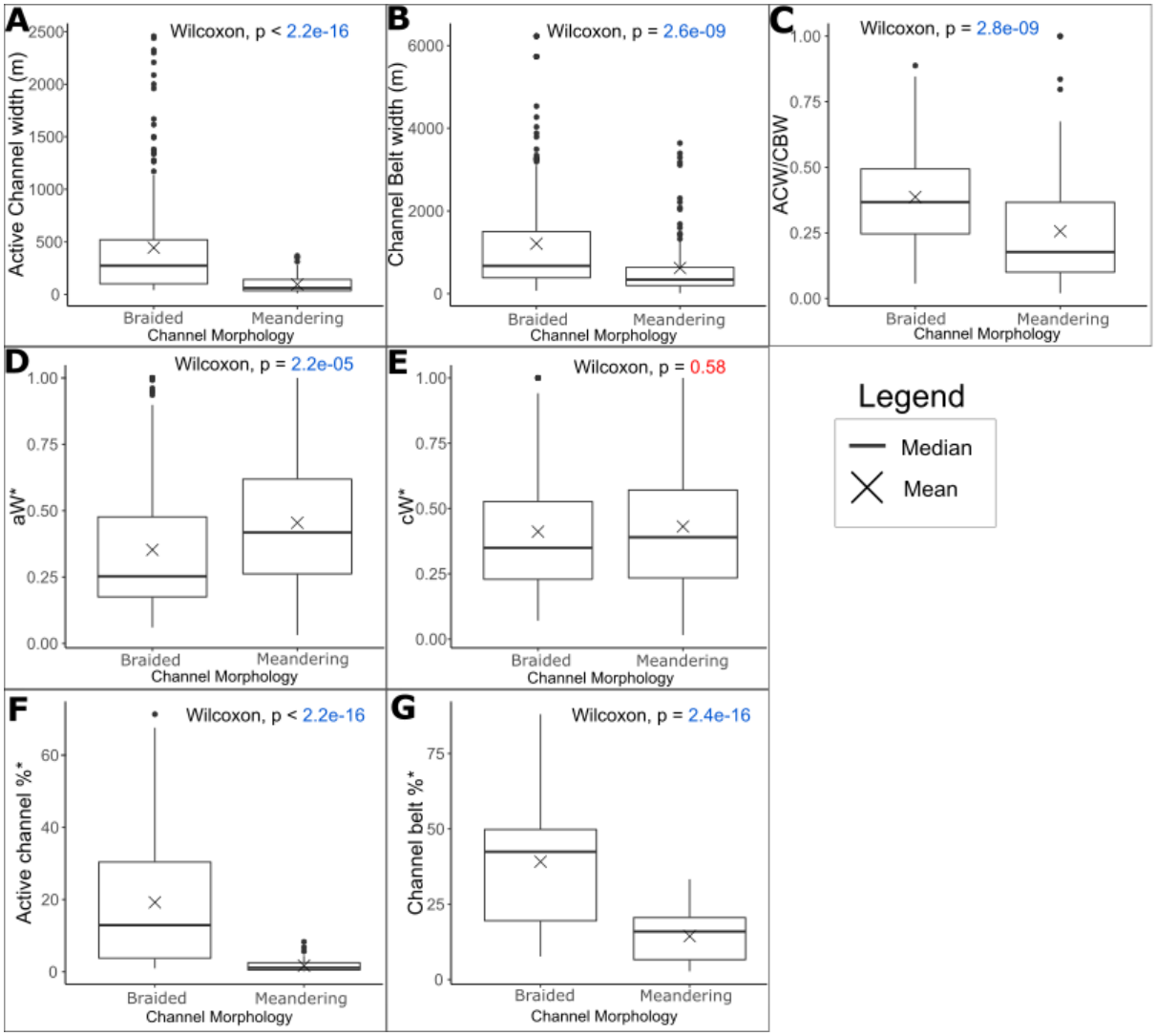

Figure 4.33: Boxplots comparing the channel morphology for the systems (braided and meandering)) against the measured parameters: active channel width (ACW), normalised ACW (aW), channel belt width (CBW), normalised CBW (cW*), ACW/CBW, active channel %, channel belt %. Wilcoxon test P values annotated, and values < 0.05 are statistically significant.*

Active Channel Width (ACW)

Normalised ACW (aW*) shows a statistical difference (P = 0.000022) where the single thread systems are larger than braided systems. However, when considering the absolute values, single thread is considerably smaller (11.1 m to 366.9 m, mean: 94.4 m), and braided active channels being much wider (41.4 m to 2457.7 m, mean: 443.9 m).

Channel Belt Width (CBW)

The normalised cW* has no statistical difference in widths between the planforms (P = 0.58), however it is apparent from **Figure 4.33e** that there is a highly significant difference between the absolute CBW between braided and meandering planforms (P = 2.6e-09). Similar to ACW, the single thread/meandering systems are much smaller in width (11.1 m to 3641.2 m, mean: 621.2 m) than the braided/multi-thread channels (72.5 m to 6228.2 m, mean: 1209.1 m).

Active channel width / channel belt width (ACW/CBW)

ACW to CBW ratio has a statistically significant difference between meandering and braided medial zones (P = 2.8e-09); braided (0.06 to 0.89, mean: 0.39) are similar in range to meandering (0.02 to 1.0, mean: 0.26) however the mean for braided systems is higher, indicating on average ACW is closer in width to CBW.

Active channel: Channel belt : Overbank

There is a significant difference between braided and meandering for both active channel % and channel belt %, with the braided systems having a much larger proportion of active channel and channel belt. For active channel percentage, the braided group ranges from 1% to 71% (mean: 19.2%), whereas meandering ranges from 0.13% to 8.3% (mean: 1.7%). Similarly, channel belt percentage ranges from 7.6% to 88% for braided (mean: 39.1%), but 2.7% to 33.3% (mean: 14.4%) for meandering systems.

Number of Measured Channels

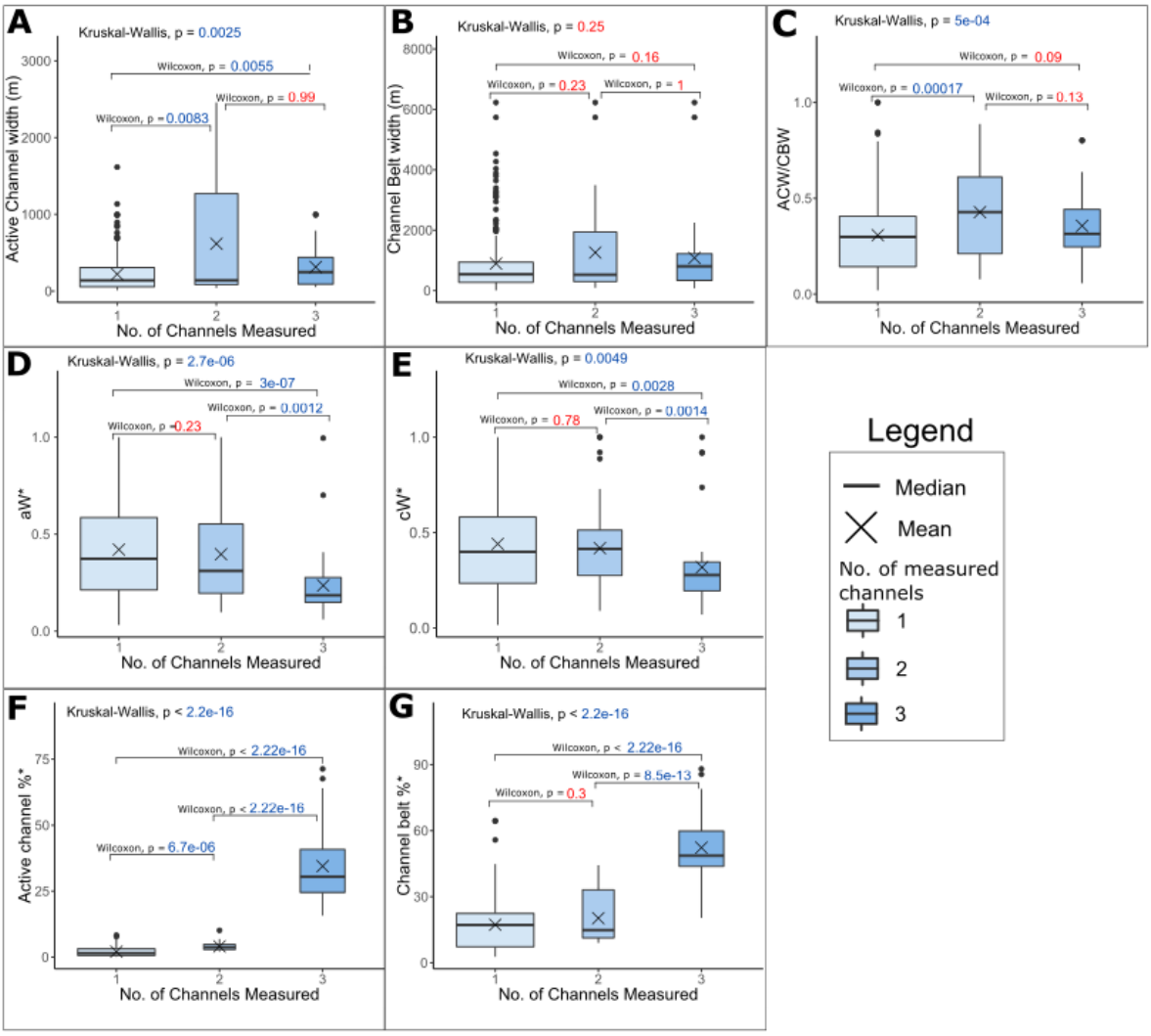

Figure 4.34: Dataset grouped based on the number of channels measured in each system (1, 2 or 3), producing boxplots plotted against the measured parameters: active channel width (ACW), normalised ACW (aW), channel belt width (CBW), normalised CBW (cW*), ACW/CBW, active channel %, channel belt %. Kruskal-Wallis test P values with Wilcoxon test pairs annotated, and values < 0.05 are statistically significant.*

Active Channel Width (ACW)

For normalised ACW (aW*, **Figure 4.34d**) there is a statistically significant difference between systems with 1, 2, and 3 measurable active channels on the DFS; active channel width decreases with increasing number of channels in the medial zone. Medial zones with 1 channel and 2 channels are not statistically different (P = 0.23), however these systems statistically differ from systems with at least 3 channels (**Figure 4.34d**).

However, absolute ACW shows less of a trend with increasing number of channels in the medial zone. Systems with 1 channel range from 11.1 m to 1615.8 m (195.4 m) and are statistically different from *2* (P= 0.0083) and *3* channels (P = 0.0055), yet there is no statistical difference between systems with 2 or 3 channels (P = 0.99). ACW are more variable systems with 2 channels (41.4 m to 424.2 m, mean: 185.2 m), whereas remains low for medial zones with 3 channels (53 m to 2457.7 m, mean: 487.5 m).

Channel Belt Width (CBW)

Normalised CBW follows a similar trend to the normalised ACW, where cW* decreases as the number of active channels in a system increases (Kruskal-Wallis P = 0.0049), however the absolute CBW has no statistical difference between the groups (Kruskal-Wallis P = 0.25). Systems with 1 channel range from 11.1 m to 4535 m (mean: 930.4 m), however systems with 2 range from 183.9 m to 1060.3 m (mean: 594.1 m), and systems with 3 72.5 m to 6228.2 m (mean: 1202.9 m).

Active channel width / channel belt width (ACW/CBW)

Based on the Kruskal-Wallis test, there *is* a significant difference between the channel number groups for the ratio of ACW to CBW (P = 0.0005), however, upon review of differences between each group, there is only a statistical difference between systems with 1 and 2 channels (P = 0.00017), in **Figure 4.34c**. There is a slight increase in ratio from 1 to 2 channel systems, where medial zones with 1 channel have ratios ranging from 0.02 to 1 (0.26), and those with 2 channels from 0.08 to 0.70 (0.31). Systems with 3 measured channels are similar in ratio to those with 2, ranging from 0.06 to 0.89 (0.43).

Active channel : Channel belt : Overbank

Finally, the percentage of active channel and channel belt show similar and distinct trends: increasing in proportion as the number of measurable channels in the medial zone increases (**Figure 4.34f** and **4.34g**). Many of the P values in **Figures 4.34f** and **4.34g** are less than 2.2e-16, indicative of highly significant variation between the three groups (noting the exception between channel number 1 and 2 with p value = 0.3). For the active channel percentage of medial zones with 1 measurable channel, values range from 0.1% to 8.3% (2.1%), and increase slightly for 2 measurable channels (2.1% to 10.1%, 1%), and substantially for systems with 3 measured channels (15.7% to 71.3%, 34.4%). Similarly, channel belt percentages range from 2.7% to 64.6% (17.3%) for system with 1 measured channel, 9% to 44.3% (20.2%) for systems with 2 measured channels, and from 20.4% to 88% (52.3%) for systems with 3 measured channels.

4.2.5 Trends in Catchment Area

As previously discussed, evaluating each systems' measured parameters against its catchment area can provide valuable information on the influence of catchment area, a function of sediment and water discharge/supply, on variability within the medial zone. Therefore, the means of each system per each parameter have been plotted against the catchment area, with the below results referring to **Figure 4.35**.

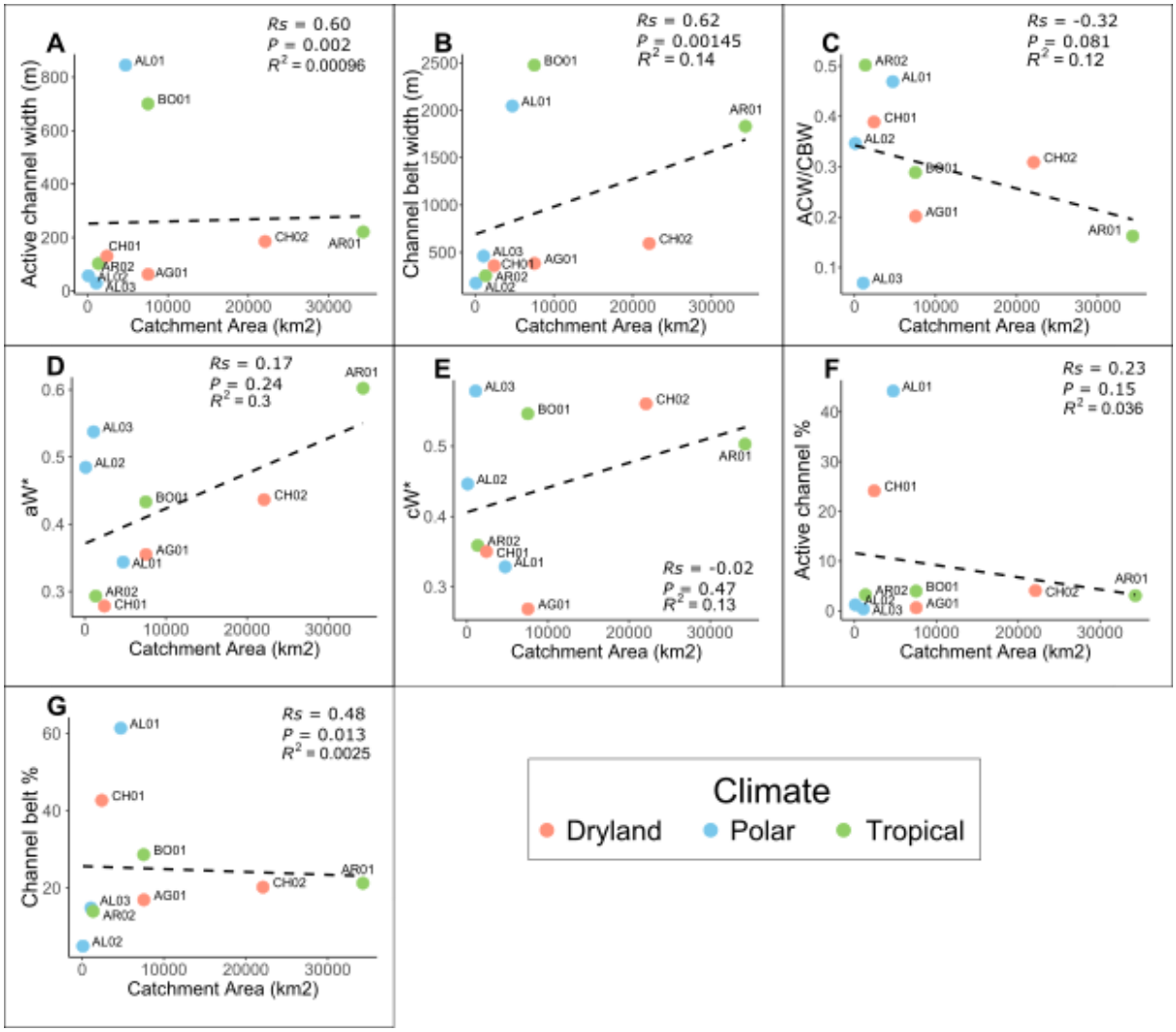

Figure 4.35: Mean values for each measured parameter (Active channel width (CBW), channel belt width (CBW), ACW/CBW, normalised ACW (aW), normalised CBW (cW*), active channel and channel belt percentage), against the upstream catchment area that supplies the DFS. Catchment areas sourced from HydroShed.*

Active Channel Width (ACW)

When plotted against catchment area (**Figure 4.35a**), ACW has moderate positive correlation (R_s 0.60, P value 0.002), however a very low R^2 (0.00096) Most of the system catchment areas are < 10,000 km^2 with mean ACW < 200 m, however AL01_POL and BO01_TROP have exceptionally high means with ACW of 844.9 m and 700 m. Without these potentially anomalous systems, the relationship between catchment area and ACW may be more significant.

Channel Belt Width (CBW)

A similar trend is observed with CBW and catchment area (**Figure 4.35b**), where there is a general trend of increasing CBW with increasing catchment area, as well as a moderate to strong positive correlation (R_s 0.62, P value 0.00145) but a weak R^2 (0.014).

Active Channel Width / Channel Belt Width (ACW/CBW)

There is a weak negative correlation (R_s -0.32, P value 0.081) and weak R^2 (0.12) where the ACW/CBW values are very scattered, particularly those with catchment areas less than 10,000km^2.

Active Channel : Channel Belt : Overbank

There is a weak correlation for the active channel percentage (R_s 0.23) and moderate for channel belt percentage (R_s 0.47), however these are statistically insignificant based on P values > 0.05. R^2 results from linear regression are also very weak (0.036 and 0.0025). The active channel percentage for all the systems lies below 5%, except for AL01_POL and CH01_DRY. These systems are also outliers for the channel belt percentage.

4.2.6 Trends in Vegetation Coverage

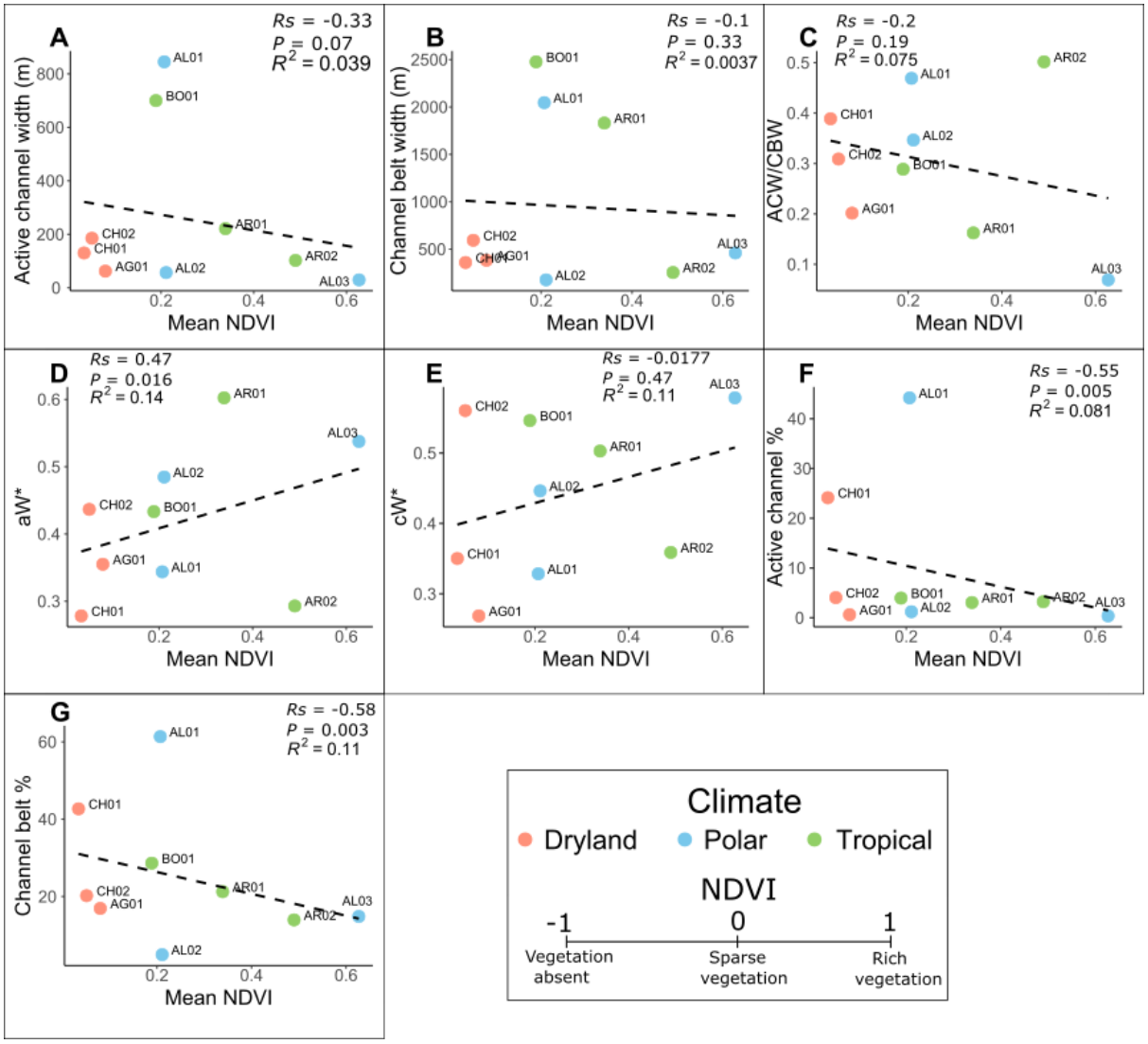

Figure 4.36: Mean values for each measured parameter (Active channel width (CBW), channel belt width (CBW), ACW/CBW, normalised ACW (aW), normalised CBW (cW*), active channel and channel belt percentage), plotted against the mean normalised difference vegetation index (NDVI) value.*

As vegetation coverage also influences channel stability and acts as a proxy for climate characteristics such as precipitation, the mean NDVI for the medial zone of a system is used to consider climate and vegetation as a control on medial characteristics. NDVI values closest to 1 indicate high vegetation coverage, whereas values close to -1 represent areas of dead or absent vegetation. This has been plotted against the system mean of each measured parameter in **Figure 4.36**.

Active Channel Width (ACW)

When mean NDVI increases, there appears to be no statistical trends when analysed with ACW, based on a weak R^2 (0.039) and R_s (-0.33, and P value 0.70). Most systems have mean widths below 300m, with AL01_POL and BO01_TROP as outlying systems.

Channel Belt Width (CBW)

There are also no significant correlations or trends for CBW, with very weak R^2 (0.0037) and R_s (-0.1, P value 0.33). Mean CBW for each system are well scattered, suggesting other factors to influence CBW over vegetation coverage (mean NDVI).

Active Channel Width / Channel Belt Width (ACW/CBW)

There is weak decreasing trend for the mean ratio against mean NDVI, however there is a very weak R^2 (0.075) and no significant correlation based on R_s (-0.2 and P value 0.19).

Active Channel : Channel Belt : Overbank

There is a moderate negative correlation for both mean active channel percentage and channel belt percentage, against mean NDVI, suggesting where vegetation coverage is higher, the proportion of active channel or channel belt decreases. Active channel percentage has a moderate R_s (-0.55, P value 0.005) but a weak R^2 (0.081). Similarly, channel belt percentage has a moderate to strong R_s (-0.58, P value 0.003), and a weak R^2 (0.11).

4.3. Discussion

4.3.1 Variability within the Medial Zone: Key Results

The second aim of this study set out to assess variability within the medial zone of modern distributive fluvial systems, to contextualise variability found in ancient rock record studies (specifically those observed in the medial zone, i.e. Martin *et al*. (2021)). Following the results presented in sections 4.1 and 4.2, variation is evident both within the medial zone of a system, and between the different systems studied.

Overall, there is a downstream decrease in both active channel width and channel belt width in the medial zone of each of the studied systems. These observations correspond to those seen on a system wide scale, in other studies of modern DFS (e.g. Kelly and Olsen, 1993; Hartley *et al.*, 2010, 2013; Weissmann *et al.*, 2011; Davidson *et al.*, 2013; Li, Tooth and Yao, 2019; Valenza *et al.*, 2020). These trends are a result of a downstream loss in discharge and sediment supply, driven by evapotranspiration, bifurcation, or infiltration (Hartley *et al.*, 2010; Weissmann *et al.*, 2010, 2013). Therefore, variability within the measured parameters (ACW and CBW) of each system is primarily related to the significantly different end member widths – a wider proximal - medial, and narrower medial – distal.

However, interestingly, for each studied system, the ACW/CBW ratio has no distinct downstream trend, but when studied a system scale study, the ratio should increase downstream as CBW narrows to a similar width as ACW. This is indicative of the downstream decrease in lateral migration of the

active channel, as the system loses energy and sediment supply depletes (Wickert *et al.*, 2013; Bufe *et al.*, 2019). While individually ACW and CBW do decrease downstream within the medial zone, this suggests that the ACW and CBW do not decrease downstream at the same rates within the medial zone, perhaps linked to variable sediment supply within the system through time. While it is suggested in this study that channel migration rates decrease from apex to toe, it is evident that this rate varies throughout the medial zone. Further study is required to fully understand why exactly this occurs. However it is postulated here that this trends may arise due to high variation in channel migration rates only observed when studying a smaller scale area of the system (e.g. the medial zone), as opposed to the trends seen in Chapter 3, where there are distinct downstream trends in the ratio in the proximal zone versus the distal zone, and variability is smoothed out of the data. As a metric in system wide studies, ACW/CBW ratio trends can indicate what DFS domain a section of a system may lie in, which is a metric that can be used in rock record bases studies using channel belt and storey widths. However, within the medial zone, it is apparent that this metric is limited as there is too much variability, thus difficult to position where in the medial zone a deposit would lie (e.g. nearer to proximal – medial, or medial – distal).

Another key result seen in section 4.1 is the downstream increase in overbank proportion. When normalised, the proportion of active channel and channel belt decrease, however while a downstream decrease in individual active channel and channel belt width are evident, the absolute proportions of these remain relatively constant. In the cases of AL01_POL and CH01_DRY, this is related to system bifurcation where active channel flow has been diverted and distributed into multiple channels. Thus, the downstream decrease in active channel and channel belt percentages are attributed to the increasing proportion of overbank deposits, where the DFS area can expand downstream, radiating into the basin. These findings are concurrent with the sweep angles measured downstream within each system, where smallest angles relate to smaller overbank proportion near the proximal – medial, and wider angles relating to larger overbank proportions near the medial – distal. However, variation from this trend is observed in some systems. For example, at AR01_TROP and AL03_POL the DFS area is constrained by neighbouring DFS or axial rivers, this has meant that the proportion of overbank also remains constant downstream as the system cannot expand further, as shown by sweep angle measurements. This has been demonstrated in **Table 4.9**, where R_s values for each parameter and system have been ranked in order of the sweep angle (SA) at the start of the medial zone. There appears to be a relationship between the percentages of active channel and channel belt, where systems with smaller sweep angles have little to no correlation, yet for systems with larger sweep angles, significant downstream decreases are apparent. Therefore, downstream trends in active channel and channel belt percentage are more apparent when the DFS is able to expand out. In narrow systems (small sweep angles), channels are more laterally confined, with smaller active channel and channel belt proportions and continuous reworking into the deposits below. Similar observations are made when comparing sweep angle to the absolute proportions of active channel and channel belt, as there are still clear decreasing trends for systems with a wide SA, yet this proportion again remains constant for narrower systems. Furthermore, when overbank area increases downstream, there is a direct influence on the percentage of channel belt recorded. Therefore, expanding, or systems with wide SA, have a decreasing downstream trend of active channel and channel belt percentages. However, the trends for the absolute values of active channel and channel belt are much less significant; weaker downstream decreases in the absolute proportions are only controlled by the decreasing width of the individual channel downstream. Thus, the confinement, or shape, of a DFS can have an impact on how sediment is distributed through the system, as in narrow systems, sediment is likely to be funnelled through. This allows for the frequent reworking of the active channel, which therefore influences the fluvial architecture of channel belt deposits preserved (e.g. reworked

channels preserved as larger amalgamated deposits). To add, there does not appear to be any link between the sweep angle and the ACW/CBW ratio, which in the event of a relationship, may have explained the variability seen, as sediment distribution varies, impacting channel mobility.

Interestingly, the channel belt proportion (both normalised and absolute) for AR01_TROP increases slightly downstream within the medial zone, this may be a result of the emergence of spring fed channels feeding the downstream portion of the medial zone (Chesley and Leier, 2018). This coincides approximately with the spring line delineated across the Chaco Plain in Hartley *et al*. (2013), although slightly more upstream than the documented spring line. Active channel proportion for AR01_TROP does not follow this same trend, slightly decreasing downstream, suggesting that some of these channel belts are relicts within the landscape: inactive related to spring fed flows, or past avulsions leaving palaeochannels, obscured by vegetation. It should be noted that these observations would require ground truthing and further study using higher resolution imagery.

SA Medial Start (°)	SA Medial End (°)	System	ACW (Rs)	CBW (Rs)	ACW/CBW (Rs)	AC% (Rs)	CB% (Rs)	Absolute AC (Rs)	Absolute CB (Rs)	Absolute OB (Rs)
92	96.5	CH01_DRY	-0.74	-0.88	+0.1	-0.66	-0.63	-0.46	-0.72	+0.98
77.1	83	Al01_POL	-0.54	-0.86	-0.12	-0.96	-0.96	-0.5	+0.45	+0.98
70.6	49.2	CH02_DRY	-0.28	-0.026	-0.18	-0.86	-0.85	-0.54	-0.85	+0.98
63.9	45	Al02_POL	-0.86	-0.85	+0.12	-0.12	-0.20	-0.02	-0.12	+0.48
60.3	83.2	BO01_TROP	-0.68	-0.84	+0.03	-0.84	-0.84	-0.78	-0.86	+0.89
54.6	25.4	AG01_DRY	-0.54	-0.41	+0.06	-0.51	-0.78	+0.1	+0.21	+0.43
35.3	19.6	Al03_POL	-0.62	-0.12	-0.42	-0.46	-0.82	0	-0.46	+0.81
20.9	22	AR02_TROP	-0.68	-0.59	+0.09	-0.36	-0.47	+0.05	-0.14	+0.90
20.6	11.5	AR01_TROP	-0.64	-0.6	+0.37	-0.18	+0.47	+0.15	+0.5	+0.26

Table 4.9: Sweep angle (SA) at the start and end of the medial zone for each system ranked in order from largest to smallest, against the Spearman's rank correlation coefficient (R_s) in different measured parameters, including active channel width (ACW), channel belt width (CBW), ratio of active channel width to channel belt width (ACW/CBW), the active channel percentage (AC%), channel belt percentage (CB%), and the absolute, unnormalized active channel (AC), channel belt (CB), and overbank (OB) proportions.

4.3.2. Drivers of Variability

In this study, the dataset has been grouped by several factors that may influence or explain variability *between* systems, including climate and morphology. Overall, it is clear, from comparison of the individual systems, there is high variation, regardless of a similar climate group, as even systems in the same climate (e.g. AR02_TROP and BO01_TROP) vastly differ. For example, the measured characteristics for AR02_TROP and BO01_TROP are not statistically significant (**Tables 4.2 – 4.8**) and the ranges in measured ACW, CBW, and ACW/CBW are much smaller for AR02_TROP. Despite belonging in the same climate group and distributing into the same sedimentary basin (Chaco Plains, with the apices situated along the Andes), other controls must influence differences between the two sites. Another example is AL01_POL, which may be considered an anomaly with its consistently outlying results for the measured parameters. This system, despite being situated within the same climate, and similar region as AL02_POL and AL03_POL, shows more similarity in its active channel

width with BO01_TROP (**Table 4.2**). Individual system comparisons showed high variation between systems of the same climatic group. However by grouping the dataset by climate helped identify if, despite internal variability within a climate group, there were differences between each climate group, or if climate groups overlapped in their ranges. Upon analysis, it is evident that when grouping by climate, there are few statistical differences between groups, with only the dryland climate group appearing to have the smallest range of active channel and channel belt widths. This is possibly linked to the infrequent nature of channel discharge in these settings. Therefore, climate alone does not explain the significant variation between the medial zones of each studied DFS, as within a climate zone these systems can vary significantly or share similarities with systems in completely different groups

When grouping by climatic zone, there are still high levels of variability within each climate zone, limiting distinct climatic related trends between the groups. While there is no distinct trend apparent between climate in this study, plotting mean NDVI for each system may show how vegetation cover influences the measured parameters, acting as a proxy for precipitation and runoff, and factors such as bank stability, considering the local impact of climate on the DFS. As there is a very weak decrease in mean active channel width with increasing mean NDVI, there is clearly still high variability between systems of similar NDVI values. For example, AL01_POL and AL02_POL are similar in vegetation coverage but significantly different in active channel width. This is attributed to vastly different river styles between the two systems, with the influencing factors for channel characteristics dominating over climate. The same is seen for the other measured parameters, again indicative of high variability between systems of a similar nature. Despite this, there is still a negative correlation between increasing vegetation cover and the proportion of active channel or channel belt, which can be related to increasing bank stability (Wickert *et al.*, 2013) limiting such extensive bifurcation; systems with higher percentages of channel belt or active channel are associated with bifurcating and avulsive channels. This again suggests that the variability seen is present due to varying river styles and channel planform, and the factors that can influence this. Finally, this method of plotting the dataset against the mean NDVI of the medial zone has its limitations; the NDVI across the medial zone may also be variable meaning the values used may not be fully representative of the medial zone. For example, vegetation cover may be more prevalent next to channels where water availability is high. Further work could be done to assess how much variability in NDVI is present across the DFS in different climates and how this impacts statistical trends.

Grouping the dataset by channel morphology, including river style and the number of measured channels (indicative of a bifurcating/multi-channel or single channel system), has shown that there are much more distinct relationships between the measured characteristics (e.g. ACW, CBW etc.) and the features of each group. Systems grouped by two or three measured channels in the medial zone represent systems that are bifurcating, and therefore distributing flow across several channels, forming much narrower channels than DFS medial zones that are characterised by one single channel. Alternatively, bifurcating, or multi-channel, systems have much higher proportions of active channel and channel belt, as more of the overbank is reworked into channel deposits. Furthermore, channel morphology has been well linked to sediment load and discharge (Hartley *et al.*, 2010; Davidson *et al.*, 2013) where coarse grained, high sediment supply and discharge creates wide braided and bifurcating systems (Friend, 1993; Hartley *et al.*, 2010), producing the wider channels seen this this study Alternatively, narrower meandering channels are associated with continuous discharge with lower sediment supply, and finer grain size. In other studies, sediment supply is found to be a significant factor in channel morphology and characteristics such as sinuosity in meandering systems (Ahmed *et al.*, 2019), potentially producing more variability within other characteristics of DFS. Therefore, when grouped as braided or meandering, there are distinct differences in the dataset, indicative of variable

sediment supply and discharges. Thus, it must be considered that the drivers of sediment supply and discharge to be the main cause of variability within the medial zone of DFS.

When group by river style, the ratio of ACW to CBW, **Figure 4.33c**, is lowest for meandering channels, suggesting higher lateral mobility than the braided channels. In this study, the active channel for braided rivers is defined as the area between the outer banks of the channel, which would be inundated with water during peak flows, including all channel threads, and the channel belt width as the area imprinted on the landscape from past flows (Limaye, 2020). This is defined similarly to the work of Limaye (2020), and the active braidplains used within Warburton (1996) and Kidová *et al.*, (2017). Therefore, channel mobility may be much higher than **Figure 4.33c** suggests, with mobility occurring within the active braidplain. Based on the differences in ACW/CBW between meandering and braided systems, this metric could be considered suitable for use in the rock record in identifying a meandering or braided DFS deposit. However, as seen in **Figure 4.33c**, there is overlap between the compared group's ranges, therefore, further study could involve the expanding the dataset, testing the validity of this method for use in the rock record.

It has been found through experimental studies of alluvial systems, that abrupt high sediment concentrations create systems with multiple channel threads (Leenman and Eaton, 2022). Episodic events are often associated with systems in dryland environments (Hartley *et al.*, 2010), inputting high sediment discharges into braided channels, of which is seen in CH01_DRY and CH02_DRY. However, AL01_POL is very similar in morphology, yet resides in a different climate group, and AG01_DRY, a similar climate, is characterised by narrow meandering channels in the medial zone, implying lower sediment supply and discharge. Therefore, while systems in similar climates can still be variable, climate is an important control in influencing sediment supply and discharges, which influences variable channel morphology and characteristics in the medial zone. However, it must be considered that other factors that influence sediment supply and discharge as a larger influence of medial variability. Furthermore, it has been proposed that as precipitation and runoff vary across climatic zones, this is not the primary factor in DFS development, and therefore variability in the medial zone, as any condition that trigger avulsions promotes the formation of a DFS (Hansford and Plink-Björklund, 2020), whether this be sediment supply or accommodation space.

In section 4.2. catchment area has also been plotted against the mean of the measured parameters per system, where it was hypothesised that a relationship between measurements such as active channel width and catchment area would exist. Previous studies have noted the relationship between catchment area and discharge (Burgers *et al*., 2014), where discharge increases with catchment area, therefore, with increasing discharge and catchment area, there will be an increase in channel width (Frasson *et al.*, 2019). However, the results produced from this study's dataset indicate weak linear regressions but moderately strong positive correlations, suggesting there is high variation in this expected trend, raising the need to widely expand the dataset. It is expected that larger catchment areas contribute larger sediment loads, and higher discharges, however in the examples of AL01_POL and BO01_TROP, catchment area is not the largest out of the dataset, but active channels and channel belts are wide and braided, suggesting high sediment loads and discharges regardless of catchment size. Similarly, the braided and bifurcating systems of CH01_DRY and AL01_POL, with the highest channel belt percentages, would be formed by high sediment supply and discharge, but is not driven by large catchment area. Furthermore, systems BO01_TROP and AR01_TROP, within the same climate and tectonic settings, differ in catchment area and morphology, with AR01_TROP a meandering channel with the largest catchment area, accounting for its wide channel width, and BO01_TROP a very wide and braided channel distributing from a smaller catchment, suggesting significantly larger sediment discharges in BO01_TROP than in AR01_TROP.

Other factors that influence sediment supply and discharge need to be investigated to understand if there is a dominating factor controlling trends, or lack of trends, observed in this study. For example, catchment lithology can vary across the different systems, regardless of climate and catchment area. In settings, where tectonic activity and climate are constant, a crystalline or hard rock lithology can limit the available sediment load, limiting aggradation of the DFS (Arzani, 2012). Alternatively, softer lithologies generate higher suspended and bedload concentrations, and where this is in excess, can develop braided morphologies (Mueller and Pitlick, 2013, 2014). Despite this, data surrounding the source rock lithology of the studied systems would need to be acquired, and this discussion on sediment supply and grain sizes makes assumptions that would need to be validated with field studies and ground truthing. Furthermore, while the systems in this study are all within a similar tectonic regime (i.e. foreland basins), rates of tectonic activity and denudation can vary between systems of a similar catchment area or climate, influencing channel morphology, and therefore causing variability in the medial zone of DFS.

Chapter 5: Overall Discussion

In Chapter 3, methods were implemented into quantifying and outlining where the boundaries for each zone of a DFS (proximal, medial, and distal) are through various criteria, including active channel width, channel belt width and channel morphology, among others. The results identified that the transitions from the proximal to medial, and medial to distal on average occur 25 – 35% and 65 – 75% downstream, with variations likely due to sediment grain size and supply. Other modern studies, such as those conducted on the Pilcomayo DFS, Argentina (Weissmann *et al.*, 2011, 2015), describe each zone based on the downstream trends in decreasing channel flows, and features including the channel avulsion and bifurcation, and identifying discrete channel belt deposits (Weissmann *et al.*, 2013). When marking the positions for the proximal, medial, and distal DFS zones, most have relied solely on qualitative observations, with some methods used limited by factors such as climate and seasonality. For example, DFS across the Chaco Plain, Argentina, experience a downstream grain size fining, which influences soil drainage, leading to the development of well-established soils in the distal zone, and immature but well-draining soils in the proximal zone (Hartley *et al.*, 2013), but in arid climates, this is difficult to observe. Other studies have identified DFS zone positions through analysis of the gravel – sand transition (Dubille and Lavé, 2015; Dingle *et al.*, 2020; 2021), related to sediment grain size and channel planform/slope, however this alone only considers the proximal – medial transition. Furthermore, a study by Davidson *et al*. (2013) has created models of three to four zones representing the different DFS domains, based on different geomorphic elements in different settings, covering a wide variety of DFS. This said, the implications of the results in Chapter 3 are the applications of a method to quantifiably define the zones of a DFS to various systems, independent of climate or channel planform, as well as identifies the need to use transition zones to mark the proximal – medial and medial – distal of approximately 10%, as the transition between each DFS zone is not abrupt.

Following this, the results in Chapter 4 have demonstrated that variability within medial zone of a DFS is associated with the downstream decrease in trends, such as active channel width and channel belt, from the proximal – medial zone and the medial – distal zone, coincident with the overall downstream trends from apex to toe seen in DFS. Then, variation between different systems has been studied, accounting most variability to be linked to variable sediment supply and discharge, independent of climatic setting, but requiring further investigation. There are also distinct differences in the proportion of channel belt and active channel, where downstream trends are only observed in systems where the DFS area is able to expand out (large sweep angle) and the proportion of overbank deposits increases. These finding have been summarised in **Figure 5.1**, where the studies DFS have been categorised into three types: *Wide sweep angle DFS, Moderate sweep angle DFS, Narrow sweep angle DFS.* Wide SA DFS consists of systems with downstream decreases in ACW and CBW, but downstream decreases in channel belt proportion are directly influenced by the expansion of the DFS and increase of overbank deposits, examples include AL01_POL and CH01_DRY. Similarly, moderate SA DFS consist of a similar trend to wide SA DFS however are characterised by single channels, and no bifurcation, examples including BO01_TROP and AR02_TROP. Finally, narrow sweep angle DFS consist of systems where there are no downstream increases in overbank deposits, and very little change in the proportions of channel belt and active channel, limited by neighbouring DFS systems or topography. Furthermore, this work has aimed to identify drivers of variability in the medial zone of modern DFS, with the implications in understanding how variability may arise through time in studying ancient DFS deposits, as discussed below.

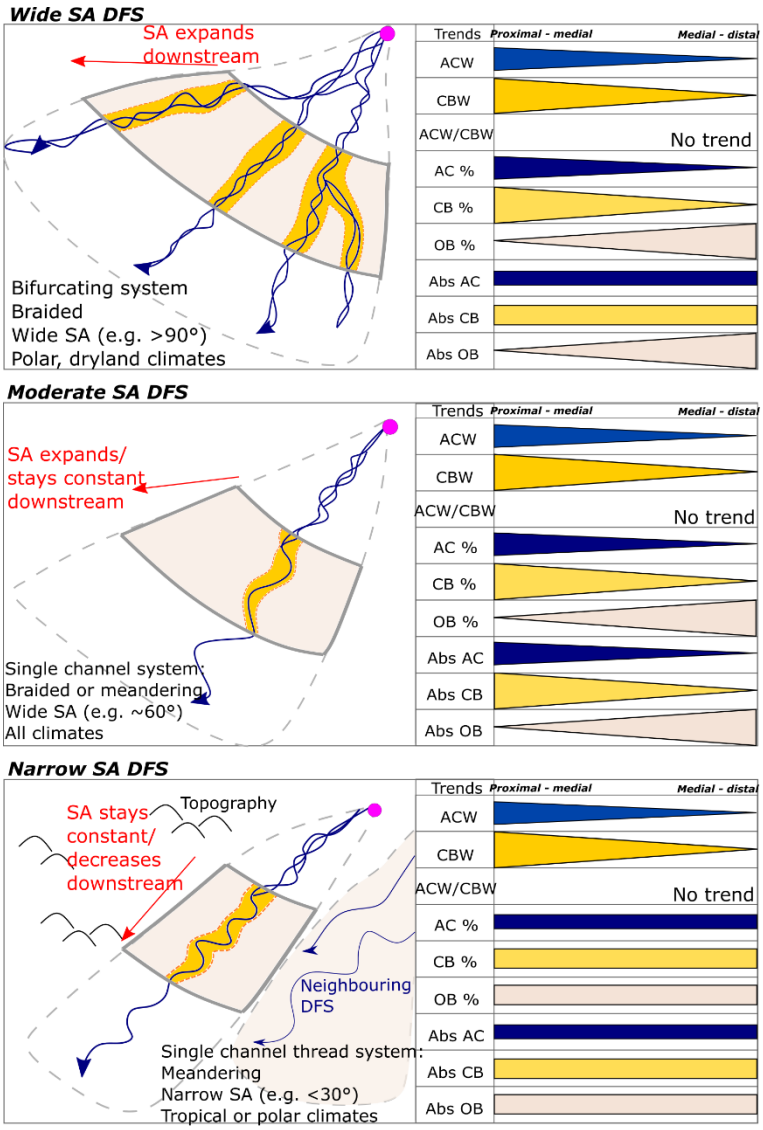

Abbreviations		Value ranges: min - max (mean)		
		Wide SA	Moderate SA	Narrow SA
ACW	Active channel width (m)	53 - 2457 (487.5)	11 - 1615 (329)	13 - 366 (92)
CBW	Channel belt width (m)	72 - 6228 (1202)	11 - 4535 (1108)	32 - 3641 (713)
ACW/ CBW	Active channel width : channel belt width	0.06 - 0.90 (0.43)	0.14 - 1.0 (0.40)	0.02 - 0.60 (0.20)
AC%	Active channel %	15 - 71 (34)	0.9 - 10 (3.7)	0.13 - 5.6 (1.3)
CB%	Channel belt %	20 - 88 (52)	4 - 65 (22)	4.7 - 33 (15)
OB%	Overbank %	12 - 80 (48)	35 - 96 (78)	66 - 98 (86)
Abs AC	Absolute active channel proportion	N/A	N/A	N/A
Abs CB	Absolute channel belt proportion	N/A	N/A	N/A
Abs OB	Absolute over-bank proportion	N/A	N/A	N/A
SA	Sweep angle (°)	~77 - 90+	~60 - 70	~20 - 35

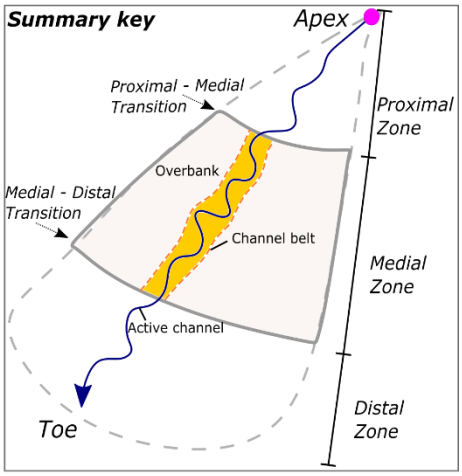

Figure 5.1: Summary diagram of the key trends observed in Chapter 4, illustrating how the downstream trends observed are directly influenced by the sweep angle (SA) of the system. Systems have been grouped into three types (wide sweep angle, moderate sweep angle, narrow sweep angle), with measured ranges for each parameter recorded in the table.

5.1 Rock Record Comparisons

While this study has focused on quantifying variability in the medial zone of modern DFS, there have been many studies that have investigated channel characteristics in the medial zone of ancient rock record deposits. Through this, variability has been observed in a number of systems, particularly the Huesca DFS, where channel body proportions in the medial zone range from 15 to 52%, with medial channel architecture ranging from isolated channel bodies to massive amalgamated belts (Martin *et al.*, 2021). Furthermore, the La Serrata portion of the Huesca DFS (medial) has observed an upwards thickening and coarsening of sand body deposits, interlaced with sporadic narrowing and thinning episodes (Burnham and Hodgetts, 2019). The overall upwards thickening sequence is coincident with the progradation of the DFS, however the narrowing episodes have been attributed to avulsion episodes directed away from the active lobe, or a reduction in deposition (Burnham and Hodgetts, 2019). In addition, the proximal and medial zone of the Huesca DFS exhibits the greatest lateral variability in net to gross, sandbody thickness and channel amalgamation (Snieder *et al.*, 2021). Furthermore, the variable channel amalgamation seen in Martin *et al*. (2021), has been related to variability in accommodation space; lower accommodation causes reworking of channel belt deposits, creating massive, amalgamated belts, whereas increasing accommodation space encourages the separation and stacking of channel deposits.

Other studies have noted high variability in the net to gross ratio (channel belt vs floodplain) of the Marilia Formation, Brazil (Führ Dal' Bó *et al.*, 2019), and high variability in channel width and thickness in the Blackhawk Formation, within an overall slight up-section increasing succession (Rittersbacher *et al*., 2014). While larger trends can be attributed to DFS progradation, many of this internal variability have been linked to autogenic controls, such as avulsion cycles and sediment supply (Owen *et al.*, 2015b). Most ancient DFS studies involve vertical trends, often informing of the controls that drive up-section trends such as progradation, and due to outcrop extent limitations, lateral trends in ancient DFS are often difficult to observe. However, where lateral trends have been studied, these have shown downstream decreasing patterns in channel belt size, and channel to floodplain ratio (Wang and Plink-Björklund, 2019), similar to those seen in the modern systems.

The results of this study have shown that through comparing different medial zones of a DFS, a common factor that causes differences in medial characteristics is varying sediment supply and discharge, controlled by a variety of factors, including catchment area, climate, and lithology. It has also been determined that most variability within a medial zone is related to the downstream trends associated with DFS on a wider scale. Therefore, as modern systems are a snapshot of conditions and processes at a set point in time for an ancient deposit, it can infer how DFS processes influence channel deposits. Firstly, as seen in progradational models of ancient studies (Weissmann *et al.*, 2013; Owen *et al.*, 2015b; Wang and Plink-Björklund, 2019; Aliyuda and Howell, 2021), an overall progradational trend may be observed, as seen at La Serrata (Burnham and Hodgetts, 2019), assuming conditions remain relatively constant. However, with changing conditions, such as sediment supply or climate, it can be inferred how these modern deposits and processes would translate to the rock record. For example, a low sediment concentration such as AR01_TROP increasing in supply, producing channel planform more similar to BO01_TROP. Thus, studying channel characteristics in the medial zone of modern systems is vital in understanding the processes that cause variability in the rock record.

5.2 Limitations

5.2.1 Preservation

While the modern systems studied here provide important context for ancient deposits in terms of the processes involved at a set point in time during specific conditions, there are limitations relating

to the preservations of deposits. Preservation of channel body, or sandbody, deposits are primarily controlled by subsidence rates, and the available accommodation space, where sediments are lowered below the level in which erosion is possible (Weissmann *et al.*, 2015). In an actively subsiding basin, with sufficient sediment supply, sediment overlies deposits, preserving the channel bodies and overbank beneath (Weissmann *et al.*, 2011), as opposed to confined axial or tributary systems which experience constant reworking and incision, producing largely amalgamated sandbodies, but no overbank material. However, sandbodies are only preserved in basins where long term subsidence can sustain the required accommodation space and preservation (Weissmann *et al.*, 2015). While increasing accommodation space is a prerequisite for channel preservation, the surface processes involved, such as avulsion, influence the formation and preservation of the channel bodies (Sheets *et al.*, 2009), through phases of channel abandonment, rapid burial, and channel reoccupation and incision of abandoned channels follows when subsidence rates lower (Mitten *et al.*, 2020). Thus, this influences how channel bodies are preserved, whether as laterally stacked channels, or massive amalgamated channel belts, featuring scoured surfaces. Therefore, a modern channel only provides context to the system processes at a fixed time, unable to predict deposition through cycles of avulsion and changing subsidence rates and accommodation space. Furthermore, the preservation of mesoscale channel architecture varies downstream on a DFS, and through variable subsidence rates, where constant reworking in the proximal zone overwrites barforms and accretionary sets that are preserved in the medial to distal zone (Mitten *et al.*, 2020). Therefore, while features such as channel bars are observed in modern systems, the existence of these may be absent from the rock record. Similarly, in modern systems, the active channels can be studied, however these are not seen in the rock record, and only preserved under certain conditions, such as the abandonment and fill of a channel.

While modern systems provide a snapshot, the channel and processes currently occurring may not make up the channel body preserved in the rock record, whether these are caused by background sedimentation, or high magnitude events. For example, deposits preserved from arid climates are likely to be produced from high sediment loads during large by infrequent flood events (Wilson *et al.*, 2014), where background processes are overprinted. Not only can climate influence what material is preserved, it may also influence the preservation potential, where arid regions such as the Atacama Desert have inactive Miocene fans preserved within (Weissmann *et al.*, 2011), where surface lithification occurs in between flood events due to high evaporation rates (Wilson *et al.*, 2014).

5.2.2 Project Limitations and Further Work

There are some limitations in this study that on reflection should be considered and improved upon if this study were to be repeated or expanded. Firstly, the analysis of the systems in this study were dependent of Sentinel 2 and Landsat 8 imagery, which is limited by resolutions of 15m and 10m. However, higher resolution imagery will greatly expand the accuracy of measurements taken (E.g. Planet Imagery), particularly for systems with much smaller channels, as well as enhance any geomorphic features that could not be observed in the imagery used. Furthermore, there could be improvements to the methods used in extracting characteristics such as active channel width, by utilising automated approaches, such as Yang *et al.* (2020) and Hayden *et al.* (2021), which would also enable the expansion of the dataset within the scope of a small project. Similarly, an automated approach to measuring active channel percentage was tested in this study, however as discussed in Chapter 2, had its own limitations that would need improvement on before being reliably utilised.

With increased project scope, other things could be measured to aid in the understanding of medial zone variability. For example, channel slope measurements can help in quantifying differences in channel planform seen across the medial zone, as was accomplished in Chapter 3 for delineating each

DFS zone. Furthermore, much of the variability in this study has been attributed to variations in sediment supply and discharge rates, which have been assumed with only limited information such as catchment area, therefore other information such as sediment flux, or denudation rates, or channel discharge rates, could be added to the database in support of this studies suggestions. Additionally, variability in channel migration rates have been discussed, where the ratio of ACW/CBW appear highly variable and lacked downstream trend, therefore, satellite imagery of the systems over several time periods could be used in quantifying channel migration rates. In improving the link between surface processes and the subsurface, channel bathymetry and depth measurements could vastly expand the scope of this project, where modelled or collected through fieldwork. For example, the work of Steel *et al*. (2022), modelled channel bathymetry of surface imagery, in order to infer channel connectivity and architecture of the subsurface.

5.3 Practical Applications

Beyond the usefulness of studying the medial zone in modern DFS to aid in other studies, ancient or modern, there are many socio-economic applications for the study of the medial zone, and DFS as a whole. Modern and ancient DFS can provide important context for the distribution and characterisation of fluvial reservoirs and is essential in improving recovery of resources (Burnham and Hodgetts, 2019) found in the channel belt deposits preserved in the rock record from modern systems. As discussed in this study, studying modern DFS is critical in understanding the processes involved in forming ancient deposits, as well as the connectivity between these. Reservoir connectivity has been directly linked to channel mobility, where processes such as avulsion, and characteristics such as discharge, sediment flux, accommodation space, and the resulting channel widths and depths (Flint and Bryant, 1993; Steel *et al.*, 2022) play an important role in the formation of channel belts, as well as the degree of lateral or vertical stacking in channel bodies. Numerical modelling of DFS has shown that these characteristics, including the proportion of channels directly influence connectivity (Flint and Bryant, 1993; Snieder *et al.*, 2021), where increasing channel proportion, and channel width or depth, means increased connectivity between sandbodies. Therefore, the characterisation undertaken in this study in variable systems, has applications for mapping the connectivity and distribution of reservoirs, similar to what has been achieved by Steel *et al*. (2022), where imagery was used in conjunction with modelled channel depth data to model the subsurface distribution of reservoirs. Thus, the characterisation of reservoirs is beneficial in understanding fluid flow of resources such as hydrocarbons, groundwater, and carbon capture and storage and hydrogen (Snieder *et al.*, 2021). Recent work has used detailed facies models in assessing the potential for using fluvial reservoirs in geothermal energy (Willems *et al.*, 2017), requiring understanding of the vertical and lateral extent of these stores.

Channel connectivity and channel body characteristics also has important environmental implications, with regards to contaminant distribution. In the Ganga Plain, many modern DFS deposits include many important aquifer stores, mapped using satellite imagery and wells across the fan surface (Van Dijk *et al.*, 2016), however, the dispersion of contaminants, such as arsenic (Shah, 2008), can occur where these are flushed through deposits with high porosity and permeability, into fine grained distal deposits, as well as through the connectivity between porous and permeable channel bodies (Anderson *et al.*, 1999). Furthermore, related to the high porosity and permeability of proximal and medial deposits, mineral resources, such as uranium, have seen a direct link between the distribution uranium and the channel percentage (Owen *et al.*, 2016); proximal and medial areas with high channel body percentage are likely to have a high accumulation of mineral resources.

Chapter 6: Conclusions

6.1. Conclusions

The first part of this study involved using quantitative methods to constrain where the proximal, medial, and distal zones were situated downstream, to enable more detailed analysis of the medial zone in the second portion of the study. From this part it can be concluded as follows:

- There are distinct downstream trends (statistically significant strong negative correlations) that can identify where the proximal to medial transition zone is, where active channel (ACW) and channel belt widths (CBW) significantly narrow, often coinciding with changes in slope and channel style change from braided to meandering.
- Trends that identify where the medial to distal transition zone is include the significant increasing (positive correlation) of ACW/CBW (to values of 1), coincident with a decrease in lateral mobility and the formation of ribbon channels or terminal splays, indicated by a series of distal avulsions.
- The average percentage downstream for each zone is 25 – 35% and 65 – 75%, with these positions being very similar across the studied systems. Variation from this trend has been attributed to higher sediment loads, through comparing the catchment area /DFS area of each system.

The second aim of this study set out to assess variability in the medial zone through measuring various channel characteristics, concluding the following;

- Within most of the studied systems' medial zone, ACW and CBW display statistically significant downstream decreases (moderate to strong negative correlation R_s values ranging -0.54 to -0.86 for ACW and -0.41 to -0.88 for CBW) from the 'proximal to medial' zone to the 'medial to distal' zone, with few anomalous systems (e.g. CH02_DRY for ACW and CBW, and AL03_POL for CBW). This is reflective of the trends observed in system scale studies. This has been related to downstream losses in discharge and sediment supply, through processes including bifurcation and evapotranspiration. Despite these trends, magnitude of ACW and CBW varies between systems, for example, AL01_POL, a small DFS, records the widest channel measurements within the dataset.
- Most systems do not statistically significant downstream trends for ACW/CBW, indicating that CBW and ACW may not decrease downstream at the same rate. This is speculated to be related to variable channel migration rates through time but would require more work to understand. Furthermore, while ACW/CBW downstream trends in most systems is similar, a comparison of each systems indicates there to be significant differences between the systems (mean values ranging 0.16 to 0.50), where some systems are likely much more laterally mobile than others, including those in similar climatic zones.
- The proportion of overbank in some systems has a direct impact on the proportion of active channel and channel belt observed and the downstream trends. In some systems channel flow is distributed across bifurcating channels and the system with a large sweep angle increases the proportion of overbank, therefore decreasing the proportion of active channel and channel belt.
- A comparison with statistical testing for the proportions of active channel, channel belt, and over bank deposits, both normalised (percentages) and with absolute values, indicated that the proportion of overbank downstream has a direct influence on the proportions of active channel and channel belt observed and the associated downstream trends. For example, AL01_POL comprises of multiple bifurcated channels, and while a general downstream

decrease in active channel width and channel belt is observed, the absolute proportions for these indicates a moderate to weak downstream trend (e.g. R^2 values of 0.28 and 0.20), but a statistically strong increase for absolute overbank proportion (R^2 0.98). As a percentage proportion there is a statistically strong downstream trend (active channel and channel belt R^2 values of 0.89 and 0.90) related to the increase in overbank deposits, which has been linked to wide sweep angles (above 60 degrees).

- Some DFS were observed to be constrained by neighbouring systems or topography (e.g. AR01_TROP and AL02_POL), and therefore sweep angle is small (less than 30 degrees). As a result, the proportion of overbank remains constant, with the active channel and channel belt proportions relatively constant often with weak correlations (e.g. AL02_POL R_s values for channel belt percentage is -0.2, and absolute active channel -0.12). Sediment is likely funnelled through the system, causing frequent reworking of channel belt deposits.
- Sweep angle therefore has a direct link to the observed DFS trends, and factors such as sediment distribution.
- Individual comparisons and grouping the dataset by climate group showed that variability within a climate zone was high and several systems of different climates shared more similarities than those within the same climate. Therefore, factors other than climate may have a more significant influence on variability.
- Multiple factors may cause variability between the different medial zones, primarily factors that control sediment supply and discharge. Comparisons by channel planform identified distinct trends between braided and meandering systems. Other comparisons showed some systems fed by small catchment areas are characterised by wide active channels and channel belts, likely related to high discharge rates and sediment supply.

References

Ahmed, J., Constantine, J.A. and Dunne, T. (2019) 'The role of sediment supply in the adjustment of channel sinuosity across the Amazon Basin', *Geology*, 47(9), pp. 807–810. doi:10.1130/G46319.1.

Ahn, J., Choi, M.H., Kim, K., Senok, S.S., Dan Cho, D. Il, Koo, K.I. and Goo, Y. (2017) 'The advantage of topographic prominence-adopted filter for the detection of short-latency spikes of retinal ganglion cells', *Korean Journal of Physiology and Pharmacology*, 21(5), pp. 555–563. doi:10.4196/kjpp.2017.21.5.555.

Aliyuda, K. and Howell, J. (2021) 'Progradation of a mid-Cretaceous distributive fluvial system: The upper member of the Bima Formation, Northern Benue Trough, Nigeria', *Sedimentology*, 68(5), pp. 1861–1876. doi:10.1111/sed.12831.

Anderson, M.P., Aiken, J.S., Webb, E.K. and Mickelson, D.M. (1999) 'Sedimentology and hydrogeology of two braided stream deposits', *Sedimentary Geology*, 129(3–4), pp. 187–199. doi:10.1016/S0037-0738(99)00015-9.

Arzani, N. (2012) 'Catchment lithology as a major control on alluvial megafan development, Kohrud Mountain range, central Iran', *Earth Surface Processes and Landforms*, 37(7), pp. 726–740. doi:10.1002/esp.3194.

Arzani, N. and Jones, S.J. (2018) 'Upstream controls on evolution of dryland alluvial megafans: Quaternary examples from the Kohrud Mountain Range, central Iran', *Geological Society Special Publication*, 440(1), pp. 245–264. doi:10.1144/SP440.2.

Attal, M. and Lavé, J. (2006) 'Changes of bedload characteristics along the Marsyandi River (central

Nepal): Implications for understanding hillslope sediment supply, sediment load evolution along fluvial networks, and denudation in active orogenic belts', in Willett, S., Hovius, N., Brandon, M., and Fisher, D. (eds) *Tectonics, Climate and Landscape Evolution: Geological Society of America Special Paper*, pp. 143–171. doi:10.1130/2006.2398(09).

Bajocco, S., De Angelis, A. and Salvati, L. (2012) 'A satellite-based green index as a proxy for vegetation cover quality in a Mediterranean region', *Ecological Indicators*, 23, pp. 578–587. doi:10.1016/j.ecolind.2012.05.013.

Blum, M.D. and Törnqvist, T.E. (2000) 'Fluvial responses to climate and sea-level change: A review and look forward', *Sedimentology*, 47(SUPPL. 1), pp. 2–48. doi:10.1046/j.1365-3091.2000.00008.x.

Brice, J.C. (1964) 'Channel patterns and terraces of the Loup Rivers in Nebraska', *U.S. Geological Survey professional paper*, 422, p. 41.

Bridge, J.S. and Tye, R.S. (2000) 'Interpreting the dimensions of ancient fluvial channel bars, channels, and channel belts from wireline-logs and cores', *AAPG Bulletin*, 84(8), pp. 1205–1228. doi:10.1306/a9673c84-1738-11d7-8645000102c1865d.

Buehler, H.A., Weissmann, G.S., Scuderi, L.A. and Hartley, A.J. (2011) 'Spatial and temporal evolution of an avulsion on the Taquari river distributive fluvial system from satellite image analysis', *Journal of Sedimentary Research*, 81(8), pp. 630–640. doi:10.2110/jsr.2011.040.

Bufe, A., Turowski, J.M., Burbank, D.W., Paola, C., Wickert, A.D. and Tofelde, S. (2019) 'Controls on the lateral channel-migration rate of braided channel systems in coarse non-cohesive sediment', *Earth Surface Processes and Landforms*, 44(14), pp. 2823–2836. doi:10.1002/esp.4710.

Buffington, J.M. and Montgomery, D.R. (2022) *Geomorphic Classification of Rivers: An Updated Review*. Second Edi, *Treatise on Geomorphology*. Second Edi. Elsevier. doi:10.1016/B978-0-12-818234-5.00077-8.

Burgers, H.E.R., Schipper, A.M. and Hendriks, A.J. (2014) 'Size relationships of water discharge in rivers : scaling of discharge with catchment area , main-stem length and precipitation', 5775(28), pp. 5769–5775. doi:10.1002/hyp.10087.

Burnham, B.S. and Hodgetts, D. (2019) 'Quantifying spatial and architectural relationships from fluvial outcrops', *Geosphere*, 15(1), pp. 236–253. doi:10.1130/GES01574.1.

Cain, S.A. and Mountney, N.P. (2009) 'Spatial and temporal evolution of a terminal fluvial fan system: The permian organ rock formation, South-east Utah, USA', *Sedimentology*, 56(6), pp. 1774–1800. doi:10.1111/j.1365-3091.2009.01057.x.

Chakraborty, T., Kar, R., Ghosh, P. and Basu, S. (2010) 'Kosi megafan: Historical records, geomorphology and the recent avulsion of the Kosi River', *Quaternary International*, 227(2), pp. 143–160. doi:10.1016/j.quaint.2009.12.002.

Chesley, J.T. and Leier, A.L. (2018) 'Sandstone-body variability in the medial-distal part of an ancient distributive fluvial system, Salt Wash Member of the Morrison Formation, Utah, USA', *Journal of Sedimentary Research*, 88, pp. 568–582.

Clarke, L.E. (2015) 'Experimental alluvial fans: Advances in understanding of fan dynamics and processes', *Geomorphology*, 244, pp. 135–145. doi:10.1016/j.geomorph.2015.04.013.

Davidson, S.K., Hartley, A.J., Weissmann, G.S., Nichols, G.J. and Scuderi, L.A. (2013) 'Geomorphic elements on modern distributive fluvial systems', *Geomorphology*, 180–181, pp. 82–95. doi:10.1016/j.geomorph.2012.09.008.

Van Dijk, W.M., Densmore, A.L., Singh, A., Gupta, S., Sinha, R., Mason, P.J., Joshi, S.K., Nayak, N.,

Kumar, M., Shekhar, S., Kumar, D. and Rai, S.P. (2016) 'Linking the morphology of fluvial fan systems to aquifer stratigraphy in the Sutlej-Yamuna plain of northwest India', *Journal of Geophysical Research: Earth Surface*, 121(2), pp. 201–222. doi:10.1002/2015JF003720.

Dingle, E.H., Kusack, K.M. and Venditti, J.G. (2021) 'The gravel-sand transition and grain size gap in river bed sediments', *Earth-Science Reviews*, 222(October), p. 103838. doi:10.1016/j.earscirev.2021.103838.

Dingle, E.H., Sinclair, H.D., Attal, M., Milodowski, D.T. and Singh, V. (2016) 'Subsidence control on river morphology and grain size in the ganga plain', *American Journal of Science*, 316(8), pp. 778–812. doi:10.2475/08.2016.03.

Dingle, E.H., Sinclair, H.D., Venditti, J.G., Attal, M., Kinnaird, T.C., Creed, M., Quick, L., Nittrouer, J.A. and Gautam, D. (2020) 'Sediment dynamics across gravel-sand transitions: Implications for river stability and floodplain recycling', *Geology*, 48(5), pp. 468–472. doi:10.1130/G46909.1.

Dong, T.Y. and Goudge, T.A. (2022) 'Quantitative relationships between river and channel-belt planform patterns', *Geology*, 50(9), pp. 1053–1057. doi:10.1130/g49935.1.

Dubille, M. and Lavé, J. (2015) 'Rapid grain size coarsening at sandstone/conglomerate transition: Similar expression in Himalayan modern rivers and Pliocene molasse deposits', *Basin Research*, 27(1), pp. 26–42. doi:10.1111/bre.12071.

Duller, R.A., Whittaker, A.C., Fedele, J.J., Whitchurch, A.L., Springett, J., Smithells, R., Fordyce, S. and Allen, P.A. (2010) 'From grain size to tectonics', *Journal of Geophysical Research: Earth Surface*, 115(3). doi:10.1029/2009JF001495.

Egozi, R. and Ashmore, P. (2008) 'Defining and measuring braiding intensity', *Earth Surface Processes and Landforms*, 33, pp. 2121–2138. doi:10.1002/esp1658.

Fielding, C.R., Ashworth, P.J., Best, J.L., Prokocki, E.W. and Smith, G.H.S. (2012) 'Tributary, distributary and other fluvial patterns: What really represents the norm in the continental rock record?', *Sedimentary Geology*, 261–262, pp. 15–32. doi:10.1016/j.sedgeo.2012.03.004.

Fisher, J.A., Nichols, G.J. and Waltham, D.A. (2007) 'Unconfined flow deposits in distal sectors of fluvial distributary systems: Examples from the Miocene Luna and Huesca Systems, northern Spain', *Sedimentary Geology*, 195(1–2), pp. 55–73. doi:10.1016/j.sedgeo.2006.07.005.

Flint, S.S. and Bryant, I.D. (1993) *The geological modelling of hydrocarbon reservoirs and outcrop analogues*. Oxford: Blackwell Scientific.

Frasson, R.P. de M., Pavelsky, T.M., Fonstad, M.A., Durand, M.T., Allen, G.H., Schumann, G., Lion, C., Beighley, R.E. and Yang, X. (2019) 'Global Relationships Between River Width, Slope, Catchment Area, Meander Wavelength, Sinuosity, and Discharge', *Geophysical Research Letters*, 46(6), pp. 3252–3262. doi:10.1029/2019GL082027.

Friend, P.F. (1993) 'Control of river morphology by the grain-size of sediment supplied', *Sedimentary Geology*, 85(1–4), pp. 171–177. doi:10.1016/0037-0738(93)90081-F.

Friend, P.F. and Sinha, R. (1993) 'Braiding and meandering parameters', *Geological Society Special Publication*, 75(1), pp. 105–111. doi:10.1144/GSL.SP.1993.075.01.05.

Fu, B. and Burgher, I. (2015) 'Riparian vegetation NDVI dynamics and its relationship with climate, surface water and groundwater', *Journal of Arid Environments*, 113, pp. 59–68. doi:10.1016/j.jaridenv.2014.09.010.

Führ Dal' Bó, P., Soares, M.V.T., Basilici, G., Rodrigues, A.G. and Menezes, M.N. (2019) 'Spatial variations in distributive fluvial system architecture of the upper cretaceous marília formation, se

brazil', *Geological Society Special Publication*, 488(1), pp. 97–118. doi:10.1144/SP488.6.

Gibling, M.R. (2006) 'Width and thickness of fluvial channel bodies and valley fills in the geological record: A literature compilation and classification', *Journal of Sedimentary Research*, 76(5–6), pp. 731–770. doi:10.2110/jsr.2006.060.

Hajek, E.A. and Edmonds, D.A. (2014) 'Is river avulsion style controlled by floodplain morphodynamics?', *Geology*, 42(3), pp. 199–202. doi:10.1130/G35045.1.

Hamer, J.M.M., Sheldon, N.D., Nichols, G.J. and Collinson, M.E. (2007) 'Late Oligocene-Early Miocene paleosols of distal fluvial systems, Ebro Basin, Spain', *Palaeogeography, Palaeoclimatology, Palaeoecology*, 247(3–4), pp. 220–235. doi:10.1016/j.palaeo.2006.10.016.

Hansford, M.R. and Plink-Björklund, P. (2020) 'River discharge variability as the link between climate and fluvial fan formation', *Geology*, 48(10), pp. 952–956. doi:10.1130/G47471.1.

Hartley, A.J., Weissmann, G.S., Bhattacharayya, P., Nichols, G.J., Scuderi, L.A., Davidson, S.K., Leleu, S., Chakraborty, T., Ghosh, P. and Mather, A.E. (2013) 'Soil development on modern distributive fluvial systems: Preliminary observations with implications for interpretation of paleosols in the rock record', *SEPM Special Publications*, 104(104), pp. 149–158. doi:10.2110/sepmsp.104.10.

Hartley, A.J., Weissmann, G.S., Nichols, G.J. and Warwick, G.L. (2010) 'Large distributive fluvial systems: Characteristics, distribution, and controls on development', *Journal of Sedimentary Research*, 80(2), pp. 167–183. doi:10.2110/jsr.2010.016.

Hayden, A.T., Lamb, M.P. and Carney, A.J. (2021) 'Similar curvature-to-width ratios for channels and channel belts: Implications for paleo-hydraulics of fluvial ridges on Mars', *Geology*, 49(7), pp. 837–841. doi:10.1130/G48370.1.

Hayden, A.T., Lamb, M.P., Fischer, W.W., Ewing, R.C., McElroy, B.J. and Williams, R.M.E. (2019) 'Formation of sinuous ridges by inversion of river-channel belts in Utah, USA, with implications for Mars', *Icarus*, 332(April), pp. 92–110. doi:10.1016/j.icarus.2019.04.019.

Hecke, T. Van (2012) 'Power study of anova versus Kruskal-Wallis test', *Journal of Statistics and Management Systems*, 15(2–3), pp. 241–247. doi:10.1080/09720510.2012.10701623.

Hirst, J.P.. (1991) *Variations in alluvial architecture across the oligo-miocene Huesca fluvial system, Ebro Basin, Spain*, *in: The three dimensional facies architecture ofterrigenous clastic sediments and its implications for hydrocarbon discovery and recovery*. Edited by A.. Miall and N. Tyler. London: Society of Economic Paleontologists and Mineralogists. doi:10.2110/csp.91.03.

Jones, L.S. and Schumm, S.A. (1999) 'Causes of avulsion : an overview', *Spec. publs int. Ass. Sedomemt*, 28, pp. 171–178.

Kelly, S.B. and Olsen, H. (1993) 'Terminal fans-a review with reference to Devonian examples', *Sedimentary Geology*, 85(1–4), pp. 339–374. doi:10.1016/0037-0738(93)90092-J.

Kidová, A., Lehotský, M. and Rusnák, M. (2017) 'Recent Channel Planform Evolution of a Braided-Wandering River Using Multitemporal Data and Gis (Case Study of the Belá River, Slovak Carpathians)', *Acta Scientiarum Polonorum Formatio Circumiectus*, 1(March), pp. 247–259. doi:10.15576/asp.fc/2017.16.1.247.

Kjemperud, A. V., Schomacker, E.R. and Cross, T.A. (2008) 'Architecture and stratigraphy of alluvial deposits, Morrison Formation (Upper Jurassic), Utah', *American Association of Petroleum Geologists Bulletin*, 92(8), pp. 1055–1076. doi:10.1306/03250807115.

Kukulski, R.B., Hubbard, S.M., Moslow, T.F. and Raines, M.K. (2013) 'Basin-scale stratigraphic architecture of upstream fluvial deposits: Jurassic-cretaceous foredeep, Alberta Basin, Canada',

Journal of Sedimentary Research, 83(8), pp. 704–722. doi:10.2110/jsr.2013.53.

Kumar, R., Ghosh, S.K. and Sangode, S.J. (1999) 'Evolution of a Neogene fluvial system in a Himalayan foreland basin, India', *Special Paper of the Geological Society of America*, 328, pp. 239–256. doi:10.1130/0-8137-2328-0.239.

Leenman, A.S. and Eaton, B.C. (2022) 'Episodic sediment supply to alluvial fans: implications for fan incision and morphometry', *Earth Surface Dynamics*, 10(6), pp. 1097–1114. doi:10.5194/esurf-10-1097-2022.

Lehner, B. and Grill, G. (2013) 'Global river hydrography and network routing : baseline data and new approaches to study the world ' s large river systems', *Hydro*, 27, pp. 2171–2186. doi:10.1002/hyp.9740.

Li, J., Tooth, S. and Yao, G. (2019) 'Cascades of sub-decadal, channel-floodplain changes in low-gradient, non-vegetated reaches near a dryland river terminus: Salar de Uyuni, Bolivia', *Earth Surface Processes and Landforms*, 44(2), pp. 490–506. doi:10.1002/esp.4512.

Limaye, A.B. (2020) 'How Do Braided Rivers Grow Channel Belts?', *Journal of Geophysical Research: Earth Surface*, 125(8), pp. 1–24. doi:10.1029/2020JF005570.

Llobera, M. (2001) 'Building past landscape perception with GIS: Understanding topographic prominence', *Journal of Archaeological Science*, 28(9), pp. 1005–1014. doi:10.1006/jasc.2001.0720.

Makaske, B., Maathuis, B.H.P., Padovani, C.R., Stolker, C., Mosselman, E. and Jongman, R.H.G. (2012) 'Upstream and downstream controls of recent avulsions on the Taquari megafan, Pantanal, south-western Brazil', *Earth Surface Processes and Landforms*, 37(12), pp. 1313–1326. doi:10.1002/esp.3278.

Martin, B., Owen, A., Nichols, G.J., Hartley, A.J. and Williams, R.D. (2021) 'Quantifying Downstream, Vertical and Lateral Variation in Fluvial Deposits: Implications From the Huesca Distributive Fluvial System', *Frontiers in Earth Science*, 8(February), pp. 1–19. doi:10.3389/feart.2020.564017.

McKight, P.E. and Najab, J. (2010) 'KRUSKAL-WALLIS TEST', in Weiner, I.B. and Craighead, W.E. (eds) *The Corsini Encyclopedia of Psychology*.

Mescolotti, P.C., Pupim, F. do N., Ladeira, F.S.B., Sawakuchi, A.O., Santa Catharina, A. and Assine, M.L. (2021) 'Fluvial aggradation and incision in the Brazilian tropical semi-arid: Climate-controlled landscape evolution of the São Francisco River', *Quaternary Science Reviews*, 263. doi:10.1016/j.quascirev.2021.106977.

Mitten, A.J., Howell, L.P., Clarke, S.M. and Pringle, J.K. (2020) 'Controls on the deposition and preservation of architectural elements within a fluvial multi-storey sandbody', *Sedimentary Geology*, 401, p. 105629. doi:10.1016/j.sedgeo.2020.105629.

Mouchené, M., Van Der Beek, P., Carretier, S. and Mouthereau, F. (2017) 'Autogenic versus allogenic controls on the evolution of a coupled fluvial megafan-mountainous catchment system: Numerical modelling and comparison with the Lannemezan megafan system (northern Pyrenees, France)', *Earth Surface Dynamics*, 5(1), pp. 125–143. doi:10.5194/esurf-5-125-2017.

Mueller, E.R. and Pitlick, J. (2013) 'Sediment supply and channel morphology in mountain river systems: 1. Relative importance of lithology, topography, and climate', *Journal of Geophysical Research: Earth Surface*, 118(4), pp. 2325–2342. doi:10.1002/2013JF002843.

Mueller, E.R. and Pitlick, J. (2014) 'Sediment supply and channel morphology in mountain river systems: 2. Single thread to braided transitions', *Journal of Geophysical Research: Earth Surface RESEARCH*, 119, pp. 1516–1541. doi:10.1002/2013JF002843.Sediment.

Myers, L. and Sirois, M.J. (2006) 'Spearman Correlation Coefficients, Differences between', in Kotz, S., Read, C.., Balakrishnan, N., Vidakovic, B., and Johnson, N.. (eds) *Encyclopedia of Statistical Sciences*. doi:10.1002/9781118445112.stat02802.

Nichols, G.J. and Fisher, J.A. (2007) 'Processes, facies and architecture of fluvial distributary system deposits', *Sedimentary Geology*, 195(1–2), pp. 75–90. doi:10.1016/j.sedgeo.2006.07.004.

Nichols, G.J., Hartley, A.J., Weissmann, G.S., Scuderi, L.A. and Davidson, S.K. (2012) 'Fluvial Reservoirs : Using the Right Architectural Models *', 50571.

Owen, A., Ebinghaus, A., Hartley, A.J., Santos, M.G.M. and Weissmann, G.S. (2017) 'Multi-scale classification of fluvial architecture: An example from the Palaeocene–Eocene Bighorn Basin, Wyoming', *Sedimentology*, 64(6), pp. 1572–1596. doi:10.1111/sed.12364.

Owen, A., Hartley, A.J., Ebinghaus, A., Weissmann, G.S. and Santos, M.G.M. (2018) 'Basin-scale predictive models of alluvial architecture: Constraints from the Palaeocene–Eocene, Bighorn Basin, Wyoming, USA', *Sedimentology*, 66(2), pp. 736–763. doi:10.1111/sed.12515.

Owen, A., Hartley, A.J., Weissmann, G.S. and Nichols, G.J. (2016) 'Uranium distribution as a proxy for basin-scale fluid flow in distributive fluvial systems', *Journal of the Geological Society*, 173(4), pp. 569–572. doi:10.1144/jgs2016-007.

Owen, A., Nichols, G.J., Hartley, A.J. and Weissmann, G.S. (2015) 'Vertical trends within the prograding Salt Wash distributive fluvial system, SW United States', *Basin Research*, 29(1), pp. 64–80. doi:10.1111/bre.12165.

Owen, A., Nichols, G.J., Hartley, A.J., Weissmann, G.S. and Scuderi, L.A. (2015) 'Quantification of a distributive fluvial system: The salt wash dfs of the Morrison Formation, SW U.S.A.', *Journal of Sedimentary Research*, 85(5), pp. 544–561. doi:10.2110/jsr.2015.35.

Paola, C., Heller, P.L. and Angevinet, C.L. (1992) 'The large-scale dynamics of grain-size variation in alluvial basins, 2: Application to syntectonic conglomerate', *Basin Research*, 4(2), pp. 91–102. doi:10.1111/j.1365-2117.1992.tb00146.x.

Parker, G. and Cui, Y. (1998) 'The arrested gravel front : stable gravel-sand transitions in rivers Part 2 : General numerical solution', 36(1), pp. 75–100.

Pereira, L.E., Lo, E. and Paranhos Filho, A.C. (2022) 'Taquari Megafan: Estimation of Water Resources in the Pantanal Wetland, Brazil', *SSRN Electronic Journal* [Preprint]. doi:10.2139/ssrn.4139627.

Priddy, C.L. and Clarke, S.M. (2021) 'Spatial variation in the sedimentary architecture of a dryland fluvial system', *Sedimentology*, 68(6), pp. 2887–2917. doi:10.1111/sed.12876.

Quick, L., Sinclair, H.D., Attal, M. and Singh, V. (2020) 'Conglomerate recycling in the Himalayan foreland basin : Implications for grain size and provenance', *Geological Society of America Bulletin*, (7), pp. 1639–1656.

Reis, A., Marlon, C., Bochi, F., Magalhães, M. De, Rossetti, M., Kifumbi, C., Galvão, E., Souza, D., Pedro, J., Ferronatto, F. and Owen, A. (2019) 'Sedimentology of the proximal portion of a large-scale , Upper Jurassic fl uvial-aeolian system in Paraná Basin , southwestern Gondwana', *Journal of South American Earth Sciences*, 95, p. 102248. doi:10.1016/j.jsames.2019.102248.

Reis, A.D. dos, Scherer, C.M. dos S., Amarante, F.B. do, Rossetti, M. de M.M., Kifumbi, C., Souza, E.G. de, Ferronatto, J.P.F. and Owen, A. (2019) 'Sedimentology of the proximal portion of a large-scale, Upper Jurassic fluvial-aeolian system in Paraná Basin, southwestern Gondwana', *Journal of South American Earth Sciences*, 95(July 2018), p. 102248. doi:10.1016/j.jsames.2019.102248.

Reitz, M.D. and Jerolmack, D.J. (2012) 'Experimental alluvial fan evolution: Channel dynamics, slope

controls, and shoreline growth', *Journal of Geophysical Research: Earth Surface*, 117(2), pp. 1–19. doi:10.1029/2011JF002261.

Rittersbacher, A., Howell, J.A. and Buckley, S.J. (2014) 'Analysis of fluvial architecture in the blackhawk formation, wasatch plateau, UTAH, U.S.A., using large 3d photorealistic models', *Journal of Sedimentary Research*, 84(2), pp. 72–87. doi:10.2110/jsr.2014.12.

Sambrook Smith, G.H., Best, J.L., Ashworth, P.J., Fielding, C.R., Goodbred, S.L. and Prokocki, E.W. (2010) 'Fluvial form in modern continental sedimentary basins: Distributive fluvial systems: Comment', *Geology*, 38(12), p. 3538944. doi:10.1130/G31507C.1.

Sassi, M.G., Hoitink, A.J.F., De Brye, B. and Deleersnijder, E. (2012) 'Downstream hydraulic geometry of a tidally influenced river delta', *Journal of Geophysical Research F: Earth Surface*, 117(4), pp. 1–13. doi:10.1029/2012JF002448.

Shah, B.A. (2008) 'Role of Quaternary stratigraphy on arsenic-contaminated groundwater from parts of Middle Ganga Plain, UP-Bihar, India', *Environmental Geology*, 53(7), pp. 1553–1561. doi:10.1007/s00254-007-0766-y.

Sheets, B.A., Paola, C. and Kelberer, J.M. (2009) 'Creation and Preservation of Channel-Form Sand Bodies in an Experimental Alluvial System', *Sedimentary Processes, Environments and Basins*, pp. 555–567. doi:10.1002/9781444304411.ch22.

Singh, H., Parkash, B. and Gohain, K. (1993) 'Facies analysis of the Kosi megafan deposits', *Sedimentary Geology*, 85(1–4), pp. 87–113. doi:10.1016/0037-0738(93)90077-I.

Singh, K.V., Setia, R., Sahoo, S., Prasad, A. and Pateriya, B. (2015) 'Evaluation of NDWI and MNDWI for assessment of waterlogging by integrating digital elevation model and groundwater level', *Geocarto International*, 30(6), pp. 650–661. doi:10.1080/10106049.2014.965757.

Sinha, R., Jain, V., Babu, G.P. and Ghosh, S. (2005) 'Geomorphic characterization and diversity of the fluvial systems of the Gangetic Plains', *Geomorphology*, 70, pp. 207–225. doi:10.1016/j.geomorph.2005.02.006.

Slingerland, R. and Smith, N.D. (2004) 'River avulsions and their deposits', *Annual Review of Earth and Planetary Sciences*, 32(Qian 1990), pp. 257–285. doi:10.1146/annurev.earth.32.101802.120201.

Snieder, S., Griffiths, C.M., Owen, A., Hartley, A.J. and Howell, J.A. (2021) 'Stratigraphic forward modelling of distributive fluvial systems based on the Huesca System, Ebro Basin, northern Spain', *Basin Research*, 33(6), pp. 3137–3158. doi:10.1111/bre.12597.

Soares, M.V.T., Basilici, G., Dal' Bó, P.F., da Silva Marinho, T., Mountney, N.P., Colombera, L., de Oliveira, E.F. and da Silva, K.E.B. (2018) 'Climatic and geomorphologic cycles in a semiarid distributive fluvial system, Upper Cretaceous, Bauru Group, SE Brazil', *Sedimentary Geology*, 372, pp. 75–95. doi:10.1016/j.sedgeo.2018.05.001.

Soares, M.V.T., Basilici, G., da Silva Marinho, T., Martinelli, A.G., Marconato, A., Mountney, N.P., Colombera, L., Mesquita, Á.F., Vasques, J.T., Junior, F.R.A. and Ribeiro, L.C.B. (2021) 'Sedimentology of a distributive fluvial system: The Serra da Galga Formation, a new lithostratigraphic unit (Upper Cretaceous, Bauru Basin, Brazil)', *Geological Journal*, 56(2), pp. 951–975. doi:10.1002/gj.3987.

Steel, E., Paola, C., Chadwick, A.J., Hariharan, J., Passalacqua, P., Xu, Z., Michael, H.A., Brommecker, H. and Hajek, E.A. (2022) 'Reconstructing subsurface sandbody connectivity from temporal evolution of surface networks', *Basin Research*, (March), pp. 1486–1506. doi:10.1111/bre.12668.

Strahler, A.N. (1957) 'Quantitative analysis of watershed geomorphology', *Eos, Transactions American Geophysical Union*, 38(6), pp. 913–920. doi:10.1029/TR038i006p00913.

Strahler, A.N. (1968) 'Dimensional Analysis Applied To Fluvially', 69(March), pp. 279–300.

Terwisscha van Scheltinga, R.C., McMahon, W.J., van Dijk, W.M., Eggenhuisen, J.T. and Kleinhans, M.G. (2020) 'Experimental distributive fluvial systems: Bridging the gap between river and rock record', *Depositional Record*, 6(3), pp. 670–684. doi:10.1002/dep2.124.

Tooth, S. (2000) 'Process, form and change in dryland rivers: A review of recent research', *Earth Science Reviews*, 51(1–4), pp. 67–107. doi:10.1016/S0012-8252(00)00014-3.

Tooth, S. (2005) 'Splay formation along the lower reaches of ephemeral rivers on the northern plains of arid central Australia', *Journal of Sedimentary Research*, 75(4), pp. 636–649. doi:10.2110/jsr.2005.052.

Ustin, S.L. and Gamon, J.A. (2010) 'Remote sensing of plant functional types', *New Phytologist*, 186(4), pp. 795–816. doi:10.1111/j.1469-8137.2010.03284.x.

Valenza, J.M., Edmonds, D.A., Hwang, T. and Roy, S. (2020) 'Downstream changes in river avulsion style are related to channel morphology', *Nature Communications*, 11(1), pp. 1–8. doi:10.1038/s41467-020-15859-9.

Vandenberghe, J. (2003) 'Climate forcing of fluvial system development: An evolution of ideas', *Quaternary Science Reviews*, 22(20), pp. 2053–2060. doi:10.1016/S0277-3791(03)00213-0.

Viseras, C., Calvache, M.L., Soria, J.M. and Fernńdez, J. (2003) 'Differential features of alluvial fans controlled by tectonics or eustatic accommodation space. Examples from the Betic Cordillera, Spain', *Geomorphology*, 50(1–3), pp. 181–202. doi:10.1016/S0169-555X(02)00214-3.

Wang, J. and Plink-Björklund, P. (2019) 'Stratigraphic complexity in fluvial fans: Lower Eocene Green River Formation, Uinta Basin, USA', *Basin Research*, 31(5), pp. 892–919. doi:10.1111/bre.12350.

Wang, Y., Straub, K.M. and Hajek, E.A. (2011) 'Scale-dependent compensational stacking: An estimate of autogenic time scales in channelized sedimentary deposits', *Geology*, 39(9), pp. 811–814. doi:10.1130/G32068.1.

Warburton, J. (1996) 'Active braidplain width, bed load transport and channel morphology in a model braided river', *Journal of Hydrology New Zealand*, 35(2), pp. 259–285.

Warren, L. V., de Andrade, A.S.M., Varejão, F.G., Promenzio, P., Santos, M.G.M., Alessandretti, L. and Assine, M.L. (2021) 'Sedimentary evolution of distributive fluvial systems within intraplate tectonic active basins: Case study of the Early Cretaceous Araripina Formation (Araripe Basin, NE Brazil)', *Journal of South American Earth Sciences*, 111(August). doi:10.1016/j.jsames.2021.103496.

Waters, J. V., Jones, S.J. and Armstrong, H.A. (2010) 'Climatic controls on late Pleistocene alluvial fans, Cyprus', *Geomorphology*, 115(3–4), pp. 228–251. doi:10.1016/j.geomorph.2009.09.002.

Weissmann, G.S., Hartley, A.J., Nichols, G.J., Scuderi, L.A., Olson, M., Buehler, H. and Banteah, R. (2010) 'Fluvial form in modern continental sedimentary basins: Distributive fluvial systems', *Geology*, 38(1), pp. 39–42. doi:10.1130/G30242.1.

Weissmann, G.S., Hartley, A.J., Nichols, G.J., Scuderi, L.A., Olson, M.E., Buehler, H.A. and Massengill, L.C. (2011) 'Alluvial Facies Distributions in Continental Sedimentary Basins—Distributive Fluvial Systems', *From River to Rock Record: The preservation of fluvial sediments and their subsequent interpretation*, (97), pp. 327–355. doi:10.2110/sepmsp.097.327.

Weissmann, G.S., Hartley, A.J., Scuderi, L.A., Nichols, G.J., Davidson, S.K., Owen, A., Atchley, S.C., Bhattacharyya, P., Chakraborty, T., Ghosh, P., Nordt, L.C., Michel, L. and Tabor, N.J. (2013) 'Prograding distributive fluvial systems-geomorphic models and ancient examples', *SEPM Special Publications*, 104, pp. 131–147. doi:10.2110/sepmsp.104.16.

Weissmann, G.S., Hartley, A.J., Scuderi, L.A., Nichols, G.J., Owen, A., Wright, S., Felicia, A.L., Holland, F. and Anaya, F.M.L. (2015) 'Fluvial geomorphic elements in modern sedimentary basins and their potential preservation in the rock record: A review', *Geomorphology*, 250, pp. 187–219. doi:10.1016/j.geomorph.2015.09.005.

Wickert, A.D., Martin, J.M., Tal, M., Kim, W., Sheets, B. and Paola, C. (2013) 'River channel lateral mobility: Metrics, time scales, and controls', *Journal of Geophysical Research: Earth Surface*, 118(2), pp. 396–412. doi:10.1029/2012JF002386.

Wilcoxon, F. (1945) 'Individual Comparison By Ranking Methods.', *Biometrics Bulletin*, 1(6), pp. 80–83.

Willems, C.J.L., Nick, H.M., Goense, T. and Bruhn, D.F. (2017) 'The impact of reduction of doublet well spacing on the Net Present Value and the life time of fluvial Hot Sedimentary Aquifer doublets', *Geothermics*, 68, pp. 54–66. doi:10.1016/j.geothermics.2017.02.008.

Wilson, A., Flint, S., Payenberg, T., Tohver, E. and Lanci, L. (2014) 'Architectural styles and sedimentology of the fluvial lower beaufort group, Karoo Basin, South Africa', *Journal of Sedimentary Research*, 84(4), pp. 326–348. doi:10.2110/jsr.2014.28.

Yang, X., Pavelsky, T.M., Allen, G.H. and Donchyts, G. (2020) 'RivWidthCloud: An Automated Google Earth Engine Algorithm for River Width Extraction from Remotely Sensed Imagery', *IEEE Geoscience and Remote Sensing Letters*, 17(2), pp. 217–221. doi:10.1109/LGRS.2019.2920225.